Composite Hydrogels of Bio-inspired Protein Polymers

Mechanical and Structural Characterization

Wolf Harald Rombouts

Composite Hydrogels of Bio-inspired Protein Polymers

Mechanical and Structural Characterization

Wolf Harald Rombouts

Contents

General Introduction

1.1 Hydrogels

Hydrogels consist of a 3D crosslinked polymer network that is swollen in water (see Figure 1.1). Despite their high water content (>50%) hydrogels behave like solids and retain their 3D structure. Hydrogels can be crosslinked by reversible physical crosslinks, chemical crosslinks, or a combination of both. Physical crosslinks are reversible non-covalent interactions such as hydrophobic interactions, entanglements, ionic bonds, hydrogen bonding, and stereocomplexation.[1–6] Chemical crosslinks are formed by permanent covalent bonds which generally cannot be remodeled after formation.
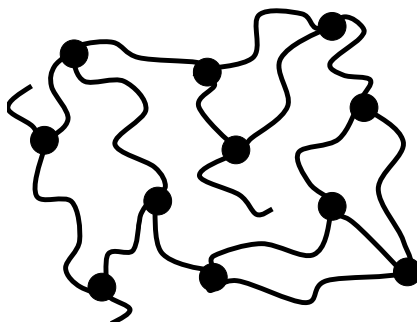
Figure 1.1: *Schematic representation of a hydrogel. Polymer chains are represented by the lines, and crosslinks are represented by the circles.*

Hydrogels can be made from synthetic polymers and polymers from natural sources. They are generally considered as biocompatible materials, because their high water content and stiffness resemble the extracellular environment (ECM) of cells. Polymers derived from natural resources such as gelatin, alginate and hyaluronic acid are generally more biocompatible than those of synthetic origin, because these polymers consist of building blocks that are present in abundance in nature. Due to their biocompatibility hydrogels are considered and used for a wide range of biomedical applications such as scaffolds, drug-delivery systems, wound dressings, super absorbents, and contact lenses.[7–13] For most of these applications it is important that properties such as the stiffness, toughness, porosity, and degradation rate of the hydrogel can be controlled to ensure proper functioning *in vivo*.[14]

1.2 Stimulus-responsive hydrogels

Stimulus-responsive hydrogels are similar to conventional hydrogels, however they have the advantage that they can respond to changes in the environment, such as temperature, pH, redox potential, and salt concentration.[15–21] In general, two types of stimulus-responsive hydrogels can be distinguished: (1) hydrogels with responsive strands and (2) hydrogels with responsive nodes.

1.2.1 Responsive strands

For the hydrogels with responsive strands, a network is formed by covalent crosslinking of the polymer chains. The responsive strands present in the hydrogel can swell or collapse due to a change in pH, salt concentration or temperature (Figure 1.2A). Most often dramatic volume changes of hydrogels are charge-related. These specific hydrogels consist of polyelectrolytes and polyampholytes, containing acidic and/or basic residues in the polymer chain, for example polyacrylic acid. These residues can be protonated or deprotonated by changing the pH, or the charges can be screened by varying the salt concentration. The osmotic pressure due to the counterions trapped in charged polymer gels leads to a strong swelling. Swelling behavior can be applied in various biomedical applications. For example superabsorbents that can hold large amounts of biological liquids. Delivery of drugs can be controlled by swelling of the hydrogel: the drugs are first loaded into polymers in dehydrated form, subsequently the drugs are released upon swelling when the polymer is rehydrated in physiological conditions.[22] pH-responsive polymers that can swell or collapse in response to pH are also interesting candidates for drug-delivery applications in the gastro-intestinal tract, where radical changes in pH are experienced. For example a hydrogel that does not swell inside the stomach at low pH, but does swell in the intestine where the pH is more alkaline, could selectively release its payload there.

Temperature-responsive behavior is observed for polymers with a temperature-dependent solubility. Two kinds of behavior can occur: lower critical solution temperature (LCST) behavior and upper critical solution temperature (UCST) behavior. Polymers that have a LCST are soluble below this temperature, while above the LCST the polymer chains collapse and phase separate. Temperature-responsive polymers with a LCST are most common, such as PNIPAm and elastin. Polymers that have a UCST in water are rare, those polymers are soluble at temperatures exceeding the

UCST, but phase separate when the temperature is below this point. For biomedical applications temperature-responsive materials are interesting for drug delivery purposes, as drugs can be mixed with a polymer that has a LCST or critical gelation temperature close to body temperature.[22–24] Because many therapeutic drugs are sensitive to the environment of the human body, a suitable carrier is necessary to guide these therapeutic drugs to the proper location.

1.2.2 Responsive nodes

In case of hydrogels with responsive nodes, the network is formed by assembly of stimulus-responsive parts of the polymer chains into crosslinking points that are called 'nodes' (Figure 1.2B). As the formation of nodes is driven by physical interactions that are generally reversible, disassembly of the network can occur if the trigger is reversed. As these nodes are formed by physical interactions they are non-permanent in nature: they have finite relaxation times. This means that physical hydrogels will flow over time. The relaxation time typically depends on the type of interaction and strength of this interaction. There are many examples of hydrogels with responsive nodes formed by physical interactions. Temperature-responsive hydrogels can be formed by gelatin, which is a well-known product derived by partial hydrolysis of natural collagen. It can form hydrogels if the solution is cooled to room temperature.[25] Gelation occurs due to the partial renaturation of triple helices: regions where triple helices are formed are connected by amorphous random-coil regions. Another example is alginate, which is a polysaccharide that can form hydrogels via the formation of ionic bonds between carboxylic acid groups in the chains and divalent ions in solution.[26] Alginate and gelatin are widely used in food industry as thickeners. Physical hydrogels that are responsive to both ionic strength and pH can be prepared from a mixture of synthetic triblock copolymers with charged end-blocks with an oppositely charged polyelectrolyte.[27] A mixture of a hydrogel-forming polymer and drug can be injected and form a hydrogel at body temperature, which then releases the drug over time.

4

A Stimulus-responsive strands

Collapsed strands   Swollen strands

Trigger 'on'

Trigger 'off'

B Stimulus-responsive nodes

Free monomers   Hydrogel with nodes

Trigger 'on'

Trigger 'off'
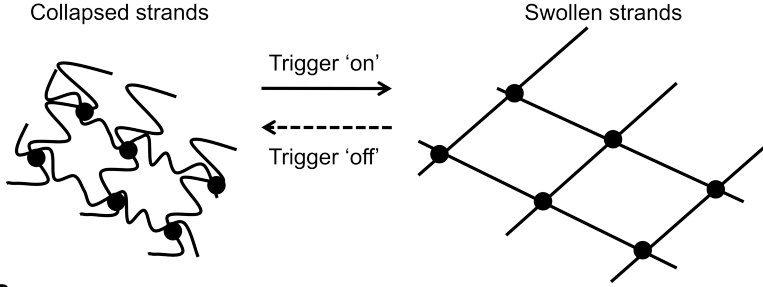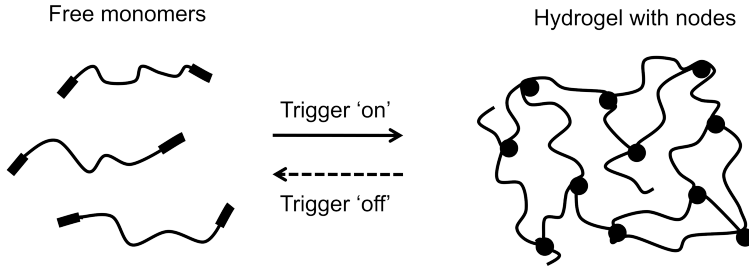
Figure 1.2: *Stimulus-responsive hydrogels. (A) Response of hydrogels with stimulus-responsive strands. The responsive strands are presented by the lines and chemical crosslinks by the circles. (B) Response of hydrogels with stimulus-responsive nodes. Physical hydrogels are formed by association of stimulus-responsive parts of the polymer chain. The soluble part of the polymer chain is represented by the lines, the stimulus-responsive parts of the polymer chain by the rectangles, and the stimulus-responsive nodes are represented by the circles.*

1.3   Mechanical properties of hydrogels

For the use of hydrogels in biomedical applications it is important that the mechanical properties meet the specific requirements for a certain application. These requirements can generally be divided in two categories: (1) modulus and (2) fracture resistance. The modulus is related to the stiffness of the material and how easily a material can be deformed.[28] According to the classical rubber theory (equation 1.1) the elastic modulus (G') of a network of flexible polymer chains scales with the number of polymer strands (n) per unit volume (V):

$$G' \approx \frac{n k_B T}{V} \tag{1.1}$$

5

where k_B is the Boltzmann constant. This relation indicates that the modulus is directly related to the number of crosslinks in the hydrogel. The crosslinking density and polymer concentration can thus be used to tune the elastic modulus of hydrogels. The fracture resistance is related to how much a material can be deformed before fracture occurs. When a polymer network is deformed beyond a certain point: (1) cracks are formed (crack nucleation), (2) these cracks can propagate as the deformation continues (crack propagation), and (3) if the network is deformed even further it results in the catastrophic fracture of the network.

The point at which cracks form is dependent on the homogeneity of the network. Inhomogeneities in the network can promote nucleation of cracks, and therefore reduce fracture resistance. Once cracks are formed they can propagate if there is sufficient energy to break crosslinks around the crack tip in the network. Crack propagation depends on the number and type of crosslinks present in the network. Because the stress is localized at the crack tip, crack propagation in single networks is relatively easy (Figure 1.3).
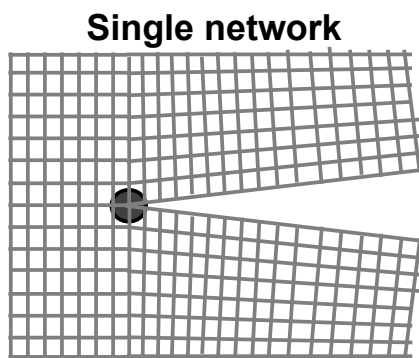
Single network

Figure 1.3: *Fracture of a single network hydrogel. The circle indicates the dissipative zone around the crack tip. In a single network the stress is localized at the crack tip.*

1.4 Design strategies for tougher hydrogels

Hydrogels can offer many benefits for biomedical applications as described earlier. However, most hydrogel systems have a poor mechanical strength, which limits their application in load-bearing applications, such as joints, cartilage, and bones. Therefore, significant improvement of the mechanical properties of hydrogels is necessary. This section describes various strategies reported in literature aimed to improve the fracture resistance of hydrogels: (1) homogenous structured hydrogels (Figure 1.4A),[29] (2) hydro-

gels with nano-fillers (Figure 1.4B),[30,31] (3) topologically interlocked hydrogels via chain-sliding crosslinking agents (Figure 1.4C),[32] (4) double network hydrogels (Figure 1.4D).[33–36] These strategies focus either on prevention of crack nucleation or crack propagation.
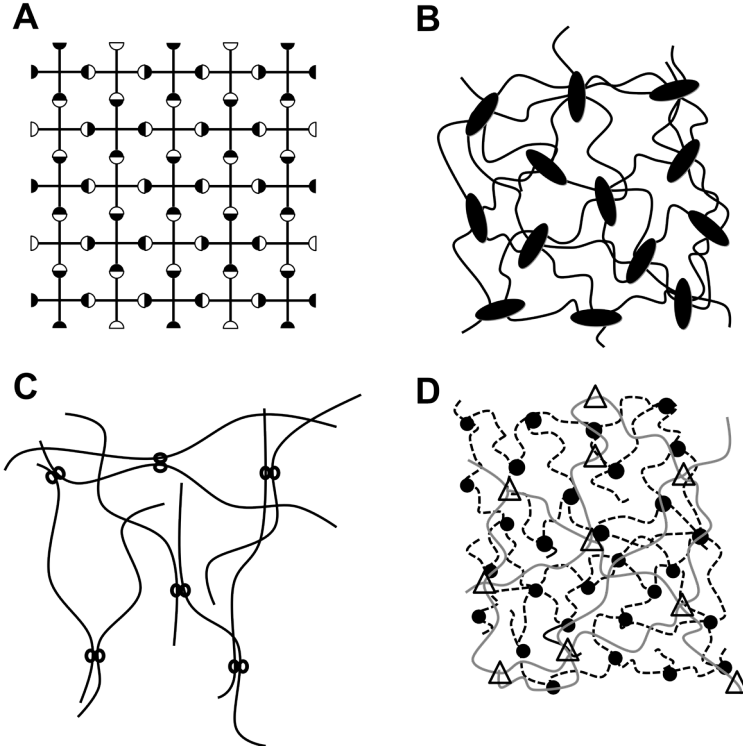
Figure 1.4: *Strategies to create tougher hydrogels. (A) Homogeneous networks.[29] (B) Hydrogels with nano-fillers.[30,31] (C) Sliding crosslinks.[32] (D) Double networks.[33–36]*

The first strategy focused on improving the fracture resistance by improving the homogeneity of the network (Figure 1.4A). It involved network formation by two different monomers, consisting of four-armed polyethylene glycol (PEG) functionalized with terminal N-Hydroxysuccinimide (NHS) and amine groups to prevent self-reaction. This approach resulted in a hydrogel with a more homogeneous structure and improved fracture resistance by impeding crack nucleation.[29] In the second strategy, inorganic clay platelets were dispersed in an aqueous medium containing N-isopropylacrylamide (NIPAAm) monomers

(Figure 1.4B). Subsequently, this NIPAAm was grafted to the clay platelets and polymerized. This resulted in highly stretchable hydrogels (up to 1500%), in which the junctions were formed by the clay platelets. In this system polymer chains with a large chain length and homogeneous length distribution were used to minimize energy localization.[30] In the third strategy chemical crosslinks are formed between cyclodextrin molecules on adjacent PEG chains resulting in chain-sliding figure-of-eight crosslinks (Figure 1.4C). A topologically interlocked network was formed as a result. This approach led to improved mechanical properties (kPa range) and deformability of the hydrogels (up to twice its length).[32] The mobile crosslinks that maintain hydrogel structure can slide along polymer chains in the hydrogel and can dissipate energy if the hydrogel is deformed. The fourth strategy, pioneered by Gong and co-workers, introduced a second loosely crosslinked polymer network to the more rigid first polymer network (Figure 1.4D). Both components formed a separate polymer network, that did not specifically interact with the other. This resulted in an interpenetrating network. They showed that these interpenetrating double-network hydrogels exhibited an extremely high mechanical strength (elastic modulus and fracture strength in MPa range).[33] This was done by combining poly(2-acrylamido-2-methylpropanesulfonic acid)(PAMPS) and poly acrylamide (PAAm). The increase of the fracture resistance is due to an increased energy dissipation around the crack tip (Figure 1.5), because the loosely crosslinked network spreads the energy at the crack site over a larger dissipation zone.[33,37] Although these hydrogels have impressive mechanical properties, these properties are lost after repeated loading of the hydrogels.
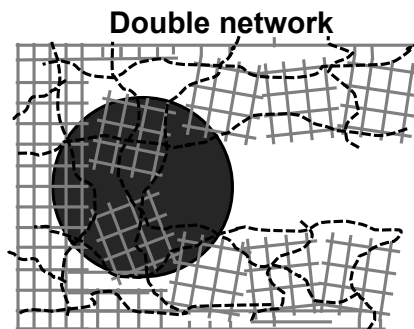
Figure 1.5: *Double network: the energy is more effectively dissipated due to the presence of a second network.*

Sun and co-workers took the next step in the development of double networks: a stiff chemically crosslinked PAAm network was combined with a soft alginate network formed by ionic bonds in the presence of calcium ions.[34] These ionic bonds can open like a zipper when stressed, and self-heal when the stress is relaxed. It was shown that double-networks of PAAm and alginate possess greatly improved mechanical properties in comparison to both single components. Furthermore, the alginate network can self-heal after failure due to the physical nature of ionic bonds.

1.5 Composites

Recent advances in the field of hydrogels led to significant improvement of the mechanical strength of these materials, which increases the potential of hydrogels for biomedical applications. However, at this moment these double network hydrogels do consist of at least one chemically crosslinked component. Generally, chemical crosslinking requires UV-curing, crosslinking agents and an initiator. As unreacted monomers can be left behind in these hydrogels, and chemicals involved in the crosslinking process can be toxic, creating biomaterials via this method is not optimal. Therefore, making tough biomaterials from natural occurring polymers should be considered. For the design of these biomaterials it should be noted that tissues are complex structures that can have a wide range of mechanical and structural properties (e.g. bone versus vitreous humor in the eye). Tissues consist of combinations of cells, proteins, polysaccharides, minerals, and other components. Often stiff fibers are combined with more soft flexible networks to provide structural integrity and mechanical strength. Tissue stiffness and elasticity are determined by the amount and orientation of the fibrous proteins collagen and elastin.[38,39] In bone, inorganic rigid hydroxyapatite crystals form a composite with more soft collagen fibers. Due to this composite structure, bone is resistant to both compression and tension.[38] In wood, long stiff cellulose fibers are bundled together by the more soft lignin, creating a composite that provides structural support, and allows trees to grow in height against gravity.[40] It is clear that the advantageous mechanical properties of composites in nature are the reason for their abundance. However, not much is known about the mechanisms behind the synergistic mechanical effects of these composites. A deeper understanding of these mechanisms is of great importance to the design strategy for new biomaterials.

1.6   Fiber networks

Many biological materials consist of semi-flexible fibers as network-formers. Semi-flexible fiber networks can be formed at low concentrations (>0.013% (w/v))[41,42] The mechanical behavior of semi-flexible fiber networks is more complicated than that of flexible polymer networks. A theoretical model describing the relation between the elastic modulus of the fiber network (G'), the persistence length (l_p), mesh size of the network (ξ) and entanglement length (L_e) was presented by MacKintosh and co-workers (equation 1.2):[43]

$$G' \approx \frac{k_B T l_p^2}{L_e^3 \xi^2} \tag{1.2}$$

where k_B is the Boltzmann constant. From this equation it can be seen that the elastic modulus of fiber networks is related to the persistence length, mesh size, and entanglement length. The persistence length is a measure of the fiber stiffness, and is determined by measuring the characteristic length scale over which the fiber maintains its orientation. Both the entanglement length and mesh size of the network depend on the fiber concentration. As the fiber concentration increases, the mesh size and entanglement length will decrease as the fibers are packed more closely together. The model of MacKintosh et al. assumes that the semi-flexible fiber network responds affinely to externally imposed strain due to stretching of the fibers only. This model is in agreement with many *in vitro* experiments done on biopolymer systems.[41,44–46] There are also models describing non-affine, bending-dominated behavior of fiber networks, where a softer network response is expected, resulting in a different scaling between the concentration and elastic modulus.[46–49]

Fiber networks generally break at low strains and are therefore brittle in nature. However, it was shown that the strain that fibers can endure can vary by orders of magnitude.[44] Nonlinear strain hardening behavior is commonly observed in both natural and synthetic fibers.[44] This behavior protects tissues against large deformation, and is thought to originate from the finite stretchability of the fibers. Recently, Brangwynne and co-workers investigated the deformation of cytoskeletal microtubules embedded in actin networks in living cells. They found that these microtubules were able to bear larger loads than expected. This effect was caused by the mechanical coupling of the microtubules to the surrounding elastic matrix: the non-affine bending modes of the microtubules were suppressed by the elastic matrix.[50] Conversely, Lin and co-workers showed that by embedding a small amount of stiff microtubules in a network of crosslinked actin filaments, the

nonlinear elastic properties of the network could be altered dramatically. Strain-stiffening was introduced by the microtubules due to suppression of non-uniform strain.[51] These studies confirm that it can be beneficial to combine rigid fibers with a more soft elastic network.

1.7   Recombinant protein polymers

Peptides that can self-assemble on demand are interesting candidates to use as scaffolds or drug carriers for biomedical applications, because these structures partially resemble the extracellular matrix (ECM) of cells. The stiffness of the scaffold provides structural support to the cells and can influence cell fate.[52] Peptide sequences can be made via chemical synthesis, however the amino acid sequence length and complexity that can be produced with this method are limited. When longer amino acid sequences and a higher complexity are required, this method is expensive. Genetic engineering allows the design of recombinant proteins with the structure of long block copolymers, and with an amino acid sequence that can be made to include supramolecular self-assembly motifs as well as recognition sites for further processing and binding of cells, enzymes, etc. A synthetic gene coding for the desired block copolymer is constructed by combining various DNA modules, coding for the different blocks, into a single sequence. The DNA modules can comprise exact copies of existing natural sequences, bioinspired (modified natural) sequences, or sequences that are designed entirely from scratch. After insertion into an expression vector, the resulting gene is finally transferred to an expression host organism for controlled expression of the polymer-encoding gene, which should result in efficient biosynthetic polymer production. The first genetically engineered protein polymers produced in this way were block copolymers consisting of silk-like and elastin-like blocks reported by Cappello and co-workers.[53] Since then many other bio-inspired designs have been reported: resilin,[54] elastin,[55] silk,[53,56,57] and collagen.[58] Both resilin and elastin are elastic proteins, providing low stiffness and high strain resistance.[54,59] Resilin can be found in certain insects, and elastin is a key ECM protein found in many vertebrate tissues. Silk is a natural fibrous protein, a stiff material providing mechanical strength, which can be found in spider webs and in cocoons of silk worms. In recent years, various protein block copolymers have been designed in our research group via genetic engineering, and were biosynthetically produced, using *Pichia pastoris* as an expression system. Important characteristics of this expression system are: (1) the

produced protein block copolymer is excreted into the culture medium, and (2) generally the yield exceeds 1 g.L^{-1} of lyophilized product. The first protein polymers produced at Wageningen University in *P. pastoris* were non-hydroxylated, non-gelling gelatins, some with natural sequence, and some with bioinspired, very hydrophilic designer sequence of amino acids.[60–63] These were followed by elastin-like and silk-like polymers consisting of only a single block,[64–66] as well as di- or triblock copolymers with tunable gel- and fiber-forming[16,20,67–72] and slow-release properties.[73] Collagen-inspired triblock copolymers were able to form soft, elastic self-healing hydrogels upon lowering the temperature.[69,74] Shape-memory behavior could be introduced to this system by chemical crosslinking of lysine residues present in the non-associating parts of the protein polymers, and by fixing the hydrogels in a temporary shape under deformation at low temperature.[75] Silk-inspired triblock copolymers were able to form rigid brittle hydrogels at low concentration (1.0% w/v) when the pH was adjusted.[16] Weak soft hydrogels could be formed with asymmetric silk-elastin-like protein polymers by fiber formation by adjusting the pH. By increasing the temperature, the fibers that were already formed were irreversibly bundled due to the LCST behavior of the elastin-like blocks.[76]

1.8 Aim and outline of thesis

The aim of this thesis is to investigate the mechanical and structural properties of composite hydrogels formed by bio-inspired protein polymers. The mechanical properties that are measured with rheology will be related to the structural properties determined with various microscopy techniques, to find new strategies for creating stronger or functional hydrogels suitable for biomedical applications. An overview of the different species of custom-designed protein polymers that are used in this thesis is given in Table 1.1.

Generally speaking, all protein polymers consist of one or two collagen-like hydrophilic random-coils providing solubility at a wide range of temperatures and pH to all designs. These blocks are designated as C_2^P and C_4^R, corresponding to a hydrophilic 198 and 396 amino acid long sequence, respectively. Most protein polymers also contain two self-assembly motifs which can associate if triggered by pH or temperature. The T_9 block is collagen-inspired, and consists of nine (Pro-Gly-Pro)$_n$ repeats that can form triple-helices when the temperature is lowered (Figure 1.6A). The T_9^* block has the exact same composition as the T_9 block,

Table 1.1: *Overview of properties of different protein block copolymers used in this thesis.*

Protein polymer	Macroscopic properties	Chapter
$T_9^* C_4^R T_9^*$	Inert, hydrophilic random-coil	2
$T_9 C_4^R T_9$	Flexible polymer networks at low T	2,3,5
C_4^R	Inert, hydrophilic random-coil	2,3,6
$C_2^P S_{48}^E C_2^P$	Forms gels <pH 4	2,3,4,6
$S_8^H C_4^R T_9$	Combines with $C_2^P S_{48}^E C_2^P$ into thermo-responsive fibers	6
$C_2^P S_{48}^H C_2^P$	Forms gels >pH 6	7
$C_2^P S_{48}^H C_2^P$-Cys	Forms gels >pH 6	7
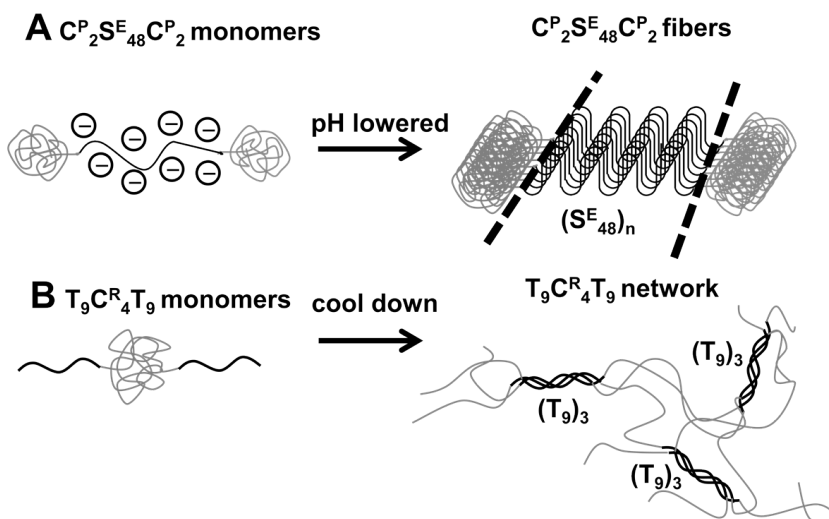
Figure 1.6: *(A) Self-assembly of $\mathbf{S^E}$ blocks into $(\mathbf{S_{48}^E})_n$ fibers when the pH is lowered. (B) Self-assembly of $\mathbf{T_9}$ blocks into triple helices $(\mathbf{T_9})_3$ if the temperature is lowered.*

however the sequence is scrambled in such a way that these blocks cannot form triple helices. The $\mathbf{S^H}$ and $\mathbf{S^E}$ blocks correspond to self-assembling blocks that can form semi-flexible fibers by stacking of β-sheet-like structures (Figure 1.6B). These blocks consist of n (Gly-Ala)$_3$-Gly-Xxx repeats, in which the Xxx contains pH-responsive residues that can be either glutamic acid (Glu) or histidine (His).

In **chapter 2** we study the mechanical and structural properties of composite hydrogels formed by elastic collagen-like ($T_9C_4^RT_9$) and silk-like ($C_2^PS_{48}^EC_2^P$) block copolymers. We show with rheology that these composite gels are significantly stronger, both in the linear and nonlinear regime, than gels of each of the consistituting components taken apart. With cryo transmission electron microscopy (Cryo-TEM) we show that the silk-like fibers in mixed conditions are bundled, most probably due to depletion attraction induced by the collagen-like block copolymers in the mixture. **Chapter 3** continues on this work by investigating the toughening mechanism observed in the previous chapter in more detail. We show with rheological stress/strain cycling tests that hysteresis occurs in the composite hydrogels. This hysteresis can be split in a part belonging to dissipation of breaking fibers, and a part belonging to the dissipation of the elastic collagen-like network. The collagen-like elastic network is able to increase the dissipated energy by the fibers tremendously. In addition, the self-healing capability of the composite hydrogels is investigated. We show that the self-healing ability of the collagen-like polymers is retained in the composite hydrogels, as these composites can partially self-heal after damaging events. In **chapter 4** we study hydrogel formation of a combination of a fiber-forming silk-like block copolymer ($C_2^PS_{48}^EC_2^P$) and a fiber-forming FMOC-functionalized dipeptide. We show with atomic force microscopy (AFM) and electron microscopy that both molecules assemble into fibers orthogonally. The composite hydrogels are significantly stronger than the single network hydrogels. In **chapter 5** we investigate the mechanical properties of hybrid networks formed by collagen-like block copolymers ($T_9C_4^RT_9$) by combination of physical and chemical crosslinks. We show that the order in which the chemical and physical crosslinks are formed does not have an influence on the final mechanical strength of the hydrogels. The hybrid networks are significantly stronger than the separate strength of the physical and chemical crosslinks combined. In **chapter 6** we investigate hydrogel formation by mixing positively charged asymmetric silk-collagen-like block copolymers ($S_8^HC_4^RT_9$) with negatively charged silk-like block copolymers ($C_2^PS_{48}^EC_2^P$). With rheology we show that these polymers can co-assemble into fibers that can form hydrogels. With confocal laser scanning microscopy (CLSM) we observe that both components are co-localized in the fibers. The composite hydrogels are responsive to temperature in a reversible manner: the storage modulus is increased as the temperature is decreased and vice versa. In **chapter 7** we study the effect of adding a cysteine-residue to the hydrophilic block of a silk-like block copolymer ($C_2^PS_{48}^HC_2^P$-Cys) on the mechanical properties. We

14

show with rheology that in oxidizing conditions stronger hydrogels are formed due to formation of disulfide-bridges by the cysteine-residues. With AFM we find a higher persistence length for the hydrogels that are formed in oxidizing conditions. In **chapter 8** we reflect on our work and we indicate future directions of possible research and applications.

References

(1) Ikada, Y.; Jamshidi, K.; Tsuji, H.; Hyon, S. H. *Macromolecules* **1987**, *20*, 904–906.

(2) Hirschberg, J. H. K. K.; Brunsveld, L.; Ramzi, A.; Vekemans, J. A. J. M.; Sijbesma, R. P.; Meijer, E. W. *Nature* **2000**, *407*, 167–170.

(3) De Jong, S. J.; De Smedt, S. C.; Demeester, J.; Van Nostrum, C. F.; Kettenes-Van Den Bosch, J. J.; Hennink, W. E. *J. Controlled Release* **2001**, *72*, 47–56.

(4) Reches, M.; Gazit, E. *Science* **2003**, *300*, 625–627.

(5) Vermonden, T.; Censi, R.; Hennink, W. E. *Chem. Rev.* **2012**, *112*, 2853–2888.

(6) Peppas, N. A.; Bures, P.; Leobandung, W.; Ichikawa, H. *Eur J. Pharm. Biopharm.* **2000**, *50*, 27–46.

(7) Bajpai, A. K.; Shukla, S. K.; Bhanu, S.; Kankane, S. *Prog. Polym. Sci.* **2008**, *33*, 1088–1118.

(8) Langer, R.; Tirrell, D. A. *Nature* **2004**, *428*, 487–492.

(9) Kim, S. J.; Hahn, S. K.; Kim, M. J.; Kim, D. H.; Lee, Y. P. *J. Controlled Release* **2005**, *104*, 323–335.

(10) Zhao, W.; Jin, X.; Cong, Y.; Liu, Y.; Fu, J. *J. Chem. Technol. Biotechnol.* **2013**, *88*, 327–339.

(11) Li, Y.; Rodrigues, J.; Tomas, H. *Chem. Soc. Rev.* **2012**, *41*, 2193–2221.

(12) Peppas, N. A.; Hilt, J. Z.; Khademhosseini, A.; Langer, R. *Adv. Mater.* **2006**, *18*, 1345.

(13) Hoffman, A. S. *Adv. Drug Delivery Rev.* **2002**, *54*, 3–12.

(14) O'Brien, F. J. *Mater. Today* **2011**, *14*, 88–95.

(15) Jeong, B.; Gutowska, A. *Trends Biotechnol.* **2002**, *20*, 305–311.

(16) Martens, A. A.; van der Gucht, J.; Eggink, G.; de Wolf, F. A.; Cohen Stuart, M. A. *Soft Matter* **2009**, *5*, 4191–4197.

(17) Petka, W. A.; Harden, J. L.; McGrath, K. P.; Wirtz, D.; Tirrell, D. A. *Science* **1998**, *281*, 389–392.

(18) Kaneko, Y.; Sakai, K.; Kikuchi, A.; Sakurai, Y.; Okano, T. *Macromol. Symp.* **1996**, *109*, 41–53.

(19) Corrente, F.; Paolicelli, P.; Matricardi, P.; Tita, B.; Vitali, F.; Casadei, M. A. *J. Pharm. Sci.* **2012**, *101*, 256–267.

(20) Werten, M. W. T.; Teles, H.; Moers, A. P. H. A.; Wolbert, E. J. H.; Sprakel, J.; Eggink, G.; de Wolf, F. A. *Biomacromolecules* **2009**, *10*, 1106–1113.

(21) Pham, T. T. H.; Skrzeszewska, P. J.; Werten, M. W. T.; Rombouts, W. H.; Cohen Stuart, M. A.; de Wolf, F. A.; van der Gucht, J. *Soft Matter* **2013**, *9*, 6391–6397.

(22) Liechty, W. B.; Kryscio, D. R.; Slaughter, B. V.; Peppas, N. A. *Annu. Rev. Chem. Biomol. Eng.* **2010**, *1*, 149–173.

(23) Schmaljohann, D. *Adv. Drug Delivery Rev.* **2006**, *58*, 1655–1670.

(24) Klouda, L.; Mikos, A. G. *Eur J. Pharm. Biopharm.* **2008**, *68*, 34–45.

(25) Bigi, A.; Panzavolta, S.; Rubini, K. *Biomaterials* **2004**, *25*, 5675–5680.

(26) Draget, K. I.; Østgaard, K.; Smidsrød, O. *Carbohydr. Polym.* **1990**, *14*, 159–178.

(27) Lemmers, M.; Sprakel, J.; Voets, I. K.; van der Gucht, J.; Cohen Stuart Martien, A. *Angew. Chem. Int. Ed.* **2010**, *49*, 708–711.

(28) Zhao, X. *Soft Matter* **2014**, *10*, 672–687.

(29) Sakai, T.; Matsunaga, T.; Yamamoto, Y.; Ito, C.; Yoshida, R.; Suzuki, S.; Sasaki, N.; Shibayama, M.; Chung, U.-i. *Macromolecules* **2008**, *41*, 5379–5384.

(30) Haraguchi, K.; Takehisa, T. *Adv. Mater.* **2002**, *14*, 1120–1124.

(31) Lin, W.-C.; Fan, W.; Marcellan, A.; Hourdet, D.; Creton, C. *Macromolecules* **2010**, *43*, 2554–2563.

(32) Okumura, Y.; Ito, K. *Adv. Mater.* **2001**, *13*, 485–487.

(33) Gong, J. P.; Katsuyama, Y.; Kurokawa, T.; Osada, Y. *Adv. Mater.* **2003**, *15*, 1155–1158.

(34) Sun, J. Y.; Zhao, X.; Illeperuma, W. R. K.; Chaudhuri, O.; Oh, K. H.; Mooney, D. J.; Vlassak, J. J.; Suo, Z. *Nature* **2012**, *489*, 133–136.

(35) Chen, Q.; Zhu, L.; Zhao, C.; Wang, Q.; Zheng, J. *Adv. Mater.* **2013**, *25*, 4171–4176.

(36) Harrass, K.; Krüger, R.; Möller, M.; Albrecht, K.; Groll, J. *Soft Matter* **2013**, *9*, 2869–2877.

(37) Webber, R. E.; Creton, C.; Brown, H. R.; Gong, J. P. *Macromolecules* **2007**, *40*, 2919–2927.

(38) Alberts, B.; Bray, D.; Hopkin, K.; Johnson, A.; Lewis, J.; Raff, M.; Roberts, K.; Walter, P., *Essential cell biology*; Garland Science: 1998.

(39) Holzapfel, G., *Biomechanics of soft tissue. In: The handbook of Materials Behavior, Nonlinear Models and Properties*; Academic New York: 2000.

(40) Thakur, V. K.; Thakur, M. K.; Raghavan, P.; Kessler, M. R. *ACS Sustainable Chem. Eng.* **2014**, *2*, 1072–1092.

(41) Kouwer, P. H. J.; Koepf, M.; Le Sage, V. A. A.; Jaspers, M.; van Buul, A. M.; Eksteen-Akeroyd, Z. H.; Woltinge, T.; Schwartz, E.; Kitto, H. J.; Hoogenboom, R., et al. *Nature* **2013**, *493*, 651–655.

(42) Adams, D. J.; Mullen, L. M.; Berta, M.; Chen, L.; Frith, W. J. *Soft Matter* **2010**, *6*, 1971–1980.

(43) MacKintosh, F. C.; Käs, J.; Janmey, P. A. *Phys. Rev. Lett.* **1995**, *75*, 4425.

(44) Storm, C.; Pastore, J. J.; MacKintosh, F. C.; Lubensky, T. C.; Janmey, P. A. *Nature* **2005**, *435*, 191–194.

(45) Lin, Y.-C.; Yao, N. Y.; Broedersz, C. P.; Herrmann, H.; MacKintosh, F. C.; Weitz, D. A. *Phys. Rev. Lett.* **2010**, *104*, 058101.

(46) Broedersz, C. P.; MacKintosh, F. C. *Rev. Mod. Phys.* **2014**, *86*, 995.

(47) Broedersz, C. P.; Sheinman, M.; MacKintosh, F. C. *Phys. Rev. Lett.* **2012**, *108*, 078102.

(48) Head, D. A.; Levine, A. J.; MacKintosh, F. C. *Phys. Rev. Lett.* **2003**, *91*, 108102.

(49) Wilhelm, J.; Frey, E. *Phys. Rev. Lett.* **2003**, *91*, 108103.

(50) Brangwynne, C. P.; MacKintosh, F. C.; Kumar, S.; Geisse, N. A.; Talbot, J.; Mahadevan, L.; Parker, K. K.; Ingber, D. E.; Weitz, D. A. *J. Cell Biol.* **2006**, *173*, 733–741.

(51) Lin, Y.-C.; Koenderink, G. H.; MacKintosh, F. C.; Weitz, D. A. *Soft Matter* **2011**, *7*, 902–906.

(52) Sun, H.; Zhu, F.; Hu, Q.; Krebsbach, P. H. *Biomaterials* **2014**, *35*, 1176–1184.

(53) Cappello, J.; Crissman, J.; Dorman, M.; Mikolajczak, M.; Textor, G.; Marquet, M.; Ferrari, F. *Biotechnol. Prog.* **1990**, *6*, 198–202.

(54) Elvin, C. M.; Carr, A. G.; Huson, M. G.; Maxwell, J. M.; Pearson, R. D.; Vuocolo, T.; Liyou, N. E.; Wong, D. C. C.; Merritt, D. J.; Dixon, N. E. *Nature* **2005**, *437*, 999–1002.

(55) Sallach, R. E.; Conticello, V. P.; Chaikof, E. L. *Biotechnol. Prog.* **2009**, *25*, 1810–1818.

(56) Krejchi, M. T.; Atkins, E. D.; Waddon, A. J.; Fournier, M. J.; Mason, T. L.; Tirrell, D. A. *Science* **1994**, *265*, 1427–1432.

(57) Krejchi, M. T.; Atkins, E. D. T.; Fournier, M. J.; Mason, T. L.; Tirrell, D. A. *J. Macromol. Sci.- Pure Appli. Chem.* **1996**, *33*, 1389–1398.

(58) Goldberg, I.; Salerno, A. J.; Patterson, T.; Williams, J. I. *Gene* **1989**, *80*, 305–314.

(59) Mithieux, S. M.; Weiss, A. S. *Adv. Protein Chem.* **2005**, *70*, 437–461.

(60) Werten, M. W. T.; van den Bosch, T. J.; Wind, R. D.; Mooibroek, H.; de Wolf, F. A. *Yeast* **1999**, *15*, 1087–1096.

(61) Werten, M. W. T.; Wisselink, W. H.; Jansen-van den Bosch, T. J.; de Bruin, E. C.; de Wolf, F. A. *Protein Eng.* **2001**, *14*, 447–454.

(62) Werten, M. W. T.; de Wolf, F. A. *Appl. Environ. Microbiol.* **2005**, *71*, 2310–2317.

(63) Rozkiewicz, D. I.; Kraan, Y.; Werten, M. W. T.; de Wolf, F. A.; Subramaniam, V.; Ravoo, B. J.; Reinhoudt, D. N. *Chem. - Eur. J.* **2006**, *12*, 6290–6297.

(64) Werten, M. W. T.; Moers, A. P. H. A.; Vong, T.; Zuilhof, H.; van Hest, J. C. M.; de Wolf, F. A. *Biomacromolecules* **2008**, *9*, 1705–1711.

(65) Schipperus, R.; Teeuwen, R. L. M.; Werten, M. W. T.; Eggink, G.; de Wolf, F. A. *Appl. Microbiol. Biotechnol.* **2009**, *85*, 293–301.

(66) Schipperus, R.; Eggink, G.; de Wolf, F. A. *Biotechnol. Prog.* **2012**, *28*, 242–247.

(67) Martens, A. A.; Portale, G.; Werten, M. W. T.; de Vries, R. J.; Eggink, G.; Cohen Stuart, M. A.; de Wolf, F. A. *Macromolecules* **2009**, *42*, 1002–1009.

(68) Moers, A. P. H. A.; Wolbert, E. J. H.; de Wolf, F. A.; Werten, M. W. T. *J. Biotechnol.* **2010**, *146*, 66–73.

(69) Skrzeszewska, P. J.; de Wolf, F. A.; Werten, M. W. T.; Moers, A. P. H. A.; Cohen Stuart, M. A.; van der Gucht, J. *Soft Matter* **2009**, *5*, 2057–2062.

(70) Teles, H.; Skrzeszewska, P. J.; Werten, M. W. T.; van der Gucht, J.; Eggink, G.; de Wolf, F. A. *Soft Matter* **2010**, *6*, 4681–4687.

(71) Silva, C. I. F.; Teles, H.; Moers, A. P. H. A.; Eggink, G.; de Wolf, F. A.; Werten, M. W. T. *Biotechnol. Bioeng.* **2011**, *108*, 2517–2525.

(72) Silva, C. I. F.; Skrzeszewska, P. J.; Golinska, M. D.; Werten, M. W. T.; Eggink, G.; de Wolf, F. A. *Biomacromolecules* **2012**, *13*, 1250–1258.

(73) Teles, H.; Vermonden, T.; Eggink, G.; Hennink, W. E.; de Wolf, F. A. *J. Controlled Release* **2010**, *147*, 298–303.

(74) Skrzeszewska, P. J.; de Wolf, F. A.; Stuart, M. A. C.; van der Gucht, J. *Soft Matter* **2010**, *6*, 416–422.

(75) Skrzeszewska, P. J.; Jong, L. N.; de Wolf, F. A.; Cohen Stuart, M. A.; van der Gucht, J. *Biomacromolecules* **2011**, *12*, 2285–2292.

(76) Golinska, M. D.; Pham, T. T. H.; Werten, M. W. T.; de Wolf, F. A.; Cohen Stuart, M. A.; van der Gucht, J. *Biomacromolecules* **2012**, *14*, 48–55.

Enhanced Rigidity and Rupture Strength of Composite Hydrogel Networks of Bio-inspired Block Copolymers

Abstract

We study self-assembled composite networks consisting of silk-like protein fibers dispersed in a soft gel matrix formed by collagen-like block copolymers. Rheological analysis shows that the composite networks have significantly higher storage moduli than either of the single networks. This is caused by bundling of the fibrils due to depletion attraction induced by the collagen-like polymers. Moreover, the soft background network significantly modifies the nonlinear response of the fibrillar network; the strain hardening disappears almost completely and the stress and strain at which the gel breaks increase strongly, resulting in tougher hydrogels.

2.1 Introduction

Hydrogels are materials consisting of a water-swollen hydrophilic polymeric network. Owing to the interesting properties of many hydrogel systems, most importantly their biocompatibility,[1,2] hydrogels are suitable for a wide range of biomedical applications, such as contact lenses, scaffolds, biosensors, and drug delivery systems.[3–5] Hydrogels can be stabilized by either chemical or physical crosslinks. Chemical crosslinks result in a permanent network, which cannot be remodelled. Physical crosslinks can be formed by a variety of non-covalent interactions or combinations thereof, such as hydrogen bonds, van der Waals interactions, electrostatic interactions, hydrophobic interactions, and stereocomplexation.[6–9] An interesting property of physical hydrogels is that they can be designed to respond to various stimuli, such as pH, temperature and (salt)concentration.[10–14]

One major drawback of most current hydrogel systems is their limited mechanical strength, which limits the application of hydrogels in situations where mechanical loading occurs.[15] However, nature provides us with ample examples of very strong polymeric materials. These biological materials are usually composite networks, consisting of structures of different length scales and components with varying stiffness. For example, the extracellular matrix, which provides structural and mechanical support in biological tissues, consists of a mixture of fibrous proteins and polysaccharides.[16] Inspired by these biological materials, a number of groups have developed synthetic composite materials. Several hydrogel systems with strongly improved mechanical properties have been presented. For example, a number of studies have reported an increase in both the elastic modulus and the toughness of hydrogels after incorporation of nano-fillers, such as silica particles,[17,18] clay platelets,[19] or biopolymer crystallites.[20,21] Others have demonstrated the toughening of a covalent network by introducing additional physical cross-links.[22] Finally, it was shown that very tough hydrogels can be made by using semi-interpenetrating networks[23] or fully interpenetrating double polymer networks.[15,24–27] However, most of these systems are chemically crosslinked hydrogels, the permanent nature of which precludes the versatility of stimulus responsiveness. To circumvent the use of chemically crosslinked composite networks, protein-engineered biomaterials have attracted interest for their tuneable material properties in the past years. Protein-based biomaterials can be produced biosynthetically or they can be harvested from natural sources, such as collagen.[12,14,28–30]

Here, we investigate composite networks consisting of two recombinant

self-assembling protein polymers. A clear advantage of the biological production of recombinant proteins is that the protein harvested is monodisperse and that all protein polymers have exactly the same amino acid sequence. One of the polymers ($C_2^P S_{48}^E C_2^P$) forms a rigid, fibrillar network, while the other ($T_9 C_4^R T_9$) forms a soft polymer gel (see Table 2.1). Both protein polymers have been studied individually by us in previous work. The first polymer, $C_2^P S_{48}^E C_2^P$, consists of a pH-responsive silk-like block (S_{48}^E), flanked by two hydrophilic blocks (C_2^P) of ~200 amino acids. The S_{48}^E block consists of 48 (Gly-Ala)$_3$-Gly-Glu repeats. At low pH the glutamic acid residue becomes protonated, allowing the S_{48}^E block to self-assemble into a β-sheet-like structure, which then stacks to form long, semi-flexible fibrils.[13,31,32] The C_2^P block remains unordered and forms a hydrophilic corona around the fibrils. At sufficiently high concentration, $C_2^P S_{48}^E C_2^P$ forms rigid fibrillar gels that break at small strains.[33] The mechanical behaviour of these gels is comparable to that of actin gels and other biological gels.[34,35] The second polymer, $T_9 C_4^R T_9$, has two collagen-inspired end blocks (T_9), consisting of nine Pro-Gly-Pro repeats. At low temperature, three of these T_9 blocks self-assemble to form a triple helix. The hydrophilic C_4^R block, which bridges between the T_9 blocks, consists of ~400 amino acids and assumes a random-coil configuration at all temperatures and pH. It has the same amino acid composition as the C_2^P block, but in a different sequence. The $T_9 C_4^R T_9$ polymer thus forms thermo-responsive trifunctional physical gels.[36,37] In this chapter, we study the mechanical properties of composite networks, formed by mixing $C_2^P S_{48}^E C_2^P$ and $T_9 C_4^R T_9$. We compare these double networks to mixed networks formed with $C_2^P S_{48}^E C_2^P$ and variants of $T_9 C_4^R T_9$ that cannot self-assemble (see Table 2.1).

Table 2.1: *Overview of properties of different protein block copolymers used in this research*

Protein polymer	Molar mass (kg.mol^{-1})	Properties
$C_2^P S_{48}^E C_2^P$	65.8	Fibrillar networks at low pH[33]
$T_9 C_4^R T_9$	41.7	Flexible polymer networks at low T[12]
C_4^R	36.8	Inert, hydrophilic random-coil[12]
$T_9^* C_4^R T_9^*$	41.7	Inert, hydrophilic random-coil[38]

2.2 Experimental Section

2.2.1 Materials

Four custom-designed protein polymers ($C_2^P S_{48}^E C_2^P$, $T_9 C_4^R T_9$, C_4^R, and $T_9^* C_4^R T_9^*$; see Table 2.1) were produced biosynthetically in the yeast *Pichia pastoris*. The biosynthetic production of $C_2^P S_{48}^E C_2^P$ and $T_9 C_4^R T_9$ has been published previously,[12,33] and the amino acid sequences of these proteins can be found in GenBank under accession numbers ABW84222 and ACF33479, respectively. To obtain the complete amino acid sequence of the mature proteins from these GenBank records, the sequence of $C_2^P S_{48}^E C_2^P$ should be preceded with Tyr-Val, and the N-terminal residues Leu-Glu-Lys-Arg-Glu-Ala-Glu-Ala in the $T_9 C_4^R T_9$ sequence should be removed. The protein polymer $T_9^* C_4^R T_9^*$ has the same middle block, but scrambled T_9 blocks that cannot self-assemble, while polymer C_4^R lacks the T_9 blocks altogether. Fed-batch fermentations were performed in 2.5 L Bioflo 3000 bioreactors (New Brunswick Scientific) according to the procedures described previously.[12,33] The protein block copolymers were purified from the fermentation broth by several ammonium sulfate precipitation steps and subsequent desalting and lyophilisation.[12,33]

2.2.2 Methods

Sample preparation

All the samples were prepared in the same way. A 10 g.L^{-1} stock solution of $C_2^P S_{48}^E C_2^P$ was prepared by dissolving a given amount of protein in 0.01 M sodium hydroxide and stored at -20 °C (final pH of the solution was around 10). The concentration of $C_2^P S_{48}^E C_2^P$ was fixed at 0.14 mM (9.2 g.L^{-1}) for all experiments. Subsequently, a chosen amount of $T_9 C_4^R T_9$ was added to the $C_2^P S_{48}^E C_2^P$ solution and dissolved by heating the solution for one hour at 50 °C in a water bath. For $T_9 C_4^R T_9$ a concentration range of 0.1 mM to 2.2 mM (4.2-91.7 g.L^{-1}) was investigated. Prior to rheological analysis, the pH of the solution was lowered to 2.0 in order to induce $C_2^P S_{48}^E C_2^P$ network formation by adding 1.0 M hydrochloric acid. The same method was used to prepare mixtures of $C_2^P S_{48}^E C_2^P$ and C_4^R and $T_9^* C_4^R T_9^*$.

Rheology

Rheological measurements were performed with an Anton Paar Physica MCR 301 rheometer equipped with a Couette geometry with a volume of 1 mL. A solvent trap was used to minimize the effects of evaporation.

24

The temperature was controlled by a Peltier element. All the rheological measurements were carried out in duplicate, unless mentioned otherwise, at 20 °C and pH 2.0. Gel formation was followed by applying an oscillatory deformation (f=1 Hz and γ=0.1%) for 15 hours, whereby the storage (G') and loss moduli (G'') were measured. Subsequently, a strain sweep (f=1 Hz and γ=0.01-1% was conducted in order to ensure that all measurements were done in the linear regime. Thereafter, viscoelastic behaviour of the steady state gel was characterised by a frequency sweep (ω=0.01-100 rad.s^{-1} and γ=0.1%). Finally, the nonlinear behaviour of the gel was evaluated by applying a constant strain rate ($\dot{\gamma}$=0.1 s^{-1}) until the gel ruptured.

Cryo transmission electron microscopy (Cryo-TEM)

Samples for Cryo-TEM were prepared by depositing a 5 mL aliquot of the induced protein solutions onto a copper grid (Quantifoil 3.5/1 400 mesh), previously glow-discharged under low pressure. After deposition, all the samples were blotted with an automated system in a controlled environment (Vitrobot, FEI) for at least 10 seconds to remove excess liquid from the copper grids to form a thin sample layer. Afterward, the samples were plunged into liquid ethane by the vitrobot and transferred to a Gatan model 626 cryo-stage precooled to -175 °C with liquid nitrogen. Imaging was carried out at 120 kV on a Philips CM12 transmission electron microscope, and images were recorded under low-dose conditions on a slow-scan CCD camera (Gatan, model 794). During imaging, the temperature of the sample holder was kept at -175 °C by liquid nitrogen to prevent crystal formation of vitrified water. The thickness of the fibrils was measured by drawing a perpendicular line on the structures in ImageJ. To prevent biased results, a nine segment grid was introduced to the images, where in each of the four outer extremes and in the middle segments, 20 measurements were done.

2.3   Results and Discussion

2.3.1   Single networks

Before discussing the composite networks consisting of $\mathbf{C_2^P S_{48}^E C_2^P}/\mathbf{T_9 C_4^R T_9}$ combinations, we first consider the single-component networks of $\mathbf{C_2^P S_{48}^E C_2^P}$ and $\mathbf{T_9 C_4^R T_9}$, respectively. Figure 2.1 presents the network formation of 0.14 mM $\mathbf{C_2^P S_{48}^E C_2^P}$ and 1.0 mM $\mathbf{T_9 C_4^R T_9}$ single networks as a function of time at various pH values. No increase in modulus above the detection limit of the rheometer could be measured for $\mathbf{C_2^P S_{48}^E C_2^P}$ at pH 5,
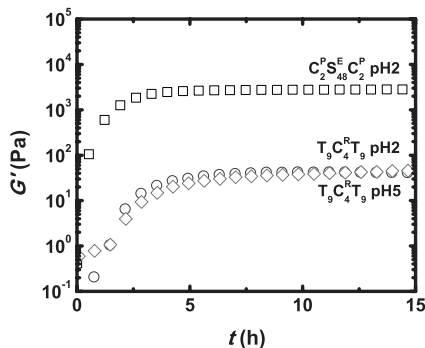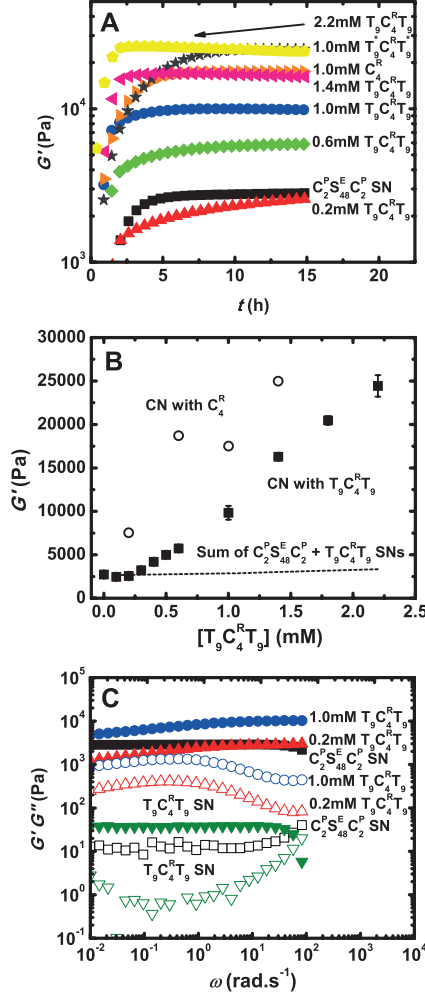
Figure 2.1: *Storage moduli (G') of single networks of 0.14 mM $C_2^P S_{48}^E C_2^P$ at pH 2 (squares), and 1.0 mM $T_9 C_4^R T_9$ at pH 2 (diamonds), and 5 (circles) as a function of time (f=1 Hz, γ=0.1% and T=20°C).*

where the negative charge of the S_{48}^E block (due to its glutamic acid residues) prevents self-assembly. However, when the pH is lowered to 2, which is below the p*Ka* of glutamic acid, $C_2^P S_{48}^E C_2^P$ forms a gel in a few hours with a final modulus of approximately 2.5 kPa. As shown previously,[33] this gelation is due to the formation of long, semi-flexible protein fibrils. The gelation of the collagen-like block copolymers ($T_9 C_4^R T_9$) depends only on temperature and not on the pH. Upon cooling to 20°C, $T_9 C_4^R T_9$ forms a soft gel within 5–10 hours. The final storage modulus of the $T_9 C_4^R T_9$ gel is approximately 50 Pa at a concentration of 1.0 mM. As shown previously,[36] it increases to approximately 500 Pa as the concentration increases to 2 mM. The rheological properties of two variants of $T_9 C_4^R T_9$ that lack the self-assembling T_9 blocks, $T_9^* C_4^R T_9^*$ and C_4^R, have been determined as well. Neither of these molecules show a significant modulus at any pH or temperature, indicating that these variants do not form gels, as expected.

2.3.2   Linear rheology of composite networks

Figure 2.2A displays the network formation of composite networks of 0.14 mM $C_2^P S_{48}^E C_2^P$ with varying concentrations of $T_9 C_4^R T_9$ as a function of time. Clearly, the modulus reaches higher values for the composite networks (CN) than for the single $C_2^P S_{48}^E C_2^P$ network. In Figure 2.2B average steady state storage moduli (values after 15 hours) are displayed as a function of the $T_9 C_4^R T_9$ concentration. In comparison with the single networks of either $C_2^P S_{48}^E C_2^P$ or $T_9 C_4^R T_9$, the $C_2^P S_{48}^E C_2^P / T_9 C_4^R T_9$

composite networks show significantly higher storage moduli. With increasing $T_9C_4^RT_9$ concentration, the modulus increases strongly and at 2.2 mM $T_9C_4^RT_9$ it is about an order of magnitude higher than that of the single $C_2^PS_{48}^EC_2^P$ network. The plateau storage modulus of the composite network (25 kPa) is much higher than the sum of the moduli of the two individual networks (2.8 kPa and 0.045 kPa, respectively). This indicates that combination of the two networks leads to a strong reinforcement. Figure 2.2C shows frequency-dependent storage and loss moduli for both single and composite networks. In all cases, the storage modulus exceeds the loss modulus. Whereas the storage modulus for the single networks is almost independent of frequency, it increases weakly with frequency for the composite networks at frequencies between 0.1 and 10 rad.s^{-1}. The loss modulus has a maximum in this frequency range. This indicates the presence of additional relaxation modes in the composite networks. However, in all networks the storage modulus goes to a plateau both at high and at low frequencies. Hence, all the networks can be considered as predominantly elastic gels. The increase of the modulus upon adding $T_9C_4^RT_9$ occurs at a concentration of approximately 0.3 mM (Figure 2.2B), which is roughly a factor of two lower than the concentration at which $T_9C_4^RT_9$ can make a percolated network.[36] This suggests that network formation of $T_9C_4^RT_9$ is not necessary for enhancing the modulus. To investigate this further, we carry out control experiments with the two variants of $T_9C_4^RT_9$ that cannot form a network, $T_9^*C_4^RT_9^*$ and C_4^R. Figure 2.2A shows the modulus as a function of time of composite networks of $C_2^PS_{48}^EC_2^P$ and these non-gelling polymers. Interestingly, these control samples show an even higher modulus than the $C_2^PS_{48}^EC_2^P/T_9C_4^RT_9$ CNs. As shown in Figure 2.2B (open symbols), the increase in modulus with varying concentration of C_4^R exceeds that of the $C_2^PS_{48}^EC_2^P/T_9C_4^RT_9$ composite network. Clearly, the enhanced modulus does not rely on the presence of a second network. This suggests that the presence of a second polymer leads to structural changes in the $C_2^PS_{48}^EC_2^P$ network.

Figure 2.2: *(A) Storage moduli (G′) of single networks (SNs) and composite networks (CNs) as a function of time (f=1 Hz, γ=0.1% and T=20°C). [$C_2^P S_{48}^E C_2^P$]=0.14 mM for all experiments. [$T_9 C_4^R T_9$], [C_4^R] and [$T_9^* C_4^R T_9^*$] varied as indicated. (B) Average plateau storage moduli (G′) of $C_2^P S_{48}^E C_2^P / T_9 C_4^R T_9$ CNs as a function of $T_9 C_4^R T_9$ concentration (closed squares) and storage moduli of $C_2^P S_{48}^E C_2^P / C_4^R$ CNs as a function of C_4^R concentration (open circles). The dashed line represents the sum of the moduli of the separate $C_2^P S_{48}^E C_2^P$ and $T_9 C_4^R T_9$ networks. (C) Frequency sweeps of $C_2^P S_{48}^E C_2^P$ and $T_9 C_4^R T_9$ SNs and $C_2^P S_{48}^E C_2^P / T_9 C_4^R T_9$ CNs. Storage moduli (G′, closed symbols) and loss moduli (G″, open symbols) are shown. [$C_2^P S_{48}^E C_2^P$]=0.14 mM for all experiments; [$T_9 C_4^R T_9$] is varied as indicated.*

2.3.3 Cryo-TEM

To investigate the structure of the single and composite networks, we carried out cryo-TEM experiments. This proved to be very difficult at the concentrations at which rheological measurements were done; no images of sufficient quality could be obtained, because the samples were overcrowded. Therefore, the measurements were done at lower $C_2^P S_{48}^E C_2^P$ concentrations (1.4 mM). Although the structure of the composite network is likely to be different at this lower fiber concentration, we assume that the effect of adding $T_9 C_4^R T_9$ on the morphology of the fibers is at least qualitatively the same as at the concentration used in the rheology experiments. Representative cryo-TEM images of $C_2^P S_{48}^E C_2^P$ SNs and $C_2^P S_{48}^E C_2^P / T_9 C_4^R T_9$ CNs at different magnifications are presented in Figure 2.3.
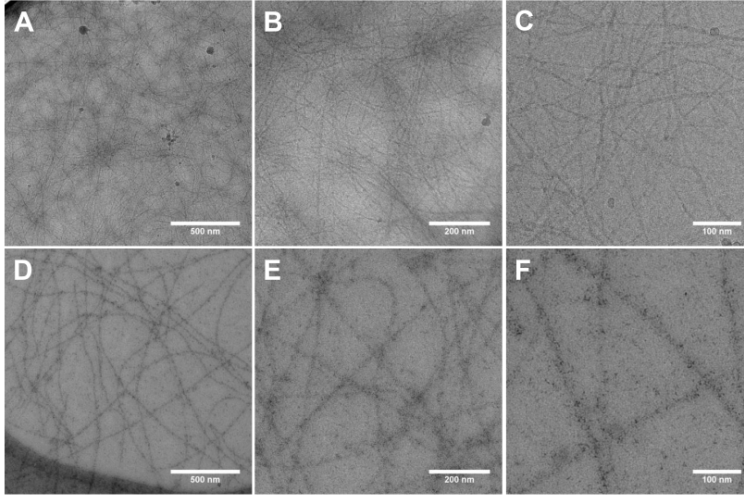
Figure 2.3: *(A-C) Cryo-TEM images of* $C_2^P S_{48}^E C_2^P$ *SNs (0.1 g.L^{-1}); (D-F) Cryo-TEM images of* $C_2^P S_{48}^E C_2^P / T_9 C_4^R T_9$ *CNs 0.1 g.L^{-1}* $C_2^P S_{48}^E C_2^P$ *and 1.0 mM* $T_9 C_4^R T_9$. *Magnifications 14,000X, the scalebar indicates 500 nm (A and D); 30,800X, the scalebar indicates 200 nm (B and E); and 49,000X, the scalebar indicates 100 nm (C and F).*

It can be observed that the fibers in the $C_2^P S_{48}^E C_2^P$ single network (Figure 2.3A-C) are much thinner than the fibers in the composite network

(Figure 2.3D-F). Image analysis of cryo-TEM pictures gives an average diameter of 10.4 nm ± 2.0 nm for the single networks, which is in accordance with earlier findings based on X-ray scattering and with model predictions.[13] However, in the composite networks the average diameter is 27.5 nm ± 4.7 nm, which is significantly larger and indicates that the fibers organize in bundles. Probably, this bundling is caused by depletion attraction[39,40] between the $C_2^P S_{48}^E C_2^P$ fibers induced by the second polymer. A similar bundling has been reported earlier for protein-polysacharide[41] systems and polymer-protein systems.[42] The increase in the diameter of the bundles makes the bending of the fibers more difficult. This explains the strong increase in modulus observed in our experiments.[42,43] It also explains why the non-gelling control molecules show an even larger increase in modulus than $T_9 C_4^R T_9$: depletion-induced bundling is probably more effective in a polymer solution than in a gel. This can be explained by the following effects: (1) the osmotic pressure, which is the main driving force for depletion bundling, is lower in a gel and (2) the gel may obstruct bundling due to kinetic hindrance.

2.3.4   Nonlinear rheology and yielding of composite networks

To see whether the composite structure of the networks has an effect on their strength and toughness, we study the nonlinear mechanical response of the samples. The networks are deformed at a constant shear rate ($\dot{\gamma}$=0.1 s^{-1}) and the stress (σ) is monitored as a function of time. Figure 2.4A shows the response of both single and composite networks. The $C_2^P S_{48}^E C_2^P$ single network strain hardens significantly before yielding at a strain of approximately 10%. This is in agreement with previous findings for this polymer[33] and for other filamentous networks.[34] Two explanations have been given for strain hardening in such systems: (1) a nonlinear entropy reduction upon filament stretching as transverse conformation fluctuations are pulled out[34] or (2) a transition from a non-affine bending-dominated response at small strains to a more affine stretching-dominated response at higher strains.[44] The $C_2^P S_{48}^E C_2^P / T_9 C_4^R T_9$ composite network can be deformed approximately two times more than the single $C_2^P S_{48}^E C_2^P$ network and breaks at a stress that is almost two times higher. Hence, the composite network is much tougher than the single $C_2^P S_{48}^E C_2^P$ network. Figure 2.4B shows that with increasing $T_9 C_4^R T_9$ concentration, the critical strain at which the composite network ruptures gradually shifts to higher values (note that the stress is normalized to the plateau modulus in this figure). Moreover, the strain hardening behaviour

of the composite network disappears at high $T_9C_4^RT_9$ concentrations, and a more ductile behaviour is observed. Interestingly, the addition of the non-assembling variants $T_9^*C_4^RT_9^*$ and C_4^R results in completely opposite behaviour. These networks break at a strain of approximately 4%, two times lower than the single $C_2^PS_{48}^EC_2^P$ network, and at a much smaller stress.
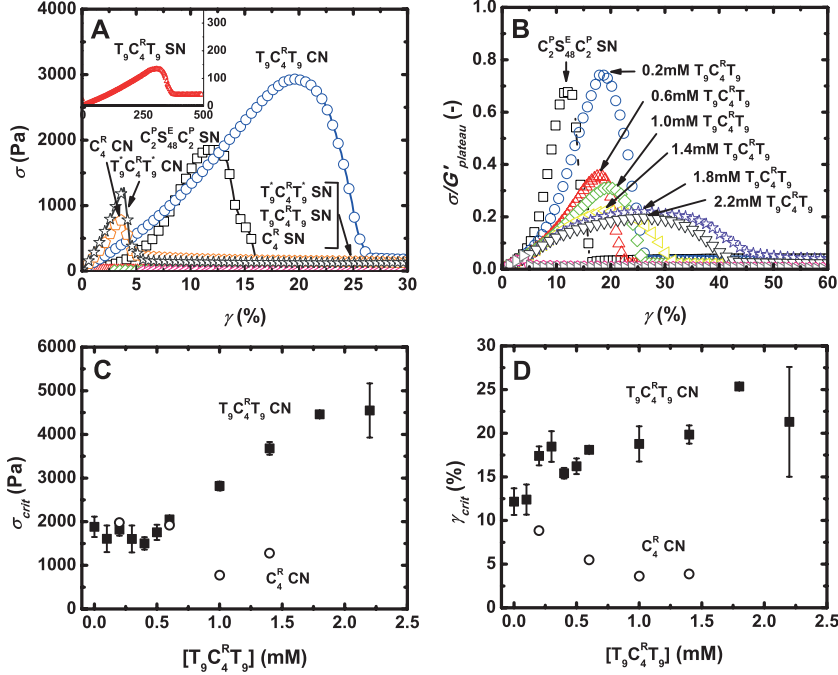
Figure 2.4: *(A) Stress response of the $C_2^PS_{48}^EC_2^P$ single network (SN) and of composite networks (CNs) with $T_9C_4^RT_9$, $T_9^*C_4^RT_9^*$, and C_4^R after applying a constant strain rate of ($\dot{\gamma}$=0.1 s^{-1}). [$C_2^PS_{48}^EC_2^P$]=0.14 mM for the $C_2^PS_{48}^EC_2^P$ SN and all CNs. [$T_9C_4^RT_9$], [C_4^R] and [$T_9^*C_4^RT_9^*$] are 1.0 mM. The inset shows the response of the $T_9C_4^RT_9$ SN (which is much softer and breaks at much lower stresses). (B) Stress response normalized by the plateau modulus after applying a constant strain rate of ($\dot{\gamma}$=0.1 s^{-1}) to $C_2^PS_{48}^EC_2^P$ SN and CNs; [$C_2^PS_{48}^EC_2^P$]=0.14 mM for $C_2^PS_{48}^EC_2^P$ SN and all CNs; [$T_9C_4^RT_9$], [C_4^R], and [$T_9^*C_4^RT_9^*$] varied as indicated. (C) Critical stress (σ_{crit}) of $C_2^PS_{48}^EC_2^P/T_9C_4^RT_9$ CNs as a function of $T_9C_4^RT_9$ concentration (closed squares) and of $C_2^PS_{48}^EC_2^P/C_4^R$ CNs as a function of C_4^R concentration (open circles); (D) critical strain (γ_{crit}) of $C_2^PS_{48}^EC_2^P/T_9C_4^RT_9$ CNs as a function of $T_9C_4^RT_9$ concentration (closed squares) and of $C_2^PS_{48}^EC_2^P/C_4^R$ CNs as a function of C_4^R concentration (open circles). pH=2 and T=20°C in all experiments.*

31

Figure 2.4C and D show the effect of $T_9C_4^RT_9$ and C_4^R on the critical strain and stress at rupture, respectively. It is clear from these results that strengthening of the composite networks is not caused by bundle formation that causes the enhanced elastic modulus: the $T_9^*C_4^RT_9^*$ and C_4^R molecules give an even stronger increase in modulus, yet the rupture strength of these composite networks has decreased compared to the single $C_2^PS_{48}^EC_2^P$ network. We conclude from this that the enhanced rupture strength of the $C_2^PS_{48}^EC_2^P/T_9C_4^RT_9$ composite network relies on the ability of $T_9C_4^RT_9$ to form a network by itself. A similar synergistic strengthening was observed recently for double network hydrogels consisting of two interpenetrating polymer networks.[24,25] The enhanced strength of these systems was attributed to a local yielding mechanism that leads to effective energy dissipation;[15] deformation of the double network leads to local rupture of the most brittle of the two networks, while the second, more ductile network bridges the damaged zones and maintains the overall integrity of the gel. A similar mechanism might explain the enhanced strength of the $C_2^PS_{48}^EC_2^P/T_9C_4^RT_9$ composite networks discussed here. The $C_2^PS_{48}^EC_2^P$ network is the brittle component that breaks locally at small strains, while the $T_9C_4^RT_9$ network is the ductile component, which bridges cracks in the $C_2^PS_{48}^EC_2^P$ network, and effectively redistributes stresses more homogeneously, making the composite network more ductile. Note that the $T_9C_4^RT_9$ network can indeed stand very large deformations without rupturing (see the inset of Figure 2.4A). This mechanism is illustrated in Figure 2.5. Local ruptures of the $C_2^PS_{48}^EC_2^P$ network might also hide the strain hardening effect in the composite networks, observed in Figure 2.4B. Another possible effect of the $T_9C_4^RT_9$ network is that it makes the deformation of the $C_2^PS_{48}^EC_2^P$ network more affine. Observations on microtubules in actin gels indicate that non-affine bending modes of filaments are suppressed in an elastic matrix.[45] This would also mean that an enthalpic strain hardening mechanism, caused by a transition from non-affine to affine deformation,[44] is less likely to occur. Moreover, the more homogeneous distribution of stresses in an affinely deformed material would slow down the nucleation and propagation of cracks.
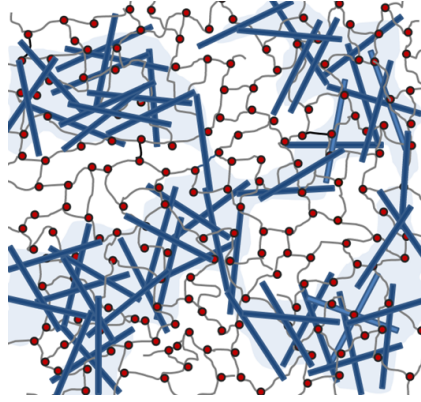
Figure 2.5: *Schematic representation of the composite network and a possible toughening mechanism. $C_2^P S_{48}^E C_2^P$ fibrils (blue rods) form a network with local cracks or defects; the $T_9 C_4^R T_9$ network (red circles represent trimeric nodes, gray lines represent C_4^R middle-blocks) in the background bridges these defects, resulting in a more homogeneous distribution of stresses and a more affine deformation.*

2.4   Conclusions

This study set out to determine the mechanical and structural properties of composite networks formed by silk-like ($C_2^P S_{48}^E C_2^P$) and collagen-like ($T_9 C_4^R T_9$) block copolymers. Composite networks of these block copolymers proved to exhibit interesting mechanical properties that exceed the contributions of the individual networks. The elastic modulus is mainly determined by the fibrillar $C_2^P S_{48}^E C_2^P$ network, but the presence of the much softer $T_9 C_4^R T_9$ polymer increases the modulus by an order of magnitude. This was shown to be due to bundling of the $C_2^P S_{48}^E C_2^P$ fibrils. In addition, a significant increase in network strength was found upon adding the $T_9 C_4^R T_9$ network. The origin of this effect is not completely clear, but a comparison to other, recently reported, tough hydrogels suggests that the ductile $T_9 C_4^R T_9$ network may be able to bridge cracks or inhomogeneities in the fibrillar network, resulting in a delocalization of the stress and a more affine deformation. We hope that this work may encourage further research on fundamental issues of fracture in soft materials and on the design of tough bio-inspired materials.

References

(1) Kopeček, J.; Yang, J. *Polym. Int.* **2007**, *56*, 1078–1098.

(2) Sallach, R. E.; Cui, W.; Balderrama, F.; Martinez, A. W.; Wen, J.; Haller, C. A.; Taylor, J. V.; Wright, E. R.; Long, R. C.; Chaikof, E. L. *Biomaterials* **2010**, *31*, 779–791.

(3) Hoffman, A. S. *Adv. Drug Delivery Rev.* **2002**, *54*, 3–12.

(4) Langer, R.; Tirrell, D. A. *Nature* **2004**, *428*, 487–492.

(5) Peppas, N. A.; Hilt, J. Z.; Khademhosseini, A.; Langer, R. *Adv. Mater.* **2006**, *18*, 1345.

(6) Reches, M.; Gazit, E. *Science* **2003**, *300*, 625–627.

(7) Hirschberg, J. H. K. K.; Brunsveld, L.; Ramzi, A.; Vekemans, J. A. J. M.; Sijbesma, R. P.; Meijer, E. W. *Nature* **2000**, *407*, 167–170.

(8) Ikada, Y.; Jamshidi, K.; Tsuji, H.; Hyon, S. H. *Macromolecules* **1987**, *20*, 904–906.

(9) De Jong, S. J.; De Smedt, S. C.; Demeester, J.; Van Nostrum, C. F.; Kettenes-Van Den Bosch, J. J.; Hennink, W. E. *J. Controlled Release* **2001**, *72*, 47–56.

(10) Jeong, B.; Gutowska, A. *Trends Biotechnol.* **2002**, *20*, 305–311.

(11) Ulijn, R. V.; Smith, A. M. *Chem. Soc. Rev.* **2008**, *37*, 664–675.

(12) Werten, M. W. T.; Teles, H.; Moers, A. P. H. A.; Wolbert, E. J. H.; Sprakel, J.; Eggink, G.; de Wolf, F. A. *Biomacromolecules* **2009**, *10*, 1106–1113.

(13) Martens, A. A.; Portale, G.; Werten, M. W. T.; de Vries, R. J.; Eggink, G.; Cohen Stuart, M. A.; de Wolf, F. A. *Macromolecules* **2009**, *42*, 1002–1009.

(14) Petka, W. A.; Harden, J. L.; McGrath, K. P.; Wirtz, D.; Tirrell, D. A. *Science* **1998**, *281*, 389–392.

(15) Gong, J. P. *Soft Matter* **2010**, *6*, 2583–2590.

(16) Kim, B. S.; Mooney, D. J. *Trends Biotechnol.* **1998**, *16*, 224–230.

(17) Lin, Y.-C.; Yao, N. Y.; Broedersz, C. P.; Herrmann, H.; MacKintosh, F. C.; Weitz, D. A. *Phys. Rev. Lett.* **2010**, *104*, 058101.

(18) Lemmers, M.; Spruijt, E.; Akerboom, S.; Voets, I. K.; van Aelst, A. C.; Cohen Stuart, M. A.; van der Gucht, J. *Langmuir* **2012**, *28*, 12311–12318.

(19) Haraguchi, K.; Li, H.-J. *Macromolecules* **2006**, *39*, 1898–1905.

(20) Zhou, C.; Wu, Q.; Zhang, Q. *Colloid Polymer Sci.* **2011**, *289*, 247–255.

(21) Capadona, J. R.; Shanmuganathan, K.; Tyler, D. J.; Rowan, S. J.; Weder, C. *Science* **2008**, *319*, 1370–1374.

(22) Jiao, Y.; Gyawali, D.; Stark, J. M.; Akcora, P.; Nair, P.; Tran, R. T.; Yang, J. *Soft matter* **2012**, *8*, 1499–1507.

(23) Dinu, M. V.; Schwarz, S.; Dinu, I. A.; Drăgan, E. S. *Colloid Polymer Sci.* **2012**, *290*, 1647–1657.

(24) Gong, J. P.; Katsuyama, Y.; Kurokawa, T.; Osada, Y. *Adv. Mater.* **2003**, *15*, 1155–1158.

(25) Sun, J. Y.; Zhao, X.; Illeperuma, W. R. K.; Chaudhuri, O.; Oh, K. H.; Mooney, D. J.; Vlassak, J. J.; Suo, Z. *Nature* **2012**, *489*, 133–136.

(26) Tako, M.; Teruya, T.; Tamaki, Y.; Ohkawa, K. *Colloid Polymer Sci.* **2010**, *288*, 1161–1166.

(27) Hyland, L. L.; Taraban, M. B.; Feng, Y.; Hammouda, B.; Yu, Y. B. *Biopolymers* **2012**, *97*, 177–188.

(28) Werten, M. W. T.; Wisselink, W. H.; Jansen-van den Bosch, T. J.; de Bruin, E. C.; de Wolf, F. A. *Protein Eng.* **2001**, *14*, 447–454.

(29) Xu, C.; Breedveld, V.; Kopecek, J. *Biomacromolecules* **2005**, *6*, 1739–1749.

(30) Huang, J.; Foo, C. W. P.; Kaplan, D. L. *J. Macromol. Sci.*, *Polym. Rev.* **2007**, *47*, 29–62.

(31) Krejchi, M. T.; Cooper, S. J.; Deguchi, Y.; Atkins, E. D. T.; Fournier, M. J.; Mason, T. L.; Tirrell, D. A. *Macromolecules* **1997**, *30*, 5012–5024.

(32) Parkhe, A. D.; Cooper, S. J.; Atkins, E. D. T.; Fournier, M. J.; Mason, T. L.; Tirrell, D. A. *Int. J. Biol. Macromol.* **1998**, *23*, 251–258.

(33) Martens, A. A.; van der Gucht, J.; Eggink, G.; de Wolf, F. A.; Cohen Stuart, M. A. *Soft Matter* **2009**, *5*, 4191–4197.

(34) Storm, C.; Pastore, J. J.; MacKintosh, F. C.; Lubensky, T. C.; Janmey, P. A. *Nature* **2005**, *435*, 191–194.

(35) Lin, Y.-C.; Koenderink, G. H.; MacKintosh, F. C.; Weitz, D. A. *Soft Matter* **2011**, *7*, 902–906.

(36) Skrzeszewska, P. J.; de Wolf, F. A.; Werten, M. W. T.; Moers, A. P. H. A.; Cohen Stuart, M. A.; van der Gucht, J. *Soft Matter* **2009**, *5*, 2057–2062.

(37) Skrzeszewska, P. J.; de Wolf, F. A.; Stuart, M. A. C.; van der Gucht, J. *Soft Matter* **2010**, *6*, 416–422.

(38) Silva, C. I. F.; Teles, H.; Moers, A. P. H. A.; Eggink, G.; de Wolf, F. A.; Werten, M. W. T. *Biotechnol. Bioeng.* **2011**, *108*, 2517–2525.

(39) Asakura, S.; Oosawa, F. *J. Polymer Sci.* **1958**, *33*, 183–192.

(40) Marenduzzo, D.; Finan, K.; Cook, P. R. *J. Cell Biol.* **2006**, *175*, 681–686.

(41) Doublier, J.-L.; Garnier, C.; Renard, D.; Sanchez, C. *Curr. Opin. Colloid Interface Sci.* **2000**, *5*, 202–214.

(42) Tharmann, R.; Claessens, M. M. A. E.; Bausch, A. R. *Biophys. J.* **2006**, *90*, 2622–2627.

(43) Gardel, M. L.; Shin, J. H.; MacKintosh, F. C.; Mahadevan, L.; Matsu-daira, P.; Weitz, D. A. *Science* **2004**, *304*, 1301–1305.

(44) Onck, P.; Koeman, T.; Van Dillen, T.; Van der Giessen, E. *Phys. Rev. Lett.* **2005**, *95*, 178102.

(45) Brangwynne, C. P.; MacKintosh, F. C.; Kumar, S.; Geisse, N. A.; Talbot, J.; Mahadevan, L.; Parker, K. K.; Ingber, D. E.; Weitz, D. A. *J. Cell Biol.* **2006**, *173*, 733–741.

Breaking and Self-Healing of Composite Hydrogels Formed by Silk-like and Collagen-like Block Copolymers

Abstract

In this chapter we present a self-assembled composite network that consists of silk-like fibers embedded in a soft collagen-like network. We find that the rupture strength of this composite network is significantly enhanced compared to the individual networks. From repeated loading/unloading cycles we show that this increase is related to mechanical hysteresis. The energy that is dissipated has two contributions: one due to permanent damage, which we ascribe to irreversible rupture of the silk-like fibers, and one due to viscoelastic dissipation, which we attribute to the disruption and reformation of triple helices in the collagen-like network. Both contributions increase strongly upon increasing the concentration of the collagen-like polymer. Moreover, the self-healing capacity of the collagen-like network imparts a partial healing to the composite network, which can recover up to 70% of the original elastic modulus after complete failure. Our results thus show that fiber networks can be toughened very effectively by embedding them in a soft viscoelastic matrix.

3.1 Introduction

Functional hydrogels have attracted significant attention in the last decade, mainly because of their potential use in biomedical applications, such as drug delivery or tissue engineering.[1–6] In many of these applications, control over the mechanical properties of the hydrogels is crucial. Most hydrogels are soft and fragile, however recent progress in polymer science has led to the development of new types of hydrogels with strongly enhanced fracture strength. In particular, double network hydrogels consisting of two interpenetrating networks swollen in water, have caught the attention.[7–9] Such double network gels were found to be remarkably tough, with a fracture energy that is comparable to that of natural materials, such as cartilage or skin. Theoretical work suggests that this toughening is caused by additional dissipation mechanisms in the mixed gels, where the most ductile of the two networks effectively redistributes stresses over a large zone around the crack tip, leading to an increase of the dissipative zone and a concomitant increase of the fracture energy.[10] Indeed, the enhancement in toughness appears to be correlated with a large mechanical hysteresis in loading/unloading experiments, which is a signature of large energy dissipation. Since the toughening relies on the irreversible rupture of bonds in the first, 'sacrificial' network, covalently linked double networks typically are not very resistant to repeated loading. This drawback can be alleviated by taking a self-healing network as one of the components, for example by using physical crosslinks rather than covalent ones.[8,9]

Most synthetic double networks that have been described consist of two flexible polymer networks, often with one of the two components carrying charges. This is in contrast to the tough materials found in nature, which usually consist of semi-flexible fibers embedded in a soft matrix.[11] Cartilage and connective tissue, for example, consist of rigid collagen fibers that are dispersed in a complex matrix of more flexible polymers.[12,13] The advantage of fibers over flexible polymers is that they can already produce elastic gels at very low volume fractions and that they are often strain hardening.[14,15] However, their rigidity usually comes at the price of a reduced fracture strength: most fiber gels are very fragile and break already at a few percent strain.[16] Moreover, recombination of broken fibers is extremely slow, therefore fiber gels cannot heal after fracture. The question therefore arises how natural fiber-based materials combine rigidity with high toughness and self-healing, and whether similar strategies can be followed for the design of synthetic fiber-based materials with high toughness.

38

Recently, we showed that it is indeed possible to toughen synthetic fiber gels by embedding the fibers in a soft elastic gel matrix.[17,18] Our composite hydrogel consisted of silk-like fibers, dispersed in a collagen-like physical hydrogel. Both components were formed by self-assembly of bio-inspired block copolymers. The fiber-forming component, $C_2^P S_{48}^E C_2^P$, consists of a silk-like middle block S_{48}^E, and two hydrophilic random-coil blocks C_2^P. The silk-like block contains 48 (Gly-Ala)$_3$-Gly-Glu repeats and can self-assemble into long semi-flexible fibers, when the glutamic acid residues are protonated at pH values below 4.1 (Figure 3.1A).
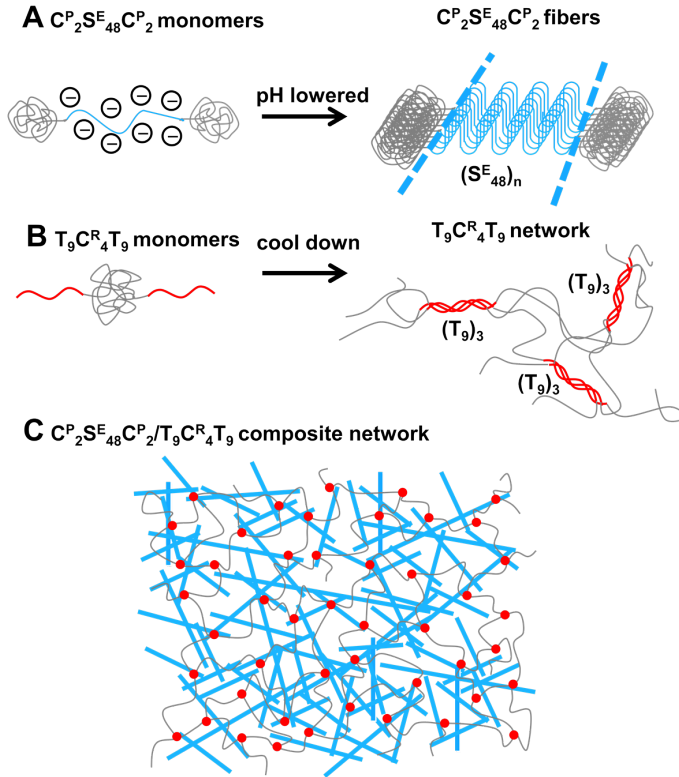
Figure 3.1: *Formation of $C_2^P S_{48}^E C_2^P / T_9 C_4^R T_9$ composite network (CN). (A) Self-assembly of S_{48}^E blocks of $C_2^P S_{48}^E C_2^P$ into fibers upon lowering the pH. (B) Self-assembly of T_9 blocks of $T_9 C_4^R T_9$ into triple helical nodes, $(T_9)_3$, upon lowering the temperature. (C) $C_2^P S_{48}^E C_2^P / T_9 C_4^R T_9$ CN, where the $C_2^P S_{48}^E C_2^P$ fibers are represented by the blue rods, the triple helical nodes formed by $T_9 C_4^R T_9$ by the red circles and the random-coil blocks by the grey lines.*

These fibers have a thickness of a few nanometers and a persistence length of several micrometers, and they are stabilized by a hydrophilic corona formed by the C_2^P blocks. The second polymer, $T_9C_4^RT_9$, consists of a hydrophilic C_4^R block (which has exactly the same composition as the C_2^P blocks, and twice their length), flanked by two self-assembling collagen-like blocks T_9. These T_9 blocks consist of nine Pro-Gly-Pro repeats, and can form triple helices at low temperature, leading to the formation of a soft polymer network with triple helices as the nodes (Figure 3.1B). We observed that the combination of these two networks yielded composite hydrogels that fractured at a strain that is up to a factor of two higher than that of the single fiber networks (Figure 3.1C). We hypothesized that this toughening was due to an increase of the dissipated energy, by a mechanism that is similar to the one used to explain the toughening of flexible double networks. In this chapter, we present evidence to support this hypothesis, by measuring the dissipated energy upon deformation and fracture. We also study whether the $T_9C_4^RT_9$ network, which is intrinsically self-healing, can induce (partial) healing to the composite gels.

3.2 Experimental Section

3.2.1 Materials

The protein polymers $C_2^PS_{48}^EC_2^P$ and $T_9C_4^RT_9$ were produced biosynthetically in the yeast *Pichia pastoris*, and purified as reported previously,[19,20] and the amino acid sequences of these proteins can be found in GenBank under accession numbers ABW84222 and ACF33479, respectively. To obtain the complete amino acid sequence of the mature proteins from these GenBank records, the sequence of $C_2^PS_{48}^EC_2^P$ should be preceded with Tyr-Val, and the N-terminal residues Leu-Glu-Lys-Arg-Glu-Ala-Glu-Ala in the $T_9C_4^RT_9$ sequence should be removed. Fed-batch fermentations were performed in 2.5 L Bioflo 3000 bioreactors (New Brunswick Scientic) according to the procedures described previously.[19,20] The protein block copolymers were purified from the fermentation broth by several ammonium sulfate precipitation steps and subsequent desalting and lyophilisation.

3.2.2 Methods

Sample preparation

To prepare the $C_2^P S_{48}^E C_2^P / T_9 C_4^R T_9$ hydrogels, a given amount of undissolved $T_9 C_4^R T_9$ was added to a 10 g.L^{-1} $C_2^P S_{48}^E C_2^P$ solution in 10 mM sodium hydroxide. The $T_9 C_4^R T_9$ was dissolved by heating the solution at 50 °C for 1 hour. Subsequently, the pH was lowered to 2.0 by adding 1.0 M hydrochloric acid to the solution. The final concentration of $C_2^P S_{48}^E C_2^P$ in the samples was fixed at 0.14 mM (0.92% (w/v)), and the concentration of $T_9 C_4^R T_9$ was varied between 0.20 and 2.60 mM (0.83-10.8% (w/v)). The temperature was kept at 20 °C for all experiments.

Rheology

Rheological measurements were performed with an Anton Paar Physica MCR 501 rheometer equipped with a Couette geometry (1 mL). A solvent trap was used to minimize the effects of evaporation. The temperature was controlled by a Peltier element. Samples were allowed to form a gel *in situ*. A time sweep was recorded to follow in-situ gel formation (f=1 Hz, and γ=0.1%), whereby the storage G' and loss moduli G'' were measured for 8 hours. After steady state was reached, the hydrogels were either subjected to recovery tests or hysteresis tests. For the hysteresis tests, the hydrogels were subjected to 11 loading/unloading cycles, in which the strain was increased with steps of 4% from 0 to 44%, at a constant strain rate $\dot{\gamma}$=0.1 s^{-1}. After each loading/unloading cycle there was a 30 minute rest period before the next cycle was initiated. For the recovery tests, shear deformation with a loading and unloading step was applied to the hydrogels until the gel fractured. Afterward, the recovery of the storage modulus was followed for 8 hours (f=1 Hz, and γ=0.1 %).

3.3 Results and Discussion

3.3.1 Fracture

To study the effect of the soft background gel on the fracture properties of the fiber network, we vary the concentration of the collagen-inspired polymer $T_9 C_4^R T_9$, while keeping the concentration of the silk-like polymer, $C_2^P S_{48}^E C_2^P$, constant. As shown previously, the modulus of the single network of $C_2^P S_{48}^E C_2^P$ fibers at the concentration employed here is 2.5 kPa, which is much larger than that of the single network of $T_9 C_4^R T_9$, which

varies between 0 and 0.5 kPa in the concentration range that we used. Hence, the background network is indeed much softer than the fiber network. To study the mechanical properties of the mixed gels, we apply a series of loading/unloading cycles in the rheometer. After each cycle, we let the sample rest for 30 minutes before continuing with the next cycle. The maximum strain increases with each cycle. The measured stress is plotted as a function of the strain in Figure 3.2 for a number of cycles and for samples with different concentrations of $\mathbf{T_9C_4^RT_9}$. For clarity, only the loading parts of the cycles are shown. Figure 3.3 shows several complete loading/unloading cycles for a representative sample. More data for other concentrations of $\mathbf{T_9C_4^RT_9}$ and for single networks (SNs) of $\mathbf{T_9C_4^RT_9}$ can be found in the Appendix (Figure A3.1).
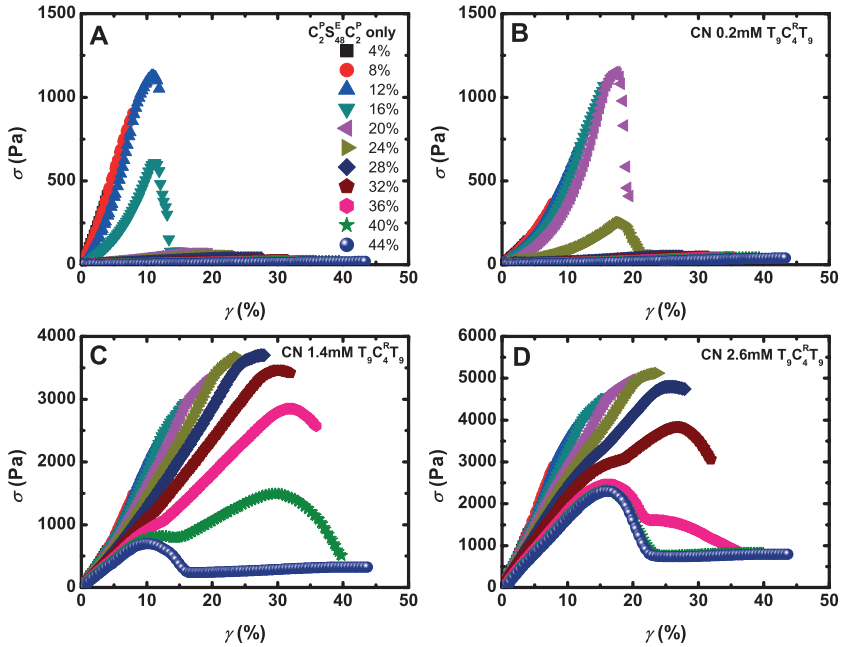
Figure 3.2: *Hysteresis experiments: stress response (σ) as function of strain (γ). (A) $\mathbf{C_2^PS_{48}^EC_2^P}$ single network (SN). (B) composite network (CN) with 0.2 mM $\mathbf{T_9C_4^RT_9}$. (C) CN with 1.4 mM $\mathbf{T_9C_4^RT_9}$. (D) CN with 2.6 mM $\mathbf{T_9C_4^RT_9}$. [$\mathbf{C_2^PS_{48}^EC_2^P}$] was 0.14 mM for all experiments. Maximum strain increases in each cycle as indicated.*
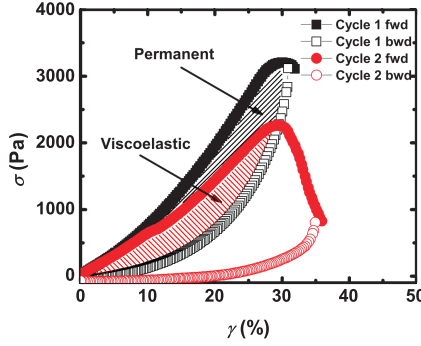
Figure 3.3: *Two consecutive loading/unloading cycles for a* $C_2^P S_{48}^E C_2^P / T_9 C_4^R T_9$ *composite network (CN, 0.14 mM/1.0 mM), showing the mechanical hysteresis. The black hatched area corresponds to the permanent damage, while the red hatched area corresponds to the viscoelastic energy dissipation (due to damage that is healed before the next cycle starts).*

The single network of $C_2^P S_{48}^E C_2^P$ (Figure 3.2A) responds completely elastically during the first strain cycles and shows very little hysteresis as long as the strain remains below 10%. When the strain reaches 16%, however, the sample fails completely and there is a large hysteresis. In the cycles after fracture, no significant stresses could be measured anymore, indicating that the gel does not recover and the damage is irreversible. When $T_9 C_4^R T_9$ is added, the strain and stress at which the network fails gradually increases (Figure 3.2B-D), indicating that the composite gels are tougher than the single fiber network, which is in agreement with our previous findings.[17] Moreover, the composite gels show a partial healing after fracture when the $T_9 C_4^R T_9$ concentration is high enough, with a modulus that recovers to approximately 60% of the initial value at the highest $T_9 C_4^R T_9$ concentration. By contrast, experiments carried out with a mixed system consisting of $C_2^P S_{48}^E C_2^P$ and a C_4^R polymer without T_9 blocks showed a decrease in fracture strain to 4%, and did not show any healing after fracture (Appendix, Figure A3.1). This clearly demonstrates that gel formation of the matrix component, $T_9 C_4^R T_9$, is necessary for toughening of the gels. We note that the initial modulus of the composite gels increases upon adding more $T_9 C_4^R T_9$, exceeding the sum of the moduli of both separate networks. As shown previously,[17] this stiffening is caused by bundling of the $C_2^P S_{48}^E C_2^P$ fibers, probably due to depletion interactions caused by the $T_9 C_4^R T_9$ polymers. We emphasize that this bundling is not responsible for the observed increase in fracture strain, because the control

experiment with unfunctionalized C_4^R did not show an improved fracture strain (but a decrease in critical strain).

To further analyze the hysteresis experiments shown in Figure 3.2 and A3.1, we extract the amount of dissipated energy from the hysteresis in the stress-strain curves. The total energy dissipation (per unit volume) in one cycle is obtained as the area enclosed between the loading and unloading curves. Part of this dissipation is due to irreversible damage of the composite network, probably in the form of broken fibers. However, another part of the dissipation is due to other dissipation mechanisms, because the loading curve of one cycle does not follow the unloading curve of the previous one. This second contribution accounts for viscoelastic dissipation and is probably due to the shear-induced unzipping of triple helices in the $T_9C_4^RT_9$ network, which can reform again during the rest period.[21] Figure 3.3 shows how these two contributions to the energy dissipation can be obtained from two successive loading/unloading cycles.

In Figure 3.4, we plot the total energy dissipated together with the permanent and viscoelastic contributions, as a function of the maximum strain reached in the cycle for the various composite networks. More data for other concentrations of $T_9C_4^RT_9$ and for single networks (SNs) of $T_9C_4^RT_9$ can be found in the Appendix (Figure A3.2). Figure 3.4A shows that for the $C_2^PS_{48}^EC_2^P$ single network, nearly all the dissipated energy is due to permanent damage. After fracture has occurred, no more energy is dissipated, because the gel is fractured and does not reform. This result confirms our previous findings that breakage of $C_2^PS_{48}^EC_2^P$ fibers is irreversible. When a small amount of $T_9C_4^RT_9$ was added, the curves for the total energy dissipation and the permanent dissipation still overlap (Figure 3.4B). However, the amount of dissipated energy is higher than in the fiber-only case, and the dissipation occurs at larger strain values. As the concentration of $T_9C_4^RT_9$ is increased above its gel point ($\sim$0.8 mM), the viscoelastic contribution to the dissipated energy begins to increase (Figure 3.4C) and finally becomes dominant (Figure 3.4D). After the fiber network is fractured, there is no further permanent damage and the later cycles only show viscoelastic dissipation due to the breakage and reformation of triple helices.
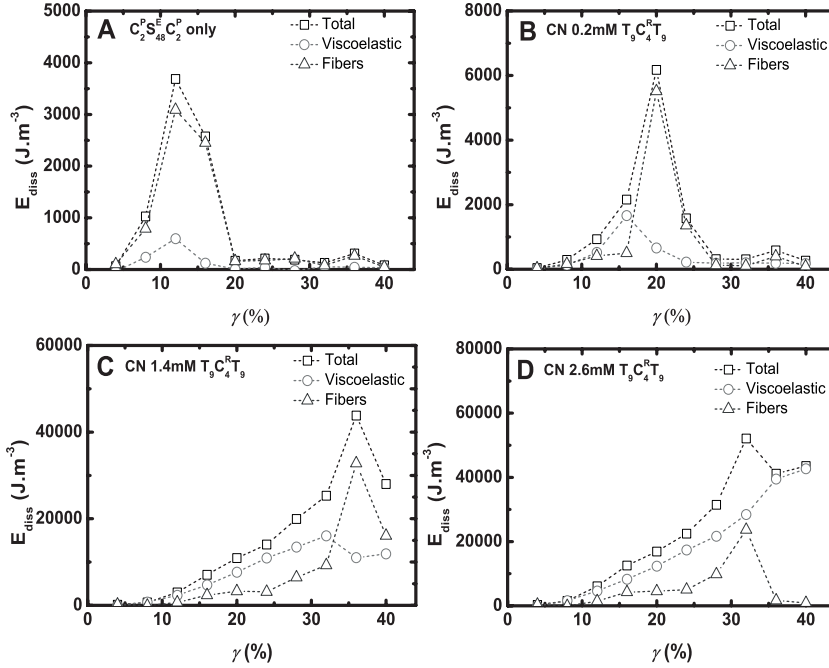
Figure 3.4: *Total energy dissipation (squares), viscoelastic contribution (circles) and permanent contribution (triangles) versus strain (γ). (A) $C_2^P S_{48}^E C_2^P$ single network (SN), (B) composite network (CN) with 0.2 mM $T_9 C_4^R T_9$, (C) CN with 1.4 mM $T_9 C_4^R T_9$, (D) CN with 2.6 mM $T_9 C_4^R T_9$. The dashed lines are a guide to the eye. [$C_2^P S_{48}^E C_2^P$] is 0.14 mM for all experiments.*

Hence, from Figure 3.4 we can conclude that the addition of $T_9 C_4^R T_9$ indeed leads to a strong increase of the dissipated energy, and thereby to an increase of the fracture toughness. Part of this toughening effect is due to viscoelastic dissipation in the $T_9 C_4^R T_9$ network itself, which is probably related to the unzipping of triple helices. However, we see that the permanent dissipation, which we attributed to fiber breakage, also increases upon adding $T_9 C_4^R T_9$. This is shown more clearly in Figure 3.5, where we plotted the total dissipated energy due to permanent damage, obtained by summing the permanent dissipation over all cycles, as a function of the $T_9 C_4^R T_9$ concentration. We find that the $T_9 C_4^R T_9$ network increases the energy dissipated by fiber breakage by approximately a factor of 7. The reason for this is probably that the soft elastic matrix redistributes the stresses around small cracks over a larger region, effectively increasing the size of the dissipative zone.[22,23]
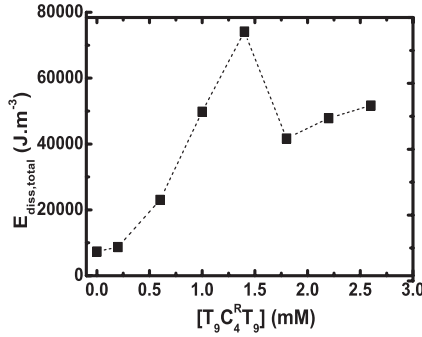
Figure 3.5: *Cumulative amount of dissipated energy of* $C_2^P S_{48}^E C_2^P$ *fibers in* $C_2^P S_{48}^E C_2^P / T_9 C_4^R T_9$ *composite networks (CNs) versus* $[T_9 C_4^R T_9]$. *The dashed lines are a guide to the eye.*

3.3.2 Self-healing

Our results in Figure 3.2 show that in the composite gels with sufficient $T_9 C_4^R T_9$ concentration, the modulus partially recovers after fracture. Since the damage to the fiber network is irreversible, this partial healing must be due to the $T_9 C_4^R T_9$ network, which has been shown previously to be capable of self-healing.[21] To quantify the degree of healing, we obtain the modulus of the gel after each cycle from the slopes of the loading curves. Figure 3.6A shows the measured modulus as a function of the strain reached in the previous cycle for the different samples. It can be observed that for the single $C_2^P S_{48}^E C_2^P$ network, the modulus drops abruptly to nearly zero after the fracture strain has been exceeded, indicating once more that the fractured fiber gel does not heal. For the $C_2^P S_{48}^E C_2^P$ network with added C_4^R (the control experiment), we also found a complete vanishing of the modulus after fracture (which occurs at lower strains than for the $C_2^P S_{48}^E C_2^P$ network alone) and no signs of healing. In contrast, in the presence of $T_9 C_4^R T_9$, the fracture proceeds more gradually (and at higher strains), and the modulus partially recovers even at the highest applied strains, to a value which is approximately 60% of the initial value at the highest $T_9 C_4^R T_9$ concentration. We also carried out self-healing tests on freshly prepared samples, to make sure this observed partial healing is not related to the repeated loading in the experiments in Figure 3.2, and to probe its kinetics. For each sample (all at the same concentration of $C_2^P S_{48}^E C_2^P$ and $T_9 C_4^R T_9$), we formed the gels in the rheometer for 8 hours, which was sufficient to reach a steady state. Then we subjected the hydrogels to a single loading/unloading cycle (Figure 3.6B, inset), and we subsequently monitored the recovery of

the elastic modulus during another 8 hours (Figure 3.6B). This measurement was repeated for different applied strains. A fresh sample was prepared for each datapoint. The recovery step shows that most of the self-healing occurs within the first half hour, while optimal self-healing is reached after 2 hours. This observation is in accordance with those done in previous work on $T_9C_4^RT_9$ gels.[21]
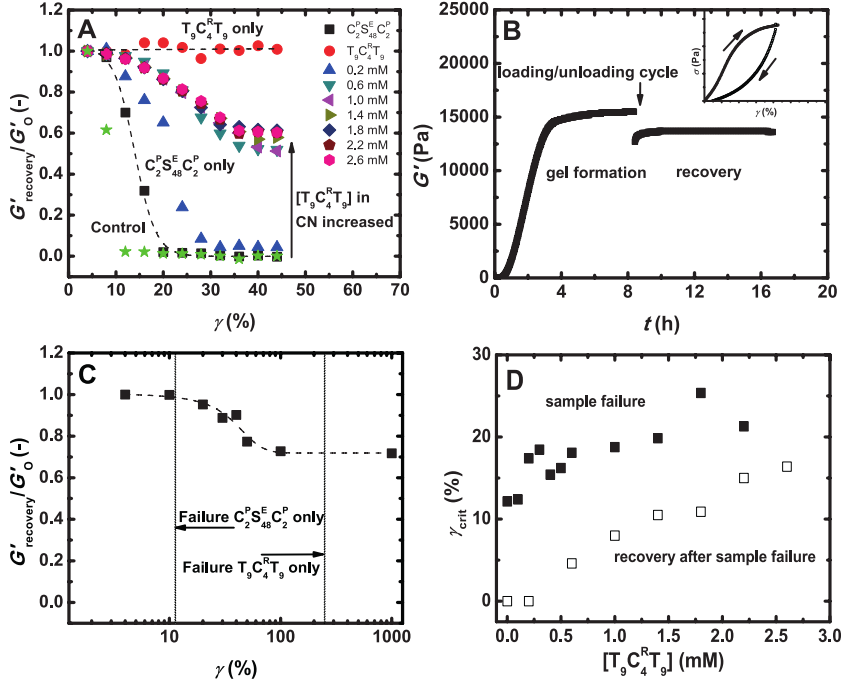
Figure 3.6: *(A) Self-healing after multi-step strain cycles: storage moduli after recovery normalized by the steady state moduli before the strain cycle as a function of strain (γ) for various [$T_9C_4^RT_9$]. (B) Time-resolved progress of gel formation of a mixture of 0.14 mM $C_2^PS_{48}^EC_2^P$ and 1.4 mM $T_9C_4^RT_9$ monitored by rheology, and hydrogel recovery of 1.4 mM $T_9C_4^RT_9$ in $C_2^PS_{48}^EC_2^P/T_9C_4^RT_9$ composite network (CN) after 30% deformation. Inset shows loading and unloading step. (C) Self-healing after 1-step strain cycle: storage moduli after recovery normalized by the steady state moduli before the strain cycle as a function of strain for 1.4 mM $T_9C_4^RT_9$ in $C_2^PS_{48}^EC_2^P/T_9C_4^RT_9$ CN. The dashed line is a guide to the eye. (D) Critical strain versus [$T_9C_4^RT_9$] for fresh hydrogels (closed squares),[17] and after recovery (open squares).*

In Figure 3.6C, we plot the recovered modulus (after 8 hours) divided by the initial modulus as a function of the applied strain. These results are very

similar to those presented in Figure 3.6A, although the recovered modulus (70%) is slightly higher than in Figure 3.6A. Most likely because the damage to the fiber network is a bit lower in these single loading cycle experiments. We conclude that the $T_9C_4^RT_9$ network is to some extent able to repair the damage in the composite gel. Probably, the soft network is able to bridge the cracks that were formed in the fiber network and reconnect the crack faces (Figure 3.7). Since the fibers themselves do not heal, these 'repaired cracks' remain weak spots of the gel. This explains why the recovered gel already breaks at lower strains than the initial gels, as shown in Figure 3.6D.
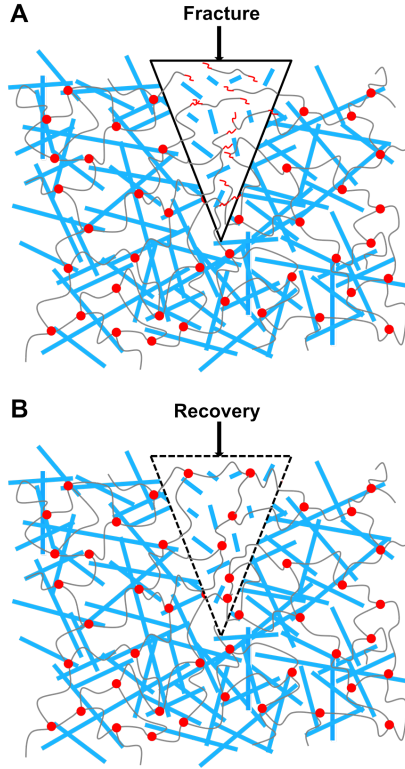

Figure 3.7: *Schematic representation of (A) failure, and (B) partial healing in* $C_2^PS_{48}^EC_2^P/T_9C_4^RT_9$ *composite networks (CN). The* $C_2^PS_{48}^EC_2^P$ *fibers are represented by the blue rods, the triple helical nodes,* $(T_9)_3$*, formed by* $T_9C_4^RT_9$ *by the red circles, dissociated* T_9 *blocks with the red lines, and the random-coil blocks by the grey lines.*

3.4 Conclusions

This study set out to obtain more insight into the mechanism that causes toughening in silk-like fiber networks embedded in a collagen-like elastic matrix. We found that a combination of two different dissipation mechanisms is responsible for the toughening of the composite networks. Firstly, when the collagen-like network was added, the amount of energy dissipated by the fibers alone increased strongly. This effect is probably related to a more homogeneous distribution of the stress throughout the network, which results in enhanced storage moduli and resistance to fracture of the composite network. Secondly, as the amount of the collagen-like component was increased in the composite network, an additional viscoelastic dissipation mechanism became important, related to the unzipping and reformation of triple helices. In addition, the composite networks were capable of partial self-healing after fracturing events. These results show that it is advantageous to reinforce fiber-networks with self-healing physical networks. With this work we shed new insight into the mechanics of fiber-containing composite networks. This might be used for optimization of the mechanical properties of fiber-reinforced composite materials.

Appendix
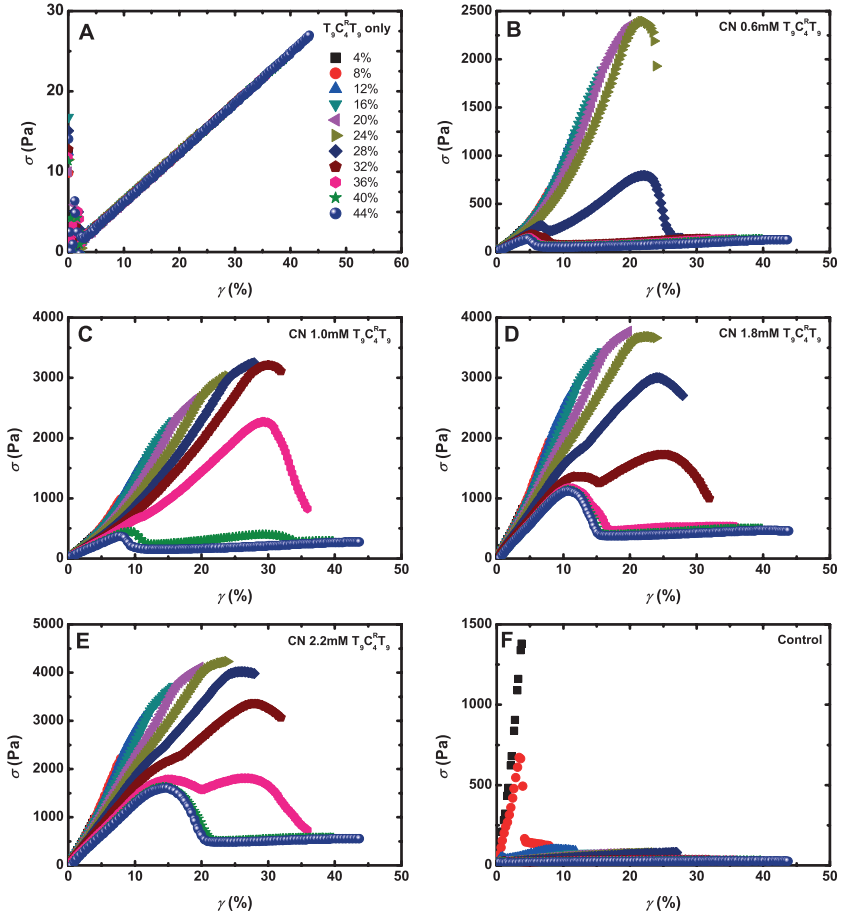
Figure A3.1: *Hysteresis experiments: stress response (σ) as function of strain (γ). (A) 1.0 mM $T_9C_4^RT_9$ single network (SN). (B) composite network (CN) with 0.6 mM $T_9C_4^RT_9$. (C) CN with 1.0 mM $T_9C_4^RT_9$. (D) CN with 1.8 mM $T_9C_4^RT_9$. (E) CN with 2.2 mM $T_9C_4^RT_9$. (F) Control: CN with 1.4 mM C_4^R. $[C_2^PS_{48}^EC_2^P]$ was 0.14 mM for all experiments shown in B-F. Maximum strain increases in each cycle as indicated.*
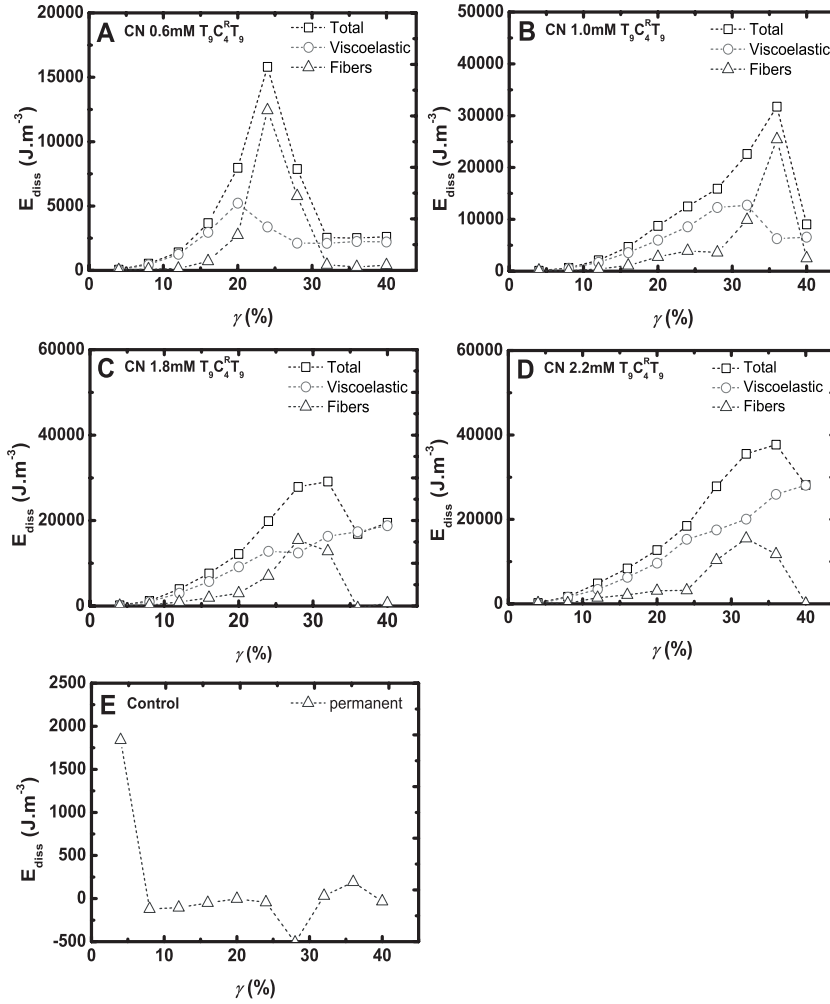
Figure A3.2: *Total energy dissipation (squares), viscoelastic component (circles) and fiber component (triangles) versus strain. (A) composite network (CN) with 0.6 mM* $T_9C_4^RT_9$. *(B) CN with 1.0 mM* $T_9C_4^RT_9$. *(C) CN with 1.8 mM* $T_9C_4^RT_9$. *(D) CN with 2.2 mM* $T_9C_4^RT_9$. *(E) Control: CN with 1.4 mM* C_4^R. *The dashed lines are a guide to the eye.* $[C_2^PS_{48}^EC_2^P]$ *was 0.14 mM for all experiments.*

References

(1) Nicodemus, G. D.; Bryant, S. J. *Tissue Eng., Part B* **2008**, *14*, 149–165.

(2) Ahn, B. K.; Lee, D. W.; Israelachvili, J. N.; Waite, J. H. *Nat. Mater.* **2014**, *13*, 867–872.

(3) Hoare, T. R.; Kohane, D. S. *Polymer* **2008**, *49*, 1993–2007.

(4) Zhu, J.; Marchant, R. E. *Expert Rev. Med. Devices* **2011**, *8*, 607–626.

(5) Vermonden, T.; Censi, R.; Hennink, W. E. *Chem. Rev.* **2012**, *112*, 2853–2888.

(6) Van Vlierberghe, S.; Dubruel, P.; Schacht, E. *Biomacromolecules* **2011**, *12*, 1387–1408.

(7) Gong, J. P.; Katsuyama, Y.; Kurokawa, T.; Osada, Y. *Adv. Mater.* **2003**, *15*, 1155–1158.

(8) Sun, J. Y.; Zhao, X.; Illeperuma, W. R. K.; Chaudhuri, O.; Oh, K. H.; Mooney, D. J.; Vlassak, J. J.; Suo, Z. *Nature* **2012**, *489*, 133–136.

(9) Chen, Q.; Zhu, L.; Zhao, C.; Wang, Q.; Zheng, J. *Adv. Mater.* **2013**, *25*, 4171–4176.

(10) Webber, R. E.; Creton, C.; Brown, H. R.; Gong, J. P. *Macromolecules* **2007**, *40*, 2919–2927.

(11) Kim, B. S.; Mooney, D. J. *Trends Biotechnol.* **1998**, *16*, 224–230.

(12) Eyre, D. *Arthritis Res.* **2002**, *4*, 30–35.

(13) Frantz, C.; Stewart, K. M.; Weaver, V. M. *J. Cell Sci.* **2010**, *123*, 4195–4200.

(14) Kouwer, P. H. J.; Koepf, M.; Le Sage, V. A. A.; Jaspers, M.; van Buul, A. M.; Eksteen-Akeroyd, Z. H.; Woltinge, T.; Schwartz, E.; Kitto, H. J.; Hoogenboom, R., et al. *Nature* **2013**, *493*, 651–655.

(15) Adams, D. J.; Mullen, L. M.; Berta, M.; Chen, L.; Frith, W. J. *Soft Matter* **2010**, *6*, 1971–1980.

(16) Storm, C.; Pastore, J. J.; MacKintosh, F. C.; Lubensky, T. C.; Janmey, P. A. *Nature* **2005**, *435*, 191–194.

(17) Rombouts, W. H.; Colomb-Delsuc, M.; Werten, M. W. T.; Otto, S.; de Wolf, F. A.; van der Gucht, J. *Soft Matter* **2013**, *9*, 6936–6942.

(18) Rombouts, W. H.; Giesbers, M.; van Lent, J.; de Wolf, F. A.; van der Gucht, J. *Biomacromolecules* **2014**, *15*, 1233–1239.

(19) Martens, A. A.; Portale, G.; Werten, M. W. T.; de Vries, R. J.; Eggink, G.; Cohen Stuart, M. A.; de Wolf, F. A. *Macromolecules* **2009**, *42*, 1002–1009.

(20) Werten, M. W. T.; Teles, H.; Moers, A. P. H. A.; Wolbert, E. J. H.; Sprakel, J.; Eggink, G.; de Wolf, F. A. *Biomacromolecules* **2009**, *10*, 1106–1113.

(21) Skrzeszewska, P. J.; de Wolf, F. A.; Stuart, M. A. C.; van der Gucht, J. *Soft Matter* **2010**, *6*, 416–422.

(22) Gong, J. P. *Soft Matter* **2010**, *6*, 2583–2590.

(23) Brown, H. R. *Macromolecules* **2007**, *40*, 3815–3818.

Synergistic Stiffening in Double-Fiber Networks

4

Abstract

Many biological materials are composite structures, interpenetrating networks of different types of fibers. The composite nature of such networks leads to superior mechanical properties, but the origin of this mechanical synergism is still poorly understood. Here we study soft composite networks, made by mixing two self-assembling fiber-forming components. We find that the elastic moduli of the composite networks significantly exceed the sum of the moduli of the two individual networks. This mechanical enhancement is in agreement with recent simulations, where it was attributed to a suppression of non-affine deformation modes in the most rigid fiber network due to the reaction forces in the softer network. The increase in affinity also causes a loss of strain hardening and an increase in the critical stress and stain at which the network fails.

4.1 Introduction

Fiber networks are important structural components in many biological systems, food products, and biomedical applications. Their primary function is to provide mechanical strength and stability. The elastic properties of fiber networks depend on the persistence length of the fibers, on the fiber concentration, and on the presence and type of crosslinks. Recent experimental and theoretical work has shown that loosely crosslinked fiber networks deform very inhomogeneously. The lowest-energy deformation modes are strongly non-affine, meaning that locally the network deformation can be significantly greater than the average deformation. These "floppy", non-affine deformation modes are crucial for determining network elasticity.[1–7] They are also responsible for stress localization, which can lead to network fracture already at very low overall strains. Another characteristic feature of fiber networks is their pronounced nonlinear response, which typically exhibits strong strain stiffening.[7–10] Several explanations have been proposed for this. In one of these, the strain stiffening of the fiber network is attributed to a nonlinear stretching response of the individual fibers in the network.[11] Alternatively, the nonlinear elasticity may be due to a transition from a non-affine bending-dominated response at low strains to a more affine stretching-dominated response at higher strains.[12,13] In biology, soft tissues are often composite materials, consisting of a fiber network embedded in a soft elastic matrix. This composite structure has a major impact on the resulting mechanical properties of the material.[14–17] An experimental study with microtubules in an elastic medium has shown that non-affine bending modes of individual fibers are suppressed by the elastic matrix.[18] Recent simulations show that a similar suppression of non-affine deformation modes occurs in fiber networks embedded in an elastic matrix, leading to an increase in the storage modulus of the composite structure.[19] Furthermore, the stress distribution becomes more homogeneous, resulting in a higher critical stress of the network.[19] These enhancements of mechanical properties might explain why composite structures are so abundant in living organisms. However, an experimental validation of these simulation results is still lacking. In this chapter, we aim to test this for a model composite fiber network. Here, we investigate physical composite networks formed by the simultaneous self-assembly of two fiber-forming components. The first component, Fmoc-Leu-Gly (FMOC-LG), is a Fmoc dipeptide (see Figure 4.1A for the molecular structure).
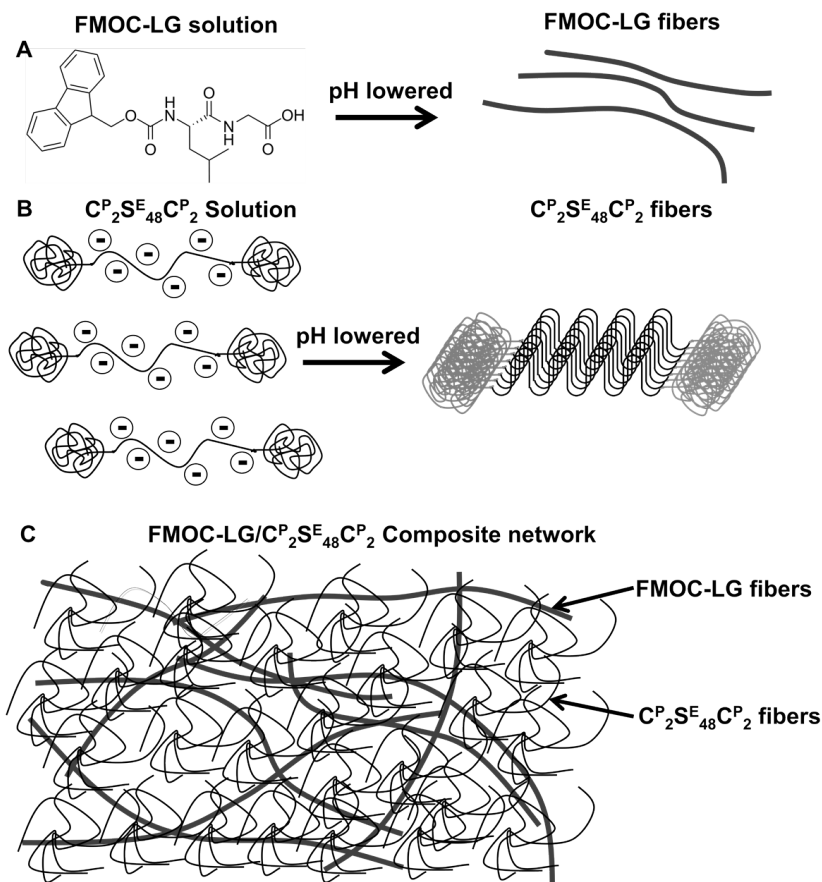
Figure 4.1: *(A) Molecular structure of FMOC-LG. When the pH is lowered, FMOC-LG self-assembles into stiff fibers. (B) Self-assembly mechanism of $C^P_2S^E_{48}C^P_2$. At low pH, the silk-like middle blocks fold and stack to form fibers. (C) Impression of the composite network formed by FMOC-LG (thick lines) mixed with $C^P_2S^E_{48}C^P_2$ (thin lines). The FMOC-LG fibers are much stiffer than the $C^P_2S^E_{48}C^P_2$ fibers.*

At high pH, when the terminal acid group of the glycine residue is deprotonated, self-assembly of the dipeptide is prevented by the repulsion between the negative charges. However, when the pH is decreased below the p*Ka* of ~5.8, the charge is removed and the dipeptide self-assembles into long, stiff fibers that entangle to form a self-supporting hydrogel.[20–28] The driving force for this self-assembly process is thought to be a combination of $\pi - \pi$ stacking and hydrophobic interactions

between the Fmoc groups and hydrogen bonding between the peptide side chains.[20,22,25,26] The second component, a silk-like block copolymer ($C_2^P S_{48}^E C_2^P$), is an ABA block copolymer consisting of a pH-sensitive middle block (S_{48}^E), consisting of 48 (Gly-Ala)$_3$-Gly-Glu octapeptide repeats, and hydrophilic, gelatin-inspired end blocks (C_2^P) that each consist of approximately 200 amino acids (Figure 4.1B). The C_2^P blocks assume a random-coil conformation at all relevant pH values and have been described by us previously.[29] When the pH is decreased below the pKa value of the glutamic acid residues present in the S_{48}^E block, the glutamic acid residues become protonated. This allows the S_{48}^E block to fold into a β-sheet-like structure, which then assembles into long semiflexible fibers. The design of $C_2^P S_{48}^E C_2^P$ was inspired by natural spider silk, and it can be produced biosynthetically. $C_2^P S_{48}^E C_2^P$ has been characterized by us in previous work.[30,31] In addition, the role of $C_2^P S_{48}^E C_2^P$ in a physical composite network consisting of $C_2^P S_{48}^E C_2^P$ fibers dispersed in a soft elastic matrix has been studied.[15] In this chapter, we study the structural and mechanical properties of composite networks, formed by mixing FMOC-LG and $C_2^P S_{48}^E C_2^P$. As we will show below, the FMOC-LG fibers are much more rigid than the $C_2^P S_{48}^E C_2^P$ fibers. A schematic picture of the composite network is shown in Figure 4.1C.

4.2 Experimental Section

4.2.1 Materials

Two bioinspired protein polymers, $C_2^P S_{48}^E C_2^P$ and C_4^R, were produced biosynthetically in the yeast *Pichia pastoris*. The biosynthetical production of $C_2^P S_{48}^E C_2^P$ and C_4^R has been described previously,[29,30] and the amino acid sequences of these proteins can be found in GenBank as entries ABW84222 and ACF33477, respectively. To obtain the complete amino acid sequence of the mature proteins from these GenBank records, the sequence of $C_2^P S_{48}^E C_2^P$ should be preceded with Tyr-Val and the N-terminal residues (Leu-Glu-Lys-Arg-Glu-Ala-Glu-Ala) in the C_4^R sequence should be removed. Fed-batch fermentations were performed in 2.5 L Bioflo 3000 bioreactors (New Brunswick Scientific), according to the procedures described previously.[30,32] The protein polymers were purified from the fermentation broth by two consecutive ammonium sulfate precipitation steps followed by desalting and lyophilization. FMOC-LG (Bachem) was used as received.

4.2.2 Methods

Sample preparation

Stock solutions of $C_2^P S_{48}^E C_2^P$ (1.7 and 6.0% (w/v)), C_4^R (0.58% (w/v)), and FMOC-LG (0.60% (w/v)) were prepared by dissolving fixed amounts of chemicals in deionized water. The sample preparation for all experiments was conducted at 20 °C. The pH of the stock solutions was carefully adjusted to 10.0 by addition of small amounts of 1.0 M sodium hydroxide. After pH adjustment, the stock solutions were filter sterilized (0.2 μm). Samples were prepared by mixing fixed amounts of stock solutions and complemented with 0.1 mM sodium hydroxide (pH 10.0) to a final volume of 1.2 mL. The concentration of FMOC-LG was fixed to 0.25% (w/v) for all experiments, unless mentioned otherwise. The concentration of $C_2^P S_{48}^E C_2^P$ was varied between 0.05 and 3.0% (w/v) in the composite networks. To induce gelation of both $C_2^P S_{48}^E C_2^P$ and FMOC-LG, glucono delta-lactone (GDL) in solid form was added to the samples. After dissolving, GDL causes a gradual decrease in the pH to a final value of 3.0-3.7 within approximately 2 hours. As shown previously,[21] such a gradual pH reduction leads to more homogeneous and stiffer hydrogels than a rapid pH quench with, for example, hydrochloric acid.

Rheology

Rheological measurements were performed with an Anton Paar Physica MCR 301 rheometer equipped with a Couette geometry (1 mL). A solvent trap was used to minimize the effects of evaporation. The temperature was controlled with a Peltier element. All measurements were taken at 20 °C. Samples were allowed to form a gel *in situ*. *In situ* gel formation was followed by measuring a time sweep (f=1 Hz and γ=0.1%), whereby the storage (G') and loss (G'') moduli were measured for 10 h. Thereafter, the viscoelastic behavior of the steady state gel was characterized by a frequency sweep (ω=0.01-100 rad.s^{-1} and γ=0.05 %). Finally, the nonlinear behavior of the gel was evaluated by two different methods: by increasing the strain at a constant strain rate ($\dot{\gamma}$=0.1 s^{-1}) and by applying an oscillatory strain sweep (f=1 Hz and γ=0.01-10%) until the gel ruptured.

Atomic Force Microscopy (AFM)

Samples for AFM were prepared by depositing a 5 μL aliquot of solutions of $C_2^P S_{48}^E C_2^P$, FMOC-LG, and FMOC-LG mixed with $C_2^P S_{48}^E C_2^P$ immediately after induction on silica wafers. The AFM samples were not diluted. The

silica wafers were glow-discharged under vacuum before being used to improve the surface hydrophilicity. Afterward, the samples were dried in air. Subsequently, the air-dried samples were washed with deionized water and dried under a nitrogen flow to remove nonadsorbed material. Analysis was conducted with a Bruker Nanoscope V instrument in peak force tapping mode: the AFM tip is oscillated in a sinusoidal manner in the vertical direction, while the peak force is used as a feedback signal. This mode allows for direct force control and avoids damage due to lateral forces. In the images, we show the peak force error (the feedback signal). As shown previously,[33] peak force images show better resolution than height images, especially for soft samples. Corresponding height images are shown in Figure A4.1 of the Appendix. Silicon nitride tips with a typical radius of 2 nm (Bruker SCANASYST-AIR) were used for samples in the dilute regime, and silicon nitride tips with a typical radius of 20 nm (Bruker NP-10) were used for samples in the concentrated regime. To test whether the drying rate has an influence on the morphology of the fibers, we also observed samples that were dried at a high controlled humidity, so that the drying occurs more slowly. As shown in Figure A4.1 of the Appendix, the drying rate does not affect the morphology of the fibers, although the number of fibers is significantly higher in these samples, because the slower drying process gives the fibers more time to form.

Scanning Electron Microscopy (SEM)

Samples for SEM were induced for 24 h. Thin slices of the hydrogels were cut with a razor blade and mounted on brass sample holders coated with carbon adhesive tabs. Subsequently, the sample holders were plunged into liquid nitrogen and transferred to a freeze-dryer (Labconco) for 24 h. After the water had been removed, the samples were sputter-coated with a 5 nm layer of iridium to prevent charging of the sample during analysis. The analysis was performed with a FEI Magellan FESEM scanning electron microscope at a working distance of 4 mm, with SE detection at 2 kV and 6 pA. All images were recorded digitally.

Cryo-Transmission Electron Microscopy (Cryo-TEM)

Samples for cryo-TEM were prepared below the gelation concentration of both $C_2^P S_{48}^E C_2^P$ and FMOC-LG, to investigate fiber morphology in the dilute regime. Copper TEM grids (C-Flat 4/1 400 mesh and Lacey carbon 400 mesh) were exposed to a glow-discharge in air prior to being used. Subsequently, 3 μL aliquots of induced protein solutions were deposited on

copper grids. To obtain a thin vitrified sample film, the excess was removed by blotting in a Vitrobot Mark IV instrument (FEI Co.), and the grids were plunged into liquid ethane. Grids were then transferred to a Gatan CT 3500 cryo-stage and analyzed in a JEOL JEM2100 transmission electron microscope. Images were recorded at 200 kV under low-dose conditions with a 4K x 4K Gatan US4000 digital camera. Images were processed with ImageJ. To remove noise, a Gaussian blur filter was applied. Finally, the image brightness and contrast were optimized to improve the contrast of the images.

## 4.3   Results and Discussion

4.3.1   Structure

Before studying the linear and nonlinear rheological properties of the FMOC-LG/$C_2^P S_{48}^E C_2^P$ composite networks (CNs), we first studied the structural characteristics of these composite networks via AFM and SEM. Both $C_2^P S_{48}^E C_2^P$ and FMOC-LG are known to form fibers.[15,21,25,30] In this study, however, combinations of $C_2^P S_{48}^E C_2^P$ and FMOC-LG were studied. It is therefore important to confirm that both components are also able to form fibers in mixed systems. Figure 4.2 presents AFM peak force error pictures (see Methods) and SEM images of FMOC-LG single networks (SNs), the $C_2^P S_{48}^E C_2^P$ SN, and FMOC-LG/$C_2^P S_{48}^E C_2^P$ CNs. In all experiments, the conditions were chosen such that the concentrations of FMOC-LG and $C_2^P S_{48}^E C_2^P$ both exceeded their respective gelation concentrations. For the FMOC-LG SN, twisted ribbons can be observed. This is in agreement with previous findings in the literature.[25] With the $C_2^P S_{48}^E C_2^P$ SN, single fibers cannot be resolved via AFM and SEM. Apparently, the sample preparation for AFM and SEM, which involves drying of the networks, prohibits the visualization of individual $C_2^P S_{48}^E C_2^P$ fibers in the gels. In the FMOC-LG/$C_2^P S_{48}^E C_2^P$ CN, similar twisted ribbons like the ones seen in the FMOC-LG SN are observed via AFM and SEM. The general network structure is similar to that in the FMOC-LG SN. The surfaces of the FMOC-LG fibers in the composite network have a more irregular appearance, probably because the FMOC-LG fibers are covered with $C_2^P S_{48}^E C_2^P$ fibers (Figure 4.2F). However, no single $C_2^P S_{48}^E C_2^P$ fibers can be distinguished in the composite network, just as in the $C_2^P S_{48}^E C_2^P$ SN. Hence, AFM and SEM on dried gels allow us to confirm the presence of the FMOC-LG fibers, but not of $C_2^P S_{48}^E C_2^P$ fibers.
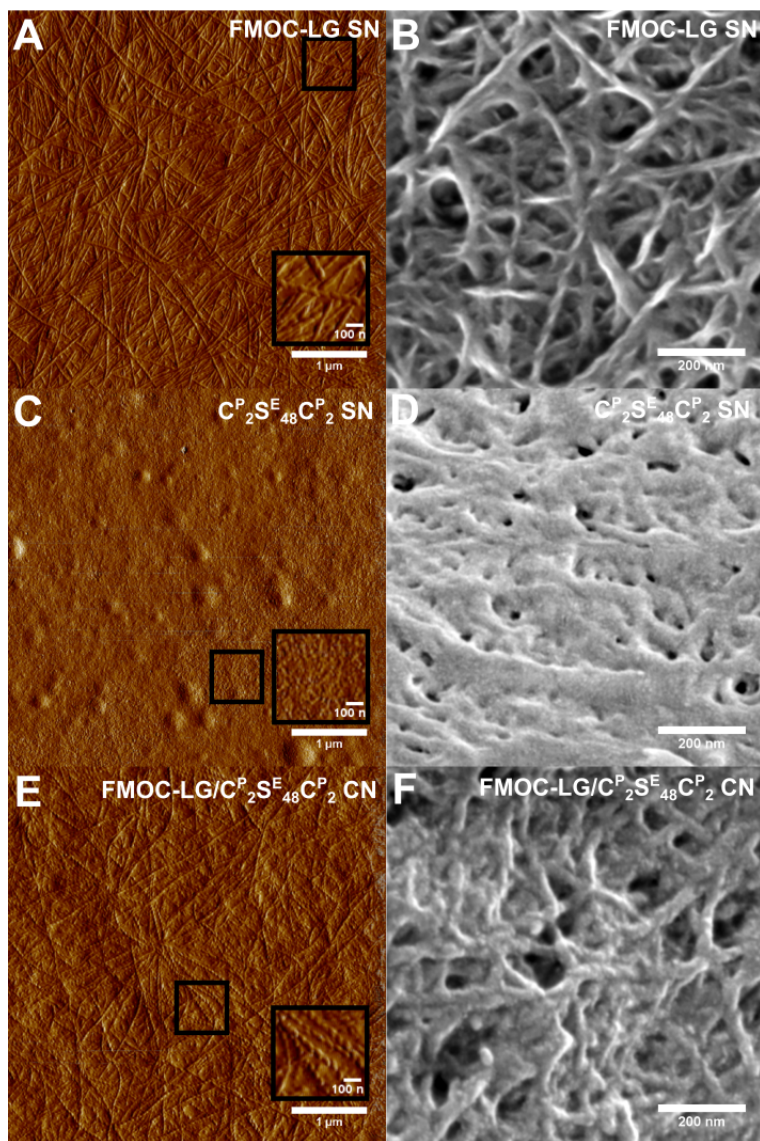
Figure 4.2: *(A, C, and E) AFM peak force error images of (A) the FMOC-LG single network (SN) at 0.25% (w/v), (C) the $C_2^P S_{48}^E C_2^P$ single network (SN) at 0.50% (w/v), and (E) the composite network (CN) of FMOC-LG and $C_2^P S_{48}^E C_2^P$ at 0.25 and 0.50% (w/v), respectively. The scalebar indicates 1 μm, and 100 nm in the insets of the images. (B, D, and F) SEM images for the same samples. The scalebar indicates 200 nm.*

To circumvent the limitations of imaging concentrated gels, we performed additional experiments in dilute solutions. In all experiments, the conditions were chosen so that the concentrations of FMOC-LG and $C_2^P S_{48}^E C_2^P$ were below their gelation concentrations. Figure 4.3 presents AFM peak force error pictures and cryo-TEM images of the FMOC-LG SN, $C_2^P S_{48}^E C_2^P$ SN, and FMOC-LG/$C_2^P S_{48}^E C_2^P$ CN. For the FMOC-LG SN, twisted ribbons are again observed. However, some flat tapes are also observed (Figure 4.3A, inset). The coexistence of twisted ribbons and flat tapes for FMOC-LG has been reported previously in the literature.[25] For the $C_2^P S_{48}^E C_2^P$ SN, ribbon-like fibers are observed. This is in agreement with our previous findings.[15,30] Although the fibers are overlapping at 0.050% (w/v) $C_2^P S_{48}^E C_2^P$, it is still possible to observe single fibers via AFM at this concentration, unlike what we have seen at higher concentrations. For the FMOC-LG/$C_2^P S_{48}^E C_2^P$ CN, long twisted ribbons characteristic for FMOC-LG and shorter ribbon-like fibers characteristic of $C_2^P S_{48}^E C_2^P$ are observed together, confirming that both components form fibers in the mixed samples. We also used cryo-TEM to study the same samples. In contrast to AFM, where dry samples were analyzed, cryo-TEM allows analysis of samples in their aqueous environments. Therefore, this method provides a more realistic view of the actual structure. For the FMOC-LG SN, bundled structures of twisted ribbons are observed. This result is in accordance with observations by AFM. $C_2^P S_{48}^E C_2^P$ forms flat ribbonlike structures, which do not have a tendency to bundle. $C_2^P S_{48}^E C_2^P$ fibers formed after adding GDL have a morphology similar to the morphology of those formed after the addition of hydrochloric acid investigated previously.[15] For the FMOC-LG/$C_2^P S_{48}^E C_2^P$ CN, both long twisted bundled ribbons characteristic of FMOC-LG and shorter unbundled ribbons characteristic of $C_2^P S_{48}^E C_2^P$ are observed together (Figure 4.3F). From the combined results from AFM, SEM, and cryo-TEM, we conclude that both FMOC-LG and $C_2^P S_{48}^E C_2^P$ form fibers in composite systems, with a structure and morphology that resemble those of the respective single networks.
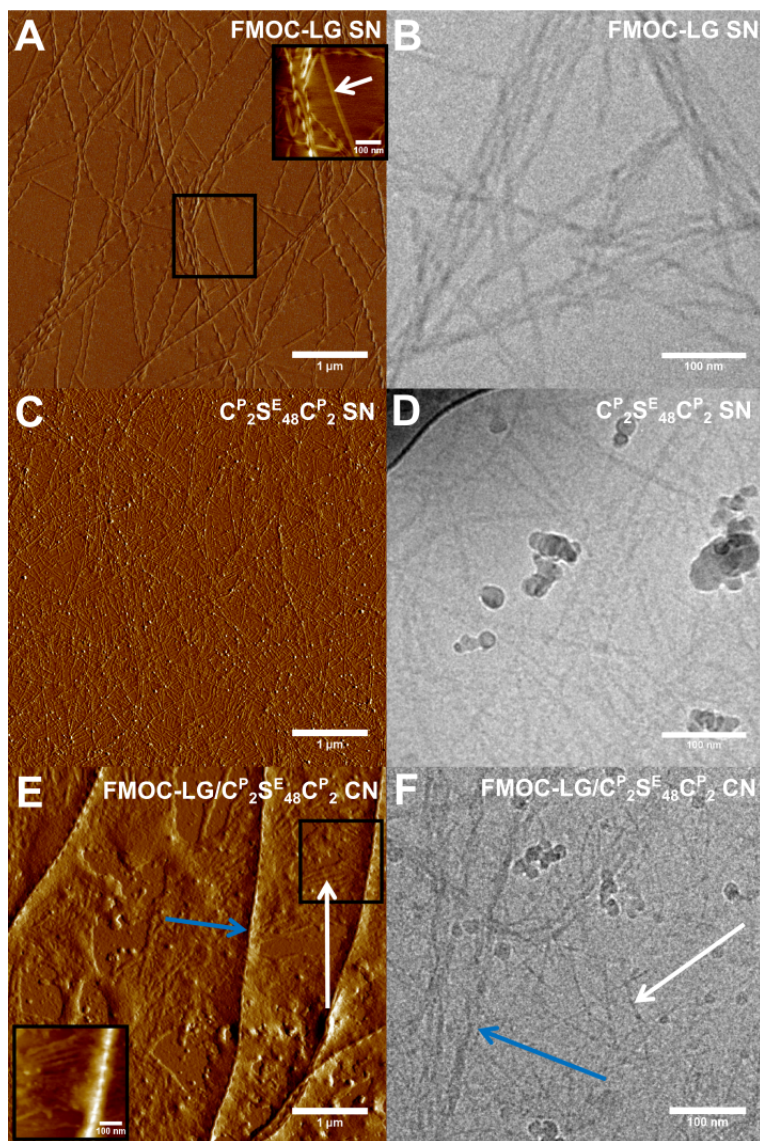
Figure 4.3: *(A, C, and E) AFM height and peak force error images of (A) the FMOC-LG single network (SN) at 0.025% (w/v), (C) the $C_2^P S_{48}^E C_2^P$ single network (SN) at 0.050% (w/v), and (E) the composite network (CN) of FMOC-LG and $C_2^P S_{48}^E C_2^P$ at 0.025 and 0.050% (w/v), respectively. In panel A, the white arrow indicates the flat FMOC-LG ribbon. In panel E, the white arrow indicates the $C_2^P S_{48}^E C_2^P$ fibers and the blue arrow FMOC-LG fibers. (A, C, and E) The scalebar indicates 1 μm. (B, D, and F) Cryo-TEM images of the same samples. The scalebar indicates 100 nm. In panel F, the white arrow indicates $C_2^P S_{48}^E C_2^P$ fibers and the blue arrow FMOC-LG fibers.*

64

4.3.2 Rheology

The *in situ* formation of the FMOC-LG SN and FMOC-LG/$\mathbf{C_2^P S_{48}^E C_2^P}$ CNs is shown in Figure 4.4A. For all combinations of FMOC-LG and $\mathbf{C_2^P S_{48}^E C_2^P}$ investigated, steady state was reached within 10 h after GDL had been added to lower the pH. Figure 4.4B presents frequency-dependent storage and loss moduli for single and composite networks. For all cases, the storage modulus is almost independent of frequency, and much higher than the loss modulus, indicating that all samples are elastic gels. To investigate possible relaxations at longer time scales, we also performed creep tests for the same samples. As shown in Figure A4.2 of the Appendix, all samples have a very high but finite viscosity and a relaxation time on the order of 10^4 s. This indicates that crosslink unbinding or disentanglement occurs very slowly in these samples. The storage modulus of fiber networks formed by 0.25% (w/v) FMOC-LG SN had an average plateau value of 75 kPa, which agrees well with other results reported in literature, where a modulus of around 200 kPa for 0.6% (w/v) FMOC-LG hydrogels was reported.[20] At the same concentration, the $\mathbf{C_2^P S_{48}^E C_2^P}$ SN had a much lower modulus (7 Pa), which is probably caused by a larger flexibility of the $\mathbf{C_2^P S_{48}^E C_2^P}$ fibers compared to that of the FMOC-LG fibers. Only at much higher $\mathbf{C_2^P S_{48}^E C_2^P}$ concentrations, between 1.5 and 2.0% (w/v), does the modulus of the $\mathbf{C_2^P S_{48}^E C_2^P}$ SN become comparable to that of the FMOC-LG SN. To study what happens in composite networks, consisting of mixtures of the two fibers, we investigated composite networks in which the FMOC-LG concentration is fixed and the $\mathbf{C_2^P S_{48}^E C_2^P}$ concentration is varied. A schematic picture of such a composite network is shown in Figure 4.1C, where the FMOC-LG fibers can be considered as long, stiff fibers, while the $\mathbf{C_2^P S_{48}^E C_2^P}$ fibers constitute a softer elastic matrix in the background. Figure 4.4C displays the average values of the steady state storage moduli of FMOC-LG/$\mathbf{C_2^P S_{48}^E C_2^P}$ CNs as a function of $\mathbf{C_2^P S_{48}^E C_2^P}$ concentration. Values for the $\mathbf{C_2^P S_{48}^E C_2^P}$ SN at the same concentration are plotted in that same figure, and the dashed line indicates the sum of the moduli of the two single networks. For all FMOC-LG/$\mathbf{C_2^P S_{48}^E C_2^P}$ CNs tested, the storage modulus exceeded the sum of the moduli of the FMOC-LG and $\mathbf{C_2^P S_{48}^E C_2^P}$ SNs (Figure 4.4C). With an increasing $\mathbf{C_2^P S_{48}^E C_2^P}$ concentration, the modulus increases strongly, until it levels off at high $\mathbf{C_2^P S_{48}^E C_2^P}$ concentrations. To test whether fiber formation of $\mathbf{C_2^P S_{48}^E C_2^P}$ is necessary for the modulus increase, we also performed an experiment with a control molecule, $\mathbf{C_4^R}$, which has the amino acid composition of the $\mathbf{C_2^P}$ blocks in $\mathbf{C_2^P S_{48}^E C_2^P}$ but lacks the self-assembling $\mathbf{S_{48}^E}$ blocks, so

it cannot form fibers. The C_4^R concentration was 0.58% (w/v) in the FMOC-LG/C_4^R CN (control). Interestingly, the storage modulus of the FMOC-LG/C_4^R CN (control) is comparable to that of the FMOC-LG SN (see Figure 4.4A-C). This result implies that the strongly enhanced storage moduli observed for the FMOC-LG/$C_2^P S_{48}^E C_2^P$ CNs can be attributed to the presence of $C_2^P S_{48}^E C_2^P$ fibers in the system. To quantify the mechanical enhancement in the composite network, we calculate an enhancement factor, defined as the storage modulus of FMOC-LG/$C_2^P S_{48}^E C_2^P$ CNs divided by the sum of the moduli of the FMOC-LG and $C_2^P S_{48}^E C_2^P$ SNs. An enhancement factor of >1 indicates that the interlocking of the two fiber networks leads to a synergistic increase in the modulus, beyond what would be expected if the contributions of the two networks would simply add up. In Figure 4.4D, we plot the enhancement factor as a function of the modulus of the background $C_2^P S_{48}^E C_2^P$ matrix. We see that the enhancement factor is >1 in all composite networks and goes through a maximum as the $C_2^P S_{48}^E C_2^P$ concentration is increased. The maximal enhancement occurs for a $C_2^P S_{48}^E C_2^P$ concentration of ~1% (w/v), corresponding to a modulus of the $C_2^P S_{48}^E C_2^P$ matrix of approximately 20 kPa. Recently, we found a similar enhancement of the elastic modulus in another composite network, consisting of $C_2^P S_{48}^E C_2^P$ fibers in a soft gelatin-like gel.[15] In that case, the increased modulus was caused by bundle formation induced by the background network, probably due to depletion attraction. In the system presented here, however, we find no evidence of an increased level of bundling in the composite networks. An alternative explanation for the mechanical enhancement has been suggested recently by Zhang et al.,[19] who conducted numerical simulations of fiber networks in an elastic matrix. Their simulations show a stiffening of the composite network, which is caused by a suppression of the floppy, non-affine deformation modes of the network due to the elastic matrix. As the modulus of the background matrix increases, the fiber network is constrained to deform more affinely, because of the external forces applied by the matrix on the fibers. Probably, a similar mechanism is behind the modulus increase in our composite networks: with an increasing $C_2^P S_{48}^E C_2^P$ concentration, the mesh size of the background network decreases (and its elasticity increases), so that deformations of the FMOC-LG fibers become more constrained and the overall network stiffness increases. The decrease in enhancement factor at very high values of the matrix modulus (Figure 4.4D) may be due to a saturation effect: when the $C_2^P S_{48}^E C_2^P$ matrix becomes very stiff, the relative contribution of the FMOC-LG network decreases.
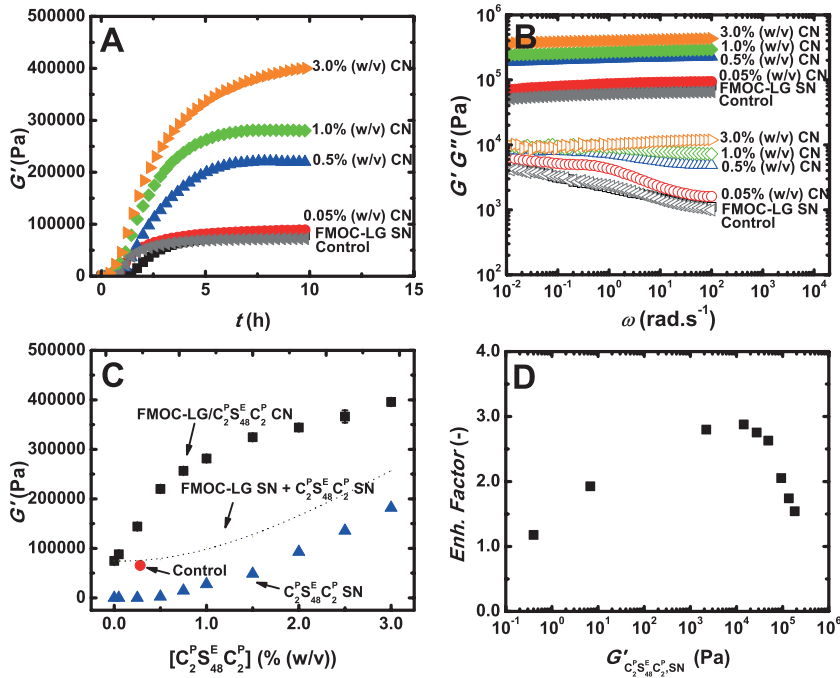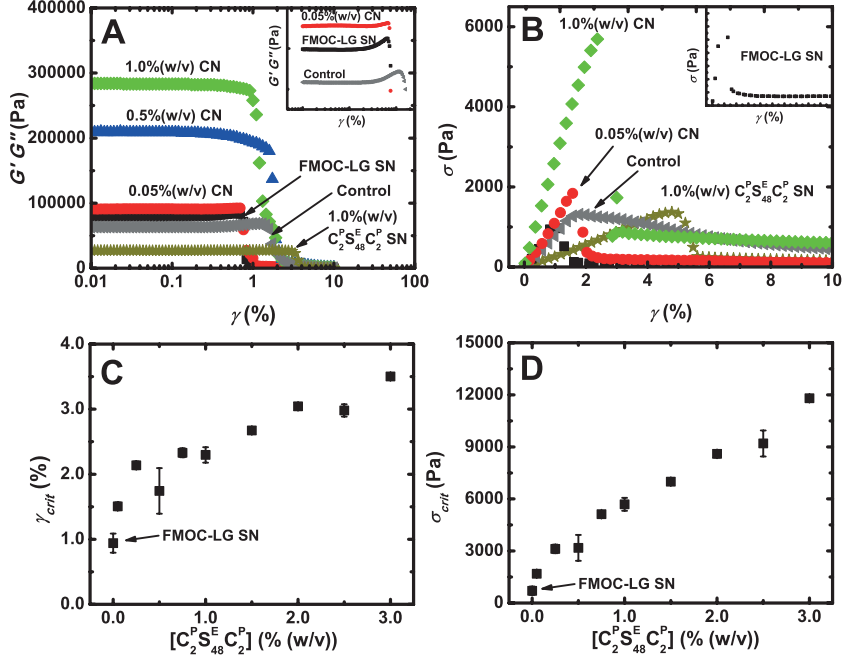
Figure 4.4: *(A) Storage moduli (G′) of single networks (SNs), composite networks (CNs), and the control as a function of time (f=1 Hz; γ=0.05%; T = 20 °C). The FMOC-LG concentration was 0.25% (w/v) for all experiments. The $C_2^P S_{48}^E C_2^P$ concentration was varied as indicated. (B) Frequency sweeps of the FMOC-LG SN, FMOC-LG/$C_2^P S_{48}^E C_2^P$ CNs, and the control. Storage moduli (G′, filled symbols) and loss moduli (G″, open symbols) are shown. The FMOC-LG concentration was 0.25% (w/v) for all experiments. The $C_2^P S_{48}^E C_2^P$ concentration was varied as indicated. (C) Average steady state storage moduli (G′) of FMOC-LG/$C_2^P S_{48}^E C_2^P$ CNs (n = 3) as a function of $C_2^P S_{48}^E C_2^P$ concentration (closed black squares). Average steady state storage moduli (G′) of $C_2^P S_{48}^E C_2^P$ SNs (n = 1) as a function of $C_2^P S_{48}^E C_2^P$ concentration (blue triangles). The dotted line represents the cumulative values of the FMOC-LG SN and $C_2^P S_{48}^E C_2^P$ SN. The red circle indicates the value for the control. (D) Enhancement factor as a function of the storage modulus of $C_2^P S_{48}^E C_2^P$ SNs. The enhancement factor is defined as storage moduli of FMOC-LG/$C_2^P S_{48}^E C_2^P$ CNs divided by the sum of the FMOC-LG SN and $C_2^P S_{48}^E C_2^P$ SN. (A-C) The control consisted of 0.58% (w/v) C_4^R mixed with 0.25% (w/v) FMOC-LG.*

The nonlinear mechanical properties of the FMOC-LG/$C_2^P S_{48}^E C_2^P$ composites were investigated by applying an oscillatory deformation of increasing amplitude to the FMOC-LG SN and FMOC-LG/$C_2^P S_{48}^E C_2^P$ CNs. In Figure 4.5A, storage moduli of various FMOC-LG/$C_2^P S_{48}^E C_2^P$ CNs are

shown as a function of strain amplitude. For all cases, at strains of <0.5%, the storage moduli are constant, indicating a linear response regime. However, when the strain is increased beyond this linear regime, the FMOC-LG SNs show a weak strain hardening. Interestingly, in the CNs investigated here, the strain hardening effect disappears completely, with an increase in the $C_2^P S_{48}^E C_2^P$ concentration in the FMOC-LG/$C_2^P S_{48}^E C_2^P$ CNs. The simulations by Zhang et al. showed a similar disappearance of strain hardening.[19] At low moduli of the embedding matrix, the fiber network strain hardens due to a transition from non-affine to affine deformation modes with increasing strain. At relatively high moduli of the elastic matrix, however, the non-affine deformation modes are suppressed already for small deformations, so that such a transition can no longer occur. We note that the strain hardening observed in the FMOC-LG networks is very weak (much weaker than, for example, for actin gels[7–9]). This is probably caused by the brittleness of the networks: before significant strain hardening can occur, the network fractures. Another method for investigating the nonlinear properties is to apply shear deformation at a constant shear rate ($\dot{\gamma}=0.1\ s^{-1}$), until the material fails. The resulting stress–strain curves for FMOC-LG/$C_2^P S_{48}^E C_2^P$ CNs are presented in Figure 4.5B. The shear stress increases more or less linearly with strain, until a point is reached where the composite network fails, resulting in a rapid decrease in shear stress with increasing strain. The values for the critical strain and the stress at which the network fails were extracted from these curves. They are shown as a function of the $C_2^P S_{48}^E C_2^P$ concentration in panels C and D of Figure 4.5, respectively. Within the range investigated, both the critical strain and stress increase with an increase in $C_2^P S_{48}^E C_2^P$ concentration. In other words, the composite networks are more resistant to failure than the single FMOC-LG network. Again, we argue that this is a result of the more homogeneous deformation of the composite network, which minimizes stress localization. An increase in fracture strength and toughness was also observed in double networks of two types of synthetic, flexible polymers.[34,35] In these systems, the enhanced toughness was ascribed to local damage of the more brittle of the two components, which dissipates energy as sacrificial bonds, thereby protecting the second network from breaking.[36–38] To test whether a similar dissipation mechanism could be acting in our composite networks, we have conducted mechanical hysteresis tests, in which the sample was deformed repeatedly at increasing strain levels. As shown in Figure A4.3 of the Appendix, however, no energy dissipation could be observed in these tests up to the point where fracture occurred. We therefore argue that

68

dissipative mechanisms are less important for the observed strengthening than the reduction of stress localization predicted by the simulations of Zhang et al.[19]

Figure 4.5: *(A) Storage moduli (G′) of the FMOC-LG single network (SN), FMOC-LG/$C_2^P S_{48}^E C_2^P$ composite networks (CNs), the and control as a function of strain (γ). The inset shows an enlarged view showing strain hardening. T = 20°C in all experiments. (B) Stress–strain (σ versus γ) curves of the FMOC-LG SN, $C_2^P S_{48}^E C_2^P$ SN, FMOC-LG/$C_2^P S_{48}^E C_2^P$ CNs, and the control. (C) Average critical strain values (γ_{crit}, n = 3) of the FMOC-LG SN and FMOC-LG/$C_2^P S_{48}^E C_2^P$ CNs as a function of $C_2^P S_{48}^E C_2^P$ concentration (closed black squares) after a constant strain rate of $\dot{\gamma}$=0.1 s^{-1} had been applied. The FMOC-LG concentration was 0.25% (w/v) for all experiments. (D) Average critical stress values (σ_{crit}, n = 3) of the FMOC-LG SN and FMOC-LG/$C_2^P S_{48}^E C_2^P$ CNs as a function of $C_2^P S_{48}^E C_2^P$ concentration (closed black squares) after a constant strain rate of ($\dot{\gamma}$=0.1 s^{-1}) had been applied. The FMOC-LG concentration was 0.25% (w/v) for all experiments. For panels A and B, the control consisted of 0.58% (w/v) C_4^R mixed with 0.25% (w/v) FMOC-LG.*

4.4 Conclusions

Composite networks formed by two fiber-forming components, $C_2^P S_{48}^E C_2^P$ and FMOC-LG, proved to have significantly increased storage moduli, exceeding the sum of the moduli of the individual FMOC-LG and $C_2^P S_{48}^E C_2^P$ networks. The storage modulus of the composite network could be tuned by changing the amount of $C_2^P S_{48}^E C_2^P$ present in the composite network. Furthermore, it was found that strain hardening, a characteristic property of both FMOC-LG and $C_2^P S_{48}^E C_2^P$, disappeared when the two components were combined. Both findings are in line with a recent simulation study done for a fiber network embedded in a soft elastic matrix.[19] The increase in the storage modulus and the disappearance of strain hardening in the composite networks are probably caused by a more affine deformation of the network as non-affine floppy modes are suppressed by the embedding matrix. With this work, we contribute to a fundamental understanding of filamentous composite networks, such as those occurring naturally in biological systems. Ultimately, this understanding should lead to new design strategies for synthetic composite networks with optimized mechanical properties.

Appendix

AFM

Additional control AFM experiments were carried out for dilute FMOC-LG SN, $C_2^P S_{48}^E C_2^P$ SN and FMOC-LG/$C_2^P S_{48}^E C_2^P$ CN samples for a different drying time. The preparation and induction of the solutions was the same as for the AFM experiments presented in the text. After depositing the 5 μL aliquot, we put all samples in a box, in which the humidity was controlled close to saturation to slow down drying. After 10 hours, the samples were taken out of the box and dried further in air overnight. In these control experiments, more fibers were observed in all samples, due to the extended period in which water was present. In all cases, however, fibers characteristic for $C_2^P S_{48}^E C_2^P$ and FMOC-LG can clearly be distinguished and their morphology is the same as at the higher drying rate used for the images in the main text. Note also that the peak force error pictures show the same structure as the height images, but with better resolution.
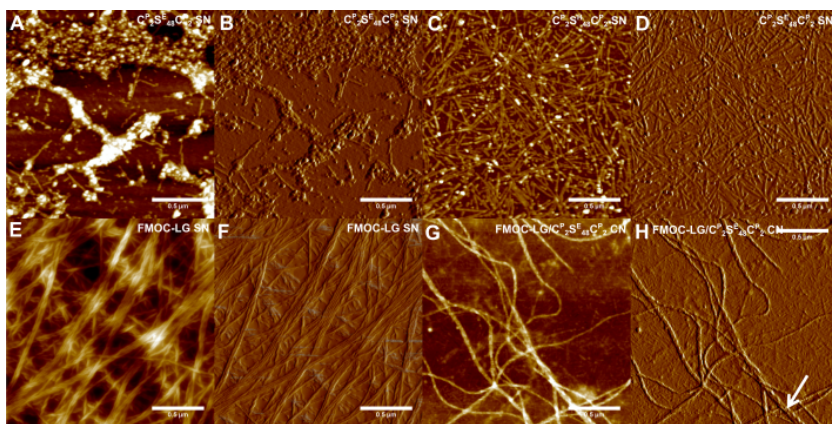
Figure A4.1: *(A, C, E, G) AFM height images of (A,C) $C_2^P S_{48}^E C_2^P$ single network (SN) at 0.05% (w/v), (E) FMOC-LG SN at 0.025% (w/v) and (G) FMOC-LG/$C_2^P S_{48}^E C_2^P$ composite network (CN) at 0.025 and 0.050% (w/v), respectively. (B, D, F, H) Corresponding AFM peak force error images of (B,D) $C_2^P S_{48}^E C_2^P$ SN at 0.05% (w/v), (F) FMOC-LG SN at 0.025% (w/v) and (H) FMOC-LG/$C_2^P S_{48}^E C_2^P$ CN at 0.025 and 0.050% (w/v), respectively. (H) White arrow indicates FMOC-LG fibers in the FMOC-LG/$C_2^P S_{48}^E C_2^P$ CN. The scalebar indicates 0.5 μm in all images.*
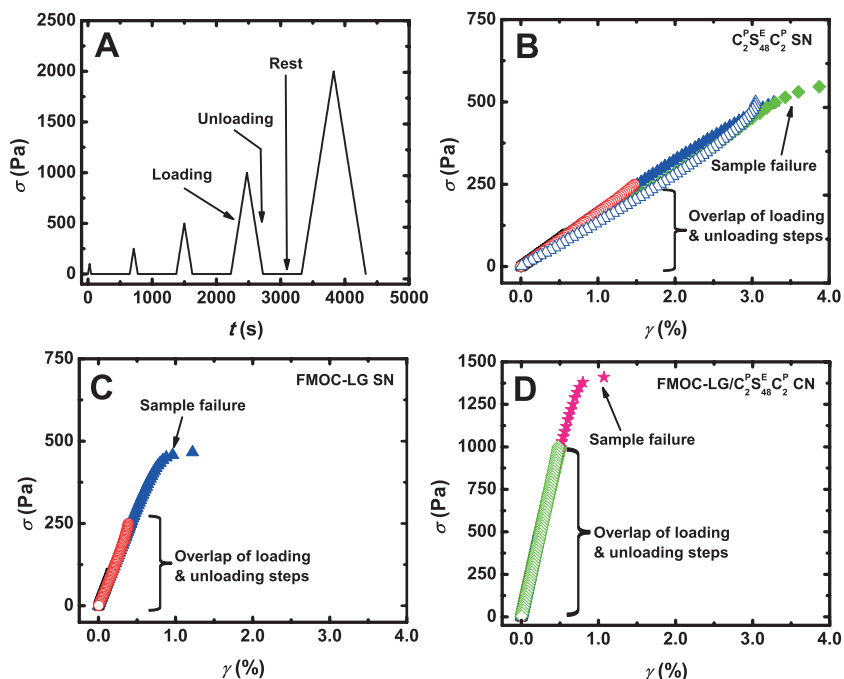
Creep experiments

Creep experiments show an elastic response followed by a slow viscous response for all samples. These results indicate that the fiber networks formed in both single networks and composite networks can relax slowly, probably because of slow dissociation of crosslinks or disentanglement. The relaxation times obtained from the creep curves for the $\mathbf{C_2^P S_{48}^E C_2^P}$ SN, FMOC-LG SN and FMOC-LG/$\mathbf{C_2^P S_{48}^E C_2^P}$ CN are estimated to be 23.3, 6.5 and 13.8 kiloseconds, respectively.
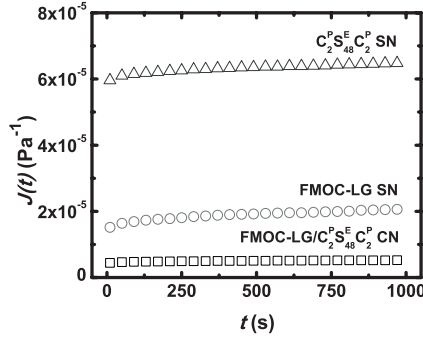
Figure A4.2: *Creep response of $\mathbf{C_2^P S_{48}^E C_2^P}$ single network (SN) at 0.75% (w/v), FMOC-LG SN at 0.25% (w/v) and FMOC-LG/$\mathbf{C_2^P S_{48}^E C_2^P}$ composite network (CN) at 0.25 and 0.75% (w/v), respectively. The applied stress for the $\mathbf{C_2^P S_{48}^E C_2^P}$ SN at 0.75% (w/v) and the FMOC-LG SN at 0.25% (w/v) was 50 Pa, while 250 Pa was used for the FMOC-LG/$\mathbf{C_2^P S_{48}^E C_2^P}$ CN at 0.25 and 0.75% (w/v), respectively.*

Hysteresis experiments

Hysteresis experiments were carried out to get insight into possible dissipative mechanisms in the networks upon deformation. A loading/unloading cycle consists of a loading step, in which the stress is increased linearly until a certain stress (σ_{crit}) is reached, immediately followed by the unloading step, in which the stress is linearly decreased to 0. The rate at which the stress is increased and decreased in all steps is fixed at 4 Pa.s^{-1}. The resting period between subsequent loading/unloading cycles is 100 s. The loading/unloading cycles used were 100 Pa, 250 Pa, 500 Pa, 1000 Pa and 2000 Pa, until sample failure occurred. For all cases, until sample failure, the unloading curves follow the trajectories of the loading curves (Figure A4.3A-C), which indicates that no stress dissipation occurs in the samples. These results imply that in both single and composite networks, no internal damage is inflicted by the loading/unloading cycles, before sample failure occurs.

Figure A4.3: *(A) Imposed stress (σ) during loading and unloading steps in the hysteresis experiments. (B) Hysteresis experiments for $C_2^P S_{48}^E C_2^P$ single network (SN) at 0.75% (w/v). (C) Hysteresis experiments for FMOC-LG SN at 0.25% (w/v). (D) Hysteresis experiments for FMOC-LG/$C_2^P S_{48}^E C_2^P$ composite network (CN) at 0.25% (w/v) and 0.75% (w/v), respectively. Closed symbols indicate loading steps, and open symbols indicate unloading steps. The loading and unloading steps are colour-coded as follows: 100 Pa (black squares), 250 Pa (red circles), 500 Pa (blue triangles), 1000 Pa (green diamonds) and 2000 Pa (pink stars). Stress is imposed on the samples by linear ramping at a speed of 4 Pa.s^{-1}. All data is shown until sample failure occurs.*

References

(1) Liu, J.; Koenderink, G. H.; Kasza, K. E.; MacKintosh, F. C.; Weitz, D. A. *Phys. Rev. Lett.* **2007**, *98*, 198304.

(2) Lin, Y.-C.; Yao, N. Y.; Broedersz, C. P.; Herrmann, H.; MacKintosh, F. C.; Weitz, D. A. *Phys. Rev. Lett.* **2010**, *104*, 058101.

(3) Heussinger, C.; Frey, E. *Phys. Rev. Lett.* **2006**, *97*, 105501.

(4) Head, D. A.; Levine, A. J.; MacKintosh, F. C. *Phys. Rev. Lett.* **2003**, *91*, 108102.

(5) Broedersz, C. P.; Sheinman, M.; MacKintosh, F. C. *Phys. Rev. Lett.* **2012**, *108*, 078102.

(6) Broedersz, C. P.; Mao, X.; Lubensky, T. C.; MacKintosh, F. C. *Nat. Phys.* **2011**, *7*, 983–988.

(7) Gardel, M. L.; Shin, J. H.; MacKintosh, F. C.; Mahadevan, L.; Matsudaira, P.; Weitz, D. A. *Science* **2004**, *304*, 1301–1305.

(8) Lieleg, O.; Claessens, M. M. A. E.; Heussinger, C.; Frey, E.; Bausch, A. R. *Phys. Rev. Lett.* **2007**, *99*, 088102.

(9) Broedersz, C. P.; Kasza, K. E.; Jawerth, L. M.; Münster, S.; Weitz, D. A.; MacKintosh, F. C. *Soft Matter* **2010**, *6*, 4120–4127.

(10) Kouwer, P. H. J.; Koepf, M.; Le Sage, V. A. A.; Jaspers, M.; van Buul, A. M.; Eksteen-Akeroyd, Z. H.; Woltinge, T.; Schwartz, E.; Kitto, H. J.; Hoogenboom, R., et al. *Nature* **2013**, *493*, 651–655.

(11) Storm, C.; Pastore, J. J.; MacKintosh, F. C.; Lubensky, T. C.; Janmey, P. A. *Nature* **2005**, *435*, 191–194.

(12) Onck, P.; Koeman, T.; Van Dillen, T.; Van der Giessen, E. *Phys. Rev. Lett.* **2005**, *95*, 178102.

(13) Huisman, E. M.; Storm, C.; Barkema, G. T. *Physical Review E: Stat., Nonlinear, Soft Matter Phys.* **2010**, *82*, 061902.

(14) Lin, Y.-C.; Koenderink, G. H.; MacKintosh, F. C.; Weitz, D. A. *Soft Matter* **2011**, *7*, 902–906.

(15) Rombouts, W. H.; Colomb-Delsuc, M.; Werten, M. W. T.; Otto, S.; de Wolf, F. A.; van der Gucht, J. *Soft Matter* **2013**, *9*, 6936–6942.

(16) Das, M.; MacKintosh, F. C. *Physical Review E: Stat., Nonlinear, Soft Matter Phys.* **2011**, *84*, 061906.

(17) Pelletier, V.; Gal, N.; Fournier, P.; Kilfoil, M. L. *Phys. Rev. Lett.* **2009**, *102*, 188303.

(18) Brangwynne, C. P.; MacKintosh, F. C.; Kumar, S.; Geisse, N. A.; Talbot, J.; Mahadevan, L.; Parker, K. K.; Ingber, D. E.; Weitz, D. A. *J. Cell Biol.* **2006**, *173*, 733–741.

(19) Zhang, L.; Lake, S. P.; Barocas, V. H.; Shephard, M. S.; Picu, R. C. *Soft matter* **2013**, *9*, 6398–6405.

(20) Adams, D. J.; Mullen, L. M.; Berta, M.; Chen, L.; Frith, W. J. *Soft Matter* **2010**, *6*, 1971–1980.

(21) Adams, D. J.; Butler, M. F.; Frith, W. J.; Kirkland, M.; Mullen, L.; Sanderson, P. *Soft Matter* **2009**, *5*, 1856–1862.

(22) Tang, C.; Ulijn, R. V.; Saiani, A. *Langmuir* **2011**, *27*, 14438–14449.

(23) Vegners, R.; Shestakova, I.; Kalvinsh, I.; Ezzell, R. M.; Janmey, P. A. *J. Pept. Sci.* **1995**, *1*, 371–378.

(24) Zhang, Y.; Gu, H.; Yang, Z.; Xu, B. *J. Am. Chem. Soc.* **2003**, *125*, 13680–13681.

(25) Tang, C.; Ulijn, R. V.; Saiani, A. *Eur. Phys. J. E: Soft Matter Biol. Phys.* **2013**, *36*, 1–11.

(26) Johnson, E. K.; Chen, L.; Kubiak, P. S.; McDonald, S. F.; Adams, D. J.; Cameron, P. J. *Chem. Commun.* **2013**, *49*, 8698–8700.

(27) Jayawarna, V.; Ali, M.; Jowitt, T. A.; Miller, A. F.; Saiani, A.; Gough, J. E.; Ulijn, R. V. *Adv. Mater.* **2006**, *18*, 611–614.

(28) Smith, A. M.; Williams, R. J.; Tang, C.; Coppo, P.; Collins, R. F.; Turner, M. L.; Saiani, A.; Ulijn, R. V. *Adv. Mater.* **2008**, *20*, 37–41.

(29) Werten, M. W. T.; Wisselink, W. H.; Jansen-van den Bosch, T. J.; de Bruin, E. C.; de Wolf, F. A. *Protein Eng.* **2001**, *14*, 447–454.

(30) Martens, A. A.; Portale, G.; Werten, M. W. T.; de Vries, R. J.; Eggink, G.; Cohen Stuart, M. A.; de Wolf, F. A. *Macromolecules* **2009**, *42*, 1002–1009.

(31) Martens, A. A.; van der Gucht, J.; Eggink, G.; de Wolf, F. A.; Cohen Stuart, M. A. *Soft Matter* **2009**, *5*, 4191–4197.

(32) Werten, M. W. T.; Teles, H.; Moers, A. P. H. A.; Wolbert, E. J. H.; Sprakel, J.; Eggink, G.; de Wolf, F. A. *Biomacromolecules* **2009**, *10*, 1106–1113.

(33) Alsteens, D.; Dupres, V.; Yunus, S.; Latgé, J.-P.; Heinisch, J. J.; Dufrêne, Y. F. *Langmuir* **2012**, *28*, 16738–16744.

(34) Sun, J. Y.; Zhao, X.; Illeperuma, W. R. K.; Chaudhuri, O.; Oh, K. H.; Mooney, D. J.; Vlassak, J. J.; Suo, Z. *Nature* **2012**, *489*, 133–136.

(35) Gong, J. P.; Katsuyama, Y.; Kurokawa, T.; Osada, Y. *Adv. Mater.* **2003**, *15*, 1155–1158.

(36) Brown, H. R. *Macromolecules* **2007**, *40*, 3815–3818.

(37) Webber, R. E.; Creton, C.; Brown, H. R.; Gong, J. P. *Macromolecules* **2007**, *40*, 2919–2927.

(38) Gong, J. P. *Soft Matter* **2010**, *6*, 2583–2590.

76

Linear and Nonlinear Properties of Collagen-inspired Hydrogels with Both Physical and Chemical Crosslinks

5

Abstract

Hydrogels are widely used in food products and biomedical applications. One major drawback of most hydrogels is their poor mechanical strength, which limits their application in mechanically demanding applications. In this chapter we study the rheological properties of hybrid collagen-inspired polymer hydrogels, prepared by combining chemical and physical crosslinks. We find that these hybrid hydrogels have significantly enhanced storage moduli, exceeding the sum of the moduli of the separate physical and chemical hydrogels. These hybrid hydrogels were also more fracture resistant than the physical hydrogels. In addition, weak strain hardening effects were observed in both chemical and hybrid hydrogels, which can be ascribed to the nonlinear stretching modulus of the polymer chains within the hydrogel.

5.1 Introduction

Hydrogels are crosslinked polymer networks with a high water content, and are widely applied as drug delivery systems, wound care materials, tissue engineering scaffolds, and food products.[1–7] Hydrogels can be formed by introducing chemical crosslinks, physical crosslinks, or by combinations of both types of crosslinks. Chemical crosslinks are permanent in nature, and can therefore not be remodelled. Physical hydrogels can be remodelled after gel formation, because these hydrogels consist of crosslinks with finite lifetimes, and can be sensitive to various triggers such as pH, temperature, and ionic strength.[8–13] One important limitation of most hydrogels is the poor mechanical strength in comparison to natural tissues, which makes them unsuitable for applications in which considerable mechanical loading occurs. However, there are various examples of strong polymeric materials, which are on the verge of overcoming these limitations. Most of these materials contain combinations of polymers with chemical and physical crosslinks, or fibers, resulting in significantly stronger materials.[14–16] In this chapter, we created hybrid hydrogels of collagen-inspired block copolymers, $T_9C_4^RT_9$, in which both physical and chemical crosslinks are present. The design of $T_9C_4^RT_9$ is inspired by natural collagen, and it can be produced biosynthetically.[13] Physical hydrogels of $T_9C_4^RT_9$ can be formed by self-assembly of three temperature-responsive end-blocks, T_9, into triple helices $(T_9)_3$, when the temperature is reduced. Each $T_9C_4^RT_9$ molecule consists of two temperature-reponsive end-blocks T_9, and a hydrophilic random-coil middle-block C_4^R, which acts as a spacer. Chemical crosslinks can be introduced by covalent coupling of lysine residues, of which 12 are present in each middle-block, with glutaraldehyde. One intriguing question is whether the pathway in which chemical crosslinks are introduced to the physical network matters. Both chemical and physical crosslinks can be formed at the same time or separately from each other. In this chapter, we study linear and nonlinear mechanical properties of hybrid collagen-inspired polymer hydrogels, prepared along different kinetic pathways.

5.2 Experimental Section

5.2.1 Materials

The protein polymer, $T_9C_4^RT_9$, was produced biosynthetically in the yeast *Pichia pastoris*. The biosynthetical production of this polymer has been published previously.[13] Fed-batch fermentations were performed in

2.5 L Bioflo 3000 bioreactors (New Brunswick Scientific) according to the procedures described previously.[13] $T_9C_4^RT_9$ was purified from the fermentation broth by two consecutive ammonium sulfate precipitation steps followed by desalting and lyophilization. Glutaraldehyde (Sigma) was used as received.

5.2.2 Methods

Sample preparation

For the physical hydrogels, solutions of $T_9C_4^RT_9$ were prepared by dissolving it in 1 mL 10 mM filtered phosphate buffer (pH 7.0) at 50 °C for 45 minutes. For the chemical and combined hydrogels, a 8.4, 12.6 and 16.8 molar excess of glutaraldehyde to lysine residues was used. Stock solutions of 70 mM glutaraldehyde were prepared by mixing it with 10 mM filtered phosphate buffer (pH 7.0) and stored at -20 °C. To prepare chemical and combined hydrogels, the procedure of preparation of $T_9C_4^RT_9$ solutions is similar, however smaller volumes of 10 mM filtered phosphate buffer (pH 7.0) were used to dissolve $T_9C_4^RT_9$. Subsequently, the $T_9C_4^RT_9$ solution was mixed with a given amount of 70 mM glutaraldehyde solution in the rheometer to get a total volume of 1 mL. For all experiments the $T_9C_4^RT_9$ concentration was fixed at 1.4 mM. Physical networks of $T_9C_4^RT_9$ were formed at 20 °C for 15 hours, whereas the chemical networks were formed at 35 °C for 15 hours. The combined networks were formed in two ways: a one-step method and a two-step method. In the one-step method, the chemical network and the physical network are formed at the same time at 20 °C for 12 hours. In the two-step method first the chemical network is formed at 35 °C for 6 hours, after which the physical network is formed at 20 °C for 6 hours.

Rheology

Rheological measurements were performed with an Anton Paar Physica MCR 301 rheometer equipped with a Couette geometry (1 mL). A solvent trap was used to minimize the effects of evaporation. The temperature was controlled by a Peltier element. Samples were allowed to form a gel *in situ*. A time sweep was recorded to follow *in situ* gel formation (f=1 Hz, and γ=0.1 %), whereby the storage (G') and loss moduli (G'') were measured for 15 hours. Subsequently, viscoelastic behaviour of the steady state gel was characterised by a frequency sweep (ω=0.01-100 rad.s^{-1}, and γ=0.1 %). Finally, nonlinear behaviour of the samples was evaluated with a hysteresis

test. In this test the samples were subjected to 10 loading/unloading cycles, in which the strain was increased stepwise with 30 or 40%, to reach a maximum strain of 300 or 400%, at a constant strain rate ($\dot{\gamma}=0.1\ s^{-1}$). Each cycle consists of a loading step, followed by an unloading step and a 30 minute rest period.

5.3 Results and Discussion

5.3.1 Linear rheology

In this study mechanical properties of physical, chemical and combined $\mathbf{T_9C_4^R T_9}$ gels were investigated. An overview of different methods that can be used to form physical, chemical, and combined $\mathbf{T_9C_4^R T_9}$ gels is presented in Figure 5.1.
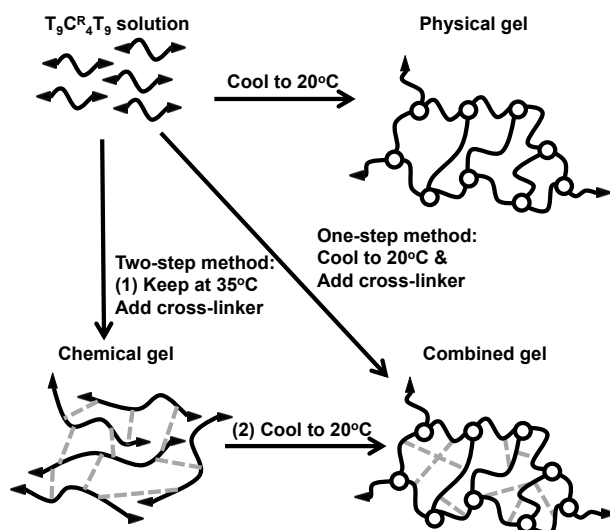
Figure 5.1: *Schematic representation of various methods to prepare $\mathbf{T_9C_4^R T_9}$ hydrogels. The triangles represent free temperature-responsive end-blocks ($\mathbf{T_9}$), the lines represent random-coil middle-blocks ($\mathbf{C_4^R}$) containing lysine residues, the circles represent triple helices (($\mathbf{T_9}$)$_3$, physical crosslinks), and the dashed lines represent chemical crosslinks formed by glutaraldehyde.*

Combined $\mathbf{T_9C_4^R T_9}$ gels were prepared in two different ways: via the one-step method and the two-step method. In the one-step method, the chemical network and the physical network are formed at the same time at 20°C for 12 hours. In the two-step method first the chemical network is

formed at 35 °C for 6 hours, and subsequently the physical network is formed at 20 °C for 6 hours. It should be noted that at 35 °C physical crosslinks are present, because at the chosen $T_9C_4^RT_9$ concentration the midpoint melting temperature of the $(T_9)_3$ triple helices is around 39 °C. However, detectable network formation will only occur well below this temperature. In Figure 5.2A a time sweep of the two methods to form combined gels, the one-step method and the two-step method, is presented. The steady state storage moduli of both methods of preparation are similar after 12 hours of gel development. This result implies that the processes of formation of chemical crosslinks and the self-assembly of $T_9C_4^RT_9$ triple helices (physical crosslinks) do not interfere with each other. Therefore, for the remaining experiments the one-step method is used to prepare the combined networks. The formation of hydrogels by physical, chemical and combined networks of $T_9C_4^RT_9$ is shown in Figure 5.2B for various amounts of added glutaraldehyde (GA). The chemical networks are formed at 35 °C, above the temperature at which gelation by means of triple helix self-assembly occurs.[17] In all cases, steady state was reached within 15 hours. Frequency-dependent storage and loss moduli for physical, chemical and combined networks of $T_9C_4^RT_9$ are shown in Figure 5.2C. For all experiments, the storage modulus is almost independent on frequency, and is much higher than the loss modulus, which indicates that elastic behaviour dominates. In Figure 5.2D average steady state storage moduli of physical, chemical and combined networks of $T_9C_4^RT_9$ as a function of molar excess GA to lysine residues in the C_4^R middle block are shown. The dotted line represents the cumulative values of the chemical and physical networks for basis of comparison. The storage moduli of the chemical networks can be increased and controlled by the amount of GA added. At the lowest amount of GA in the chemical networks (8.4 ME of GA), the storage modulus is still comparable to that of the physical networks, indicating that a high excess of GA is needed to crosslink $T_9C_4^RT_9$ molecules into chemical hydrogels. The storage moduli of the combined networks are up to two times higher than the sum of the moduli for the separate networks. This enhancement indicates that the modulus is not simply proportional to the number of crosslinks, and is probably due to the fact that the gel is relatively close to the critical gel point at this concentration. Close to the percolation point, the modulus increases much more steeply with the degree of crosslinking, because the fraction of monomers included in the gel increases as more crosslinks are formed.[17] Furthermore, many T_9 groups form loops which lead to dead ends in the network. They therefore do not contribute to the percolating network,

which leads to weaker gels. Chemical crosslinking may lead to the incorporation of these loops into the network, thereby enhancing the elastic modulus. Mechanical properties of chemical networks of $T_9C_4^RT_9$ formed by glutaraldehyde are in agreement with values published previously.[18]
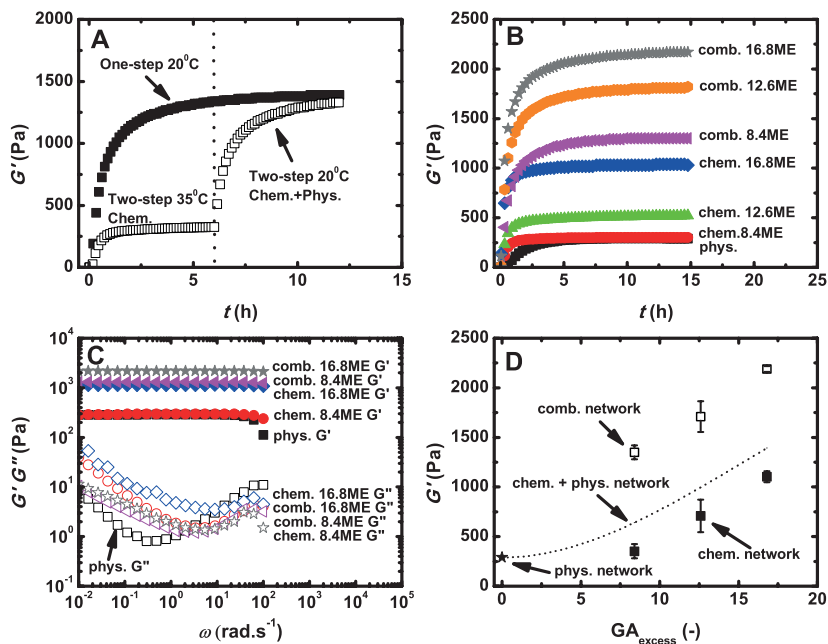

Figure 5.2: *(A) Time sweep of $T_9C_4^RT_9$ combined networks formed by the one-step method (closed squares) and two-step method (open squares). Storage moduli (G′) are plotted as a function of time (f=1 Hz, γ=0.1 %). [$T_9C_4^RT_9$]=1.4 mM and a 8.4 molar excess of glutaraldehyde to $T_9C_4^RT_9$ was used for all experiments. The temperature was varied as indicated. The dotted line represents the temperature change for the two-step method. (B) Time sweep of $T_9C_4^RT_9$ physical, chemical and combined networks. Storage moduli (G′) are plotted as a function of time (f=1 Hz, γ=0.1 %). [$T_9C_4^RT_9$]=1.4 mM for all experiments. The molar excess of glutaraldehyde (GA) to $T_9C_4^RT_9$ is varied as indicated. For physical and combined networks T=20°C and for chemical networks T=35°C. (C) Frequency sweeps of $T_9C_4^RT_9$ physical, chemical and combined networks. Storage moduli (G′, closed symbols) and loss moduli (G″, open symbols) are shown. [$T_9C_4^RT_9$]=1.4 mM for all experiments. The molar excess of glutaraldehyde to $T_9C_4^RT_9$ is varied as indicated. For physical and combined networks T=20°C and for chemical networks T=35°C. (D) Average steady state storage moduli (G′) of $T_9C_4^RT_9$ physical (closed stars), chemical (closed squares) and combined networks (open squares) as a function of the molar excess of glutaraldehyde to $T_9C_4^RT_9$. The dotted line represents the cumulative values of $T_9C_4^RT_9$ physical and chemical networks.*

5.3.2 Nonlinear rheology

The nonlinear rheological behaviour of the hydrogels was evaluated by hysteresis experiments, in which all samples were subjected to a total of ten loading cycles. A loading cycle starts with a loading step, in which the strain is increased at a constant shear rate, directly followed by an unloading step, in which the strain is removed again at the same rate. After this, the sample is left to rest for 30 minutes. With every loading cycle, the strain that is reached at the end of the loading cycle is increased with either 30 or 40%, until a maximum deformation of either 300 or 400% is reached after the tenth loading cycle. Figure 5.3A presents the hysteresis experiment for the physical networks. Not all loading cycles are shown for the sake of clarity. For stains up to 180%, the stress response of the unloading cycle exactly follows that of the loading cycle. This result indicates that up to this point, the physical network is not damaged by the loading cycles. If the strain is increased beyond 180%, hysteresis occurs: the stress response of the unloading cycle does not follow that of the loading curve anymore, indicating that energy is dissipated by damage of the physical network. Hysteresis is already present before total network failure occurs at 210% strain. If the strain is increased further, partial recovery of the physical network is observed. Physical networks of $T_9C_4^RT_9$ are able to recover their initial elastic properties and fracture strength in approximately 5 hours, even after several repeated fracturing cycles.[19] This self-healing capability of $T_9C_4^RT_9$ physical networks has been described previously.[19] In this experiment however, the samples only had a 30 minute resting period in between loading cycles, which explains the partial recovery observed for these samples. At high strains, the end-point of the unloading step does not coincide with the origin of the loading step, which indicates that already during the unloading step recovery of the physical network occurs. Figure 5.3B displays the results for the hysteresis experiment for the chemical networks. At low strains, the stress response of the loading and unloading steps overlap, which is similar to the effects observed with the physical networks. For the chemical networks, fracture occurs at higher stress and strain values than for the physical networks, probably because the chemical crosslinks are stronger than the physical crosslinks. In addition, weak strain hardening effects are observed at higher strain values. Hysteresis experiments for the combined networks are presented in Figure 5.3C. At low strains, similar to the effects observed with the physical and chemical networks, the stress response of the loading and unloading steps overlap. At high strain values, like for the chemical

networks, weak strain hardening is observed. In Figure 5.3A and C recovery after sample failure can be observed. Especially in the case of the combined networks, it should be noted that only partial recovery can occur due to the failure of irreversible chemical crosslinks. The recovery that is observed can be fully attributed to the reformation of physical crosslinks between the $T_9C_4^R T_9$ molecules.
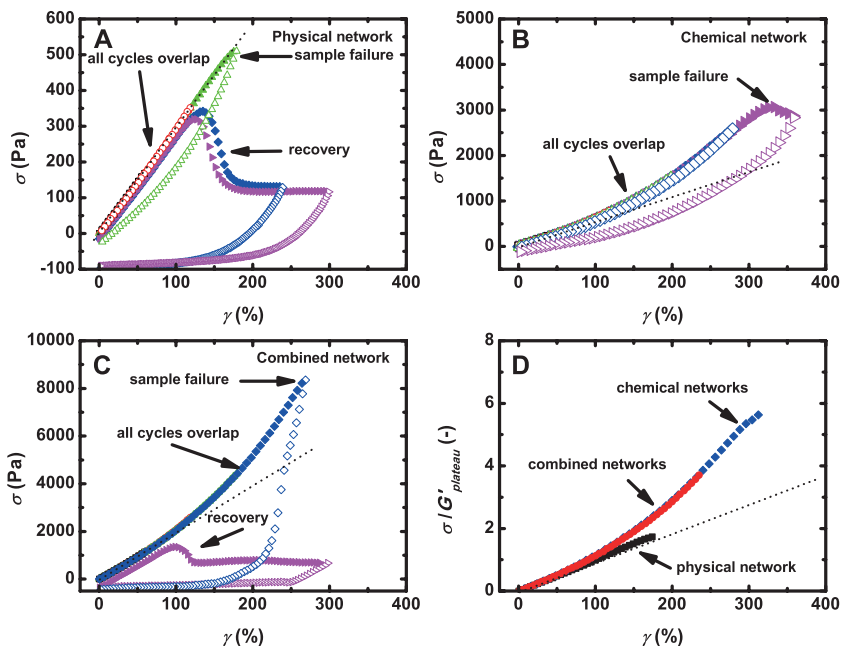

Figure 5.3: *Hysteresis experiments where the stress response (σ) is plotted as a function of strain (γ) during loading (closed symbols) and unloading steps (open symbols) for: (A) Physical networks at 20°C. (B) Chemical networks at 35°C. (C) Combined networks at 20°C. (D) Stress response during the loading step normalized by the plateau modulus of physical, chemical, and combined networks at which network failure occurs as a function of strain. For all chemical and combined networks 12.6 molar excess glutaraldehyde (GA) to $T_9C_4^R T_9$ was used. For all experiments the shear rate during loading and unloading steps was constant, $\dot{\gamma}=0.1\ s^{-1}$) and $\dot{\gamma}=-0.1\ s^{-1}$), respectively. The dotted lines indicate the initial slope in all figures.*

Figure 5.3D displays the stress response of the loading step normalized by the plateau modulus of the loading cycle at which for the first time network failure occurs for physical, chemical, and combined networks. It can be observed that the stress response of the physical networks is linear, while

the stress response of the chemical and combined networks show weak strain hardening. At the single molecule level, strain hardening can occur due to the nonlinear stretching modulus of the polymer chain as a result of its finite stretchability.[20] Strain hardening is not observed for the physical networks, probably because the weak physical crosslinks will disassemble before the stress, which is necessary for this nonlinear effect, is reached.

Estimates for the critical strain and stress values for physical, chemical and combined networks can be deduced from the curves of the loading steps where sample failure occurs (Figure 5.3A-C). It should be noted that already before complete sample failure occurs, damage accumulates in the samples, due to exposure to several loading cycles. This might result in values that are somewhat different from experiments in which sample failure is reached with a single loading cycle, without such a sample history. Critical strain and stress values as a function of the molar excess of GA to lysine residues are presented in Figure 5.4A and Figure 5.4B, respectively. Critical strain values for chemical and combined networks follow a similar trend with increasing excess of GA: they both go through an optimum at a 12.6 molar excess of glutaraldehyde.

The critical strain values found for the chemical networks are significantly higher than the values found for the physical and combined networks. Within the range investigated, the values for the critical strain of the chemical networks are higher than those found for the combined networks. This effect is also clearly visible in Figure 5.3D. However, the critical stress values found for the chemical and combined networks, increase with increasing excess of GA, and can be increased up to an order of magnitude. As can be expected, the critical stress values for combined networks are higher than those found for chemical networks and physical networks, because the contribution of both physical crosslinks and chemical crosslinks lead to a higher fracture resistance. To get an estimate of the dissipated energy, the areas under the stress-strain curves between the physical (0.15 kJ.m^{-3}), chemical (516 kJ.m^{-3}), and combined networks (915 kJ.m^{-3}) at the point of failure were compared (Figure 5.3A-C). This comparison shows that the combined networks are more fracture resistant than the chemical networks and physical networks. This shows that the combination of physical and chemical crosslinks results in an improved fracture toughness of the hydrogels.
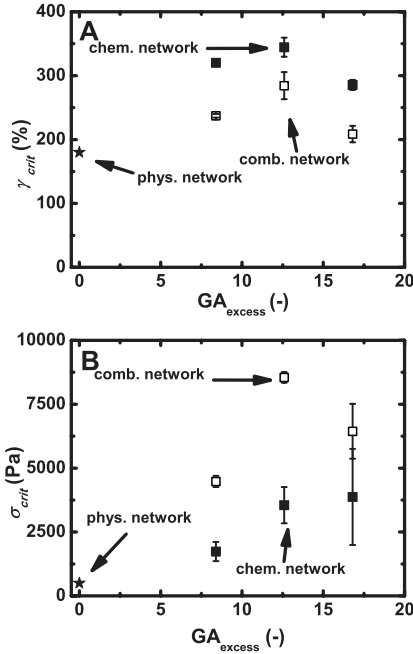
Figure 5.4: *(A) Average critical strain values (γ_{crit}) for $\mathbf{T_9 C_4^R T_9}$ physical (closed star), chemical (closed squares) and combined networks (open squares) as a function of the molar excess of glutaraldehyde (GA) to lysine residues. (B) Average critical stress values (σ_{crit}) for $\mathbf{T_9 C_4^R T_9}$ physical (closed star), chemical (closed squares) and combined networks (open squares) as a function of the molar excess of GA to lysine residues. For all experiments the shear rate during loading step was constant, $\dot{\gamma}$=0.1 s^{-1}. For chemical networks T=35 °C, and for physical and combined networks T=20 °C.*

5.4   Conclusions

Hybrid collagen-inspired polymer hydrogels have significantly enhanced mechanical properties, surpassing the combined contributions of physical and chemical crosslinked hydrogels. The storage modulus of chemical and hybrid hydrogels can be tuned by the amount of the crosslinking agent GA present. It was found that hybrid hydrogels, where both physical and chemical crosslinks were formed, are more fracture resistant than the chemical and physical hydrogels. Furthermore, it was found that weak strain hardening was introduced by the chemical crosslinks in the chemical and combined hydrogels. This appearance of strain hardening probably originates from entropic stretching of $\mathbf{T_9 C_4^R T_9}$ chains in the hydrogel due to the presence of rigid chemical crosslinks.

86

References

(1) Bajpai, A. K.; Shukla, S. K.; Bhanu, S.; Kankane, S. *Prog. Polym. Sci.* **2008**, *33*, 1088–1118.

(2) Hoffman, A. S. *Adv. Drug Delivery Rev.* **2002**, *54*, 3–12.

(3) Kim, S. J.; Hahn, S. K.; Kim, M. J.; Kim, D. H.; Lee, Y. P. *J. Controlled Release* **2005**, *104*, 323–335.

(4) Langer, R.; Tirrell, D. A. *Nature* **2004**, *428*, 487–492.

(5) Li, Y.; Rodrigues, J.; Tomas, H. *Chem. Soc. Rev.* **2012**, *41*, 2193–2221.

(6) Peppas, N. A.; Hilt, J. Z.; Khademhosseini, A.; Langer, R. *Adv. Mater.* **2006**, *18*, 1345.

(7) Zhao, W.; Jin, X.; Cong, Y.; Liu, Y.; Fu, J. *J. Chem. Technol. Biotechnol.* **2013**, *88*, 327–339.

(8) Corrente, F.; Paolicelli, P.; Matricardi, P.; Tita, B.; Vitali, F.; Casadei, M. A. *J. Pharm. Sci.* **2012**, *101*, 256–267.

(9) Jeong, B.; Gutowska, A. *Trends Biotechnol.* **2002**, *20*, 305–311.

(10) Kaneko, Y.; Sakai, K.; Kikuchi, A.; Sakurai, Y.; Okano, T. *Macromol. Symp.* **1996**, *109*, 41–53.

(11) Martens, A. A.; van der Gucht, J.; Eggink, G.; de Wolf, F. A.; Cohen Stuart, M. A. *Soft Matter* **2009**, *5*, 4191–4197.

(12) Petka, W. A.; Harden, J. L.; McGrath, K. P.; Wirtz, D.; Tirrell, D. A. *Science* **1998**, *281*, 389–392.

(13) Werten, M. W. T.; Teles, H.; Moers, A. P. H. A.; Wolbert, E. J. H.; Sprakel, J.; Eggink, G.; de Wolf, F. A. *Biomacromolecules* **2009**, *10*, 1106–1113.

(14) Gong, J. P.; Katsuyama, Y.; Kurokawa, T.; Osada, Y. *Adv. Mater.* **2003**, *15*, 1155–1158.

(15) Sun, J. Y.; Zhao, X.; Illeperuma, W. R. K.; Chaudhuri, O.; Oh, K. H.; Mooney, D. J.; Vlassak, J. J.; Suo, Z. *Nature* **2012**, *489*, 133–136.

(16) Kai, D.; Prabhakaran, M. P.; Stahl, B.; Eblenkamp, M.; Wintermantel, E.; Ramakrishna, S. *Nanotechnology* **2012**, *23*, 095705.

(17) Skrzeszewska, P. J.; de Wolf, F. A.; Werten, M. W. T.; Moers, A. P. H. A.; Cohen Stuart, M. A.; van der Gucht, J. *Soft Matter* **2009**, *5*, 2057–2062.

(18) Skrzeszewska, P. J.; Jong, L. N.; de Wolf, F. A.; Cohen Stuart, M. A.; van der Gucht, J. *Biomacromolecules* **2011**, *12*, 2285–2292.

(19) Skrzeszewska, P. J.; de Wolf, F. A.; Stuart, M. A. C.; van der Gucht, J. *Soft Matter* **2010**, *6*, 416–422.

(20) Storm, C.; Pastore, J. J.; MacKintosh, F. C.; Lubensky, T. C.; Janmey, P. A. *Nature* **2005**, *435*, 191–194.

Reversible Temperature-switching of Hydrogel Stiffness of Co-assembled, Silk-collagen-like Hydrogels

Abstract

Recombinant protein polymers, which can combine different bio-inspired self-assembly motifs in a well-defined block sequence, have large potential as building blocks for making complex, hierarchically structured materials. In this chapter we demonstrate the stepwise formation of thermo-responsive hydrogels by combination of two distinct, orthogonal self-assembly mechanisms. In the first step, fibers are co-assembled from two recombinant protein polymers: (a) a symmetric silk-like block copolymer consisting of a central silk-like block flanked by two soluble random-coil blocks and (b) an asymmetric silk-collagen-like block copolymer consisting of a central random-coil block flanked on one side by a silk-like block and on the other side a collagen-like block. In the second step, induced by cooling, the collagen-like blocks form triple helices, and thereby crosslink the fibers, leading to hydrogels with a thermo-reversibly switchable stiffness. Our work demonstrates how complex self-assembled materials can be formed through careful control of the self-assembly pathway.

6.1 Introduction

Self-assembly has proven to be a very powerful approach for the synthesis of new nano-structured materials. Many well-defined and stable structures have been presented in literature that form spontaneously from carefully designed molecular building blocks.[1,2] However, as the self-assembly process becomes more complex, for example because various self-assembly pathways compete with each other, it becomes increasingly difficult to have control over the final structure.[3–5] In many cases, the final state obtained is not simply the one that corresponds to thermodynamic equilibrium, but rather a non-equilibrium state that depends sensitively on the precise history of the sample. Predicting the outcome of the self-assembly process then becomes rather cumbersome. Yet, nature abounds in examples of complex, hierarchically structured materials resulting from extremely well-controlled self-assembly processes. Crucial elements of natural directed self-assembly processes are (1) the use of highly specific interactions, which allow for selective and orthogonal self-assembly even in complex multi-component mixtures of building blocks, and (2) the use of responsive self-assembly motifs, which allow for precise control over the assembly pathway by using external triggers.

In recent years, considerable effort has been made to mimic nature's self-assembly principles for the development of bio-inspired materials. One promising approach is the use of recombinant protein polymers, which can be produced by genetic engineering.[6–12] These are custom-designed polymers made from natural amino acids. Biological self-assembly motifs, such as those that occur in silk, collagen, or elastin, can be combined to form multi-block copolymers with different functionalities. Moreover, as compared to chemical synthesis, biosynthetic (ribosomal, DNA template-based) production has the advantage that molar mass and monomer sequence of the polymers are precisely defined, and that the resulting products are likely to be bio-compatible so that they have potential for e.g. biomedical applications, tissue engineering, and drug delivery.[6–18] In previous work we described several self-assembling protein polymers.[14,19–21] Protein polymers with silk-like domains were shown to form long, stiff fibers that can entangle to form hydrogels already at very low concentrations.[19,22] Unfolded hydrophilic polymers with collagen-like triple helix forming motifs at their ends formed soft, viscoelastic networks upon cooling.[20,21] More complex examples were also studied; for example, a block copolymer with both silk- and elastin-like blocks formed hydrogels consisting of long fibers that underwent irreversible bundling and

aggregation upon heating due to aggregation of elastin-like domains.[23] Recently, we investigated mixtures of silk- and collagen-like polymers, which formed networks of bundled fibers embedded in a soft viscoelastic gel matrix. These double networks were found to be significantly stiffer and tougher than single networks of separate components.[24] However, control over the final structure was difficult to obtain in these experiments, because the two constituent networks were not interconnected, leading to micro-phase separation and irreversible structural changes upon temperature cycling. The silk-like block copolymer used for this mixture was a triblock copolymer, $C_2^P S_{48}^E C_2^P$.[19,24] It consists of a central silk-like $((Gly\text{-}Ala)_3\text{-}Gly\text{-}Glu)_{48}$ block further denoted as 'S^E', flanked on both sides by a tandem repeat of two identical hydrophilic blocks further denoted as 'C^P', that are present as random-coils under all conditions used by us.[19,25] Each C^P block is 99 amino acids long. The S^E blocks are capable of self-assembling into long stacks of β-rolls upon charge neutralization of the Glu-residues below pH 4, leading to multiple μm long nanofibers and fiber networks.[19] The collagen-like polymer was also a triblock copolymer and is denoted as $T_9 C_4^R T_9$. It consists of a central C_4^R block flanked on both ends by a collagen-like $(Pro\text{-}Gly\text{-}Pro)_9$ block further denoted as 'T_9', which was capable of forming collagen-like $(T_9)_3$ triple helices at low temperature.[21] The behavior and amino acid composition of C^R is identical to that of C^P, only the sequence is different.[21] $T_9 C_4^R T_9$ is capable of network formation at low temperature because the $(T_9)_3$ triple helices act as trimeric network nodes. For the present study, we created a novel molecule that combines $C_4^R T_9$ with a small silk-like N-terminal $((Gly\text{-}Ala)_3\text{-}Gly\text{-}His)_8$ block, S_8^H, designed to be capable of incorporation into the silk-like core of the above-mentioned $C_2^P S_{48}^E C_2^P$ fibers. This molecule, $S_8^H C_4^R T_9$, should thus be able to eliciting temperature-dependent crosslinks between $C_2^P S_{48}^E C_2^P$ fibers through the formation of trimeric $(T_9)_3$ nodes. This approach allows us to form hydrogels in a controlled manner using a two-step approach, in which silk-like fibers are formed first at elevated temperature, and collagen-like triple helical network nodes are formed subsequently, upon cooling.

6.2 Experimental Section

6.2.1 Materials

The symmetric silk-like ($C_2^P S_{48}^E C_2^P$) and asymmetric silk-collagen-like block copolymer ($S_8^H C_4^R T_9$) were produced in *Pichia pastoris*. The production of $C_2^P S_{48}^E C_2^P$ has been reported before.[19,25] The cloning procedure for the

construction of the $S_8^H C_4^R T_9$-encoding gene can be found in the Appendix. The production of $S_8^H C_4^R T_9$ by methanol fed-batch fermentation in 2.5 L Bioflo 3000 bioreactors (New Brunswick Scientific) was as described previously.[26] The purification and characterization of $S_8^H C_4^R T_9$ is described briefly in the Appendix (Figures A6.1 and A6.2). The amino acid sequence of C_4^R and $S_8^H C_4^R T_9$ can be found in the Appendix (Figure A6.3). The protein polymers were purified from the fermentation broth by two consecutive ammoniumsulfate precipitation steps followed by desalting and lyophilization.

6.2.2 Methods

Sample preparation

The sample preparation for all experiments was done at 40 °C. $C_2^P S_{48}^E C_2^P$ and $S_8^H C_4^R T_9$ were dissolved separately in a 30 mM NaOH and 30 mM HCl solution, respectively. Adding 1 M NaOH or 1 M HCl set the pH of both solutions to pH 5.0, before solutions were mixed to get the desired final concentration. The ionic strength of the samples varied between 60 and 65 mM. The final concentration of $C_2^P S_{48}^E C_2^P$ was 1.0% (w/v), and that of $S_8^H C_4^R T_9$ was 8.1% (w/v), in the rheological, light scattering, and electron microscopy experiments. For confocal microscopy, the concentrations of $C_2^P S_{48}^E C_2^P$ and $S_8^H C_4^R T_9$ were fixed at 0.01 and 0.081% (w/v), respectively. These conditions correspond to a 12x molar excess of $S_8^H C_4^R T_9$ to $C_2^P S_{48}^E C_2^P$ in the mixed samples.

Rheology

Rheological measurements were performed with an Anton Paar Physica MCR 501 rheometer equipped with a Couette geometry (1 mL). Due to long duration of experiments, a solvent trap and direct addition of tetradecane oil on top of the sample were used to minimize evaporation. Temperature was controlled by a Peltier element. Samples were allowed to form a hydrogel *in situ*. *In situ* hydrogel formation was followed by measuring a time sweep (f=1 Hz and γ=0.1%), whereby storage (G') and loss moduli (G'') were measured. After steady state was reached, viscoelastic behaviour of the steady state gel was characterised by a frequency sweep (ω=0.01-100 rad.s^{-1}, and γ=0.1% Thereafter, temperature was cycled between 20 °C and 40 °C, to evaluate the reversible thermo-responsive behavior of the hydrogels.

Light scattering

Samples for light scattering were filtered with 0.2 μm filters prior to setting pH to 5.0 with filter sterilized 1 M NaOH and 1 M HCl. Afterward, samples were transferred to a quartz scattering cell. Light scattering was performed with an ALV light scattering setup using an ALV/LSE-5004 multiple tau digital correlator with a HeNe-laser (35 mW) operating at a wavelength of 633 nm. All experiments were carried out with a rotation unit with a rotation speed of 1.0 rpm, to increase sample scattering volume and improve statistics. The quartz scattering cell was surrounded by toluene. Temperature was varied between 20 and 40°C with a Julabo CF41 thermostat. Dynamic light scattering (DLS) experiments designed to follow network formation and investigate the effects of temperature cycling on the gels were carried out at a fixed angle of 90° (q=0.019 nm^{-1}). During static light scattering (SLS) the angle was varied in increasing steps of 5° between 25° (q=0.006 nm^{-1}) and 150° (q=0.026 nm^{-1}). At each angle, scattering intensity was measured and averaged over 10 rotations. For SLS, samples were first equilibrated for 10 hours at 20°C before SLS measurement started, then temperature was increased to 40°C and equilibrated for 10 hours before the next measurement, finally temperature was decreased to 20°C and equilibrated for 10 hours before final measurement. Scattered light intensity was normalized to the Rayleigh ratio (R_θ), which is the absolute measure of scattering intensity by the following formula:

$$R_\theta = \frac{I_{\theta,sample} - I_{\theta,solvent}}{I_{\theta,toluene}} * R_{toluene} * \frac{n^2_{solvent}}{n^2_{toluene}} \tag{6.1}$$

In which I_{sample}, $I_{solvent}$, and $I_{toluene}$ are scattered intensities of sample, solvent and toluene, $R_{toluene}$ is the known Rayleigh ratio of toluene at the wavelength used,[27] and $n_{solvent}$ and $n_{toluene}$ are the refractive indices of the solvent and toluene.

Confocal laser scanning microscopy (CLSM)

For confocal fluorescent imaging protein polymers were labelled. $\mathbf{C^P_2 S^E_{48} C^P_2}$ was labelled at the N-terminus, or at lysine residues present in the $\mathbf{C^P_2}$ blocks, with Alexa Fluor® 647 functionalized with NHS-ester. $\mathbf{S^H_8 C^R_4 T_9}$ was labelled at the N-terminus, or at lysine residues present in the $\mathbf{C^R_4}$ block, with Alexa Fluor® 488 functionalized with NHS-ester. Unreacted dye has been removed by extensive dialysis against citrate (pH 5.0, I=50 mM) and phosphate buffer (pH 8.0, I=50 mM) for $\mathbf{S^H_8 C^R_4 T_9}$ and $\mathbf{C^P_2 S^E_{48} C^P_2}$,

respectively. Attachment of the dyes to the protein polymers was verified with fluorescence correlation spectroscopy (FCS, data not shown). The light path of the microscope was chosen so that the signal from Alexa Fluor® 647 was collected with a 650 nm high pass filter, while the signal from Alexa Fluor® 488 was collected with a 500-550 nm band pass filter. Images were recorded with a confocal laser scanning microscope (Zeiss LSM exciter). The concentration of the protein polymers was 100 times lower than in the other experiments so that individual fibers can be distinguished.

NMR spectroscopy

Experiments were performed on a Bruker Avance III spectrometer, equipped with a conventional Bruker z-gradient inverse ^{1}H/^{13}C/BB 5-mm probe, at 11.7 T B_0 field strength (ωL=500 MHz for ^{1}H). For the analysis of the separate monomers, solutions of $S_8^H C_4^R T_9$ (8.1% (w/v), 1.82 mM) and $C_2^P S_{48}^E C_2^P$ (1.0% (w/v), 0.15 mM) were prepared in 90%/10% (v/v) H$_2$O/D$_2$O. ^{1}H NMR spectra of both solutions were acquired at 40 °C. The residual water signal was suppressed by presaturation (5.0 s at B_1=144 Hz). 16 transients were recorded with a repetition time of 6.5 s. For the $C_2^P S_{48}^E C_2^P$/$S_8^H C_4^R T_9$ mixture, separate solutions of 2.0% (w/v) $C_2^P S_{48}^E C_2^P$ and 16.2% (w/v) $S_8^H C_4^R T_9$ were prepared, and subsequently mixed in equal volumes, to reach a final concentration of 1.0% (w/v) and 8.1% (w/v) for $C_2^P S_{48}^E C_2^P$ and $S_8^H C_4^R T_9$, respectively. A series of 1300 consecutive ^{1}H-NMR spectra of this mixture were then recorded at 40 °C over the course of 47 h, during which gelation took place (~2 m repetition time between successive spectra). Acquisition parameters were identical to those used to acquire spectra of $S_8^H C_4^R T_9$ and $C_2^P S_{48}^E C_2^P$ solutions.

6.3   Results and Discussion

To achieve two-step self-assembly, we synthesized the new molecule $S_8^H C_4^R T_9$. The S_8^H block self-assembles when its histidine residues are deprotonated at pH values above ~6.[26] The T_9-blocks form collagen-like triple helices $(T_9)_3$ at low temperature.[20] The midpoint melting temperature of the $(T_9)_3$ triple helices is around 36 °C at a T_9 concentration corresponding to ~8% (w/v). Detectable network formation will only occur well below this temperature. As essential fiber-forming molecule we used $C_2^P S_{48}^E C_2^P$. Mixtures of these two polymers were studied at pH 5.0, halfway between the pKa values of histidine and glutamic acid, where S_8^H and S_{48}^E are oppositely charged. At this pH, $S_8^H C_4^R T_9$ and $C_2^P S_{48}^E C_2^P$ individually did

not significantly self-assemble into supramolecular structures (see Appendix Figure A6.4). However, in mixed solutions of both block copolymers, we clearly observed formation of fibers with atomic force microscopy (Appendix, Figure A6.5) and electron microscopy (Appendix, Figure A6.6), and at high polymer concentrations, a hydrogel was formed. This indicates that mixed fibers were co-assembled from the two oppositely charged block copolymers. Probably electrostatic attraction contributes to the driving force for co-assembly. Indeed, at very high ionic strength (600 mM), much weaker hydrogels are formed than at low ionic strength (60 mM) (Figure A6.4), indicating that the tendency for co-assembly is weaker when electrostatic interactions are screened. Incorporation of $S_8^H C_4^R T_9$ into $C_2^P S_{48}^E C_2^P$ fibers should lead to formation of fibers with pendant T_9 blocks that can be used for further self-assembly. Figure 6.1 shows a schematic representation of the expected temperature-dependent self-assembly process. Different assembly pathways are presumably followed at different self-assembly temperatures. When polymers are mixed at high temperature, fibers can form without association of T_9 blocks. Mixing of both polymers at low temperature, however, leads to formation of fibers in a solution where T_9 blocks of $S_8^H C_4^R T_9$ are already associated with one another.
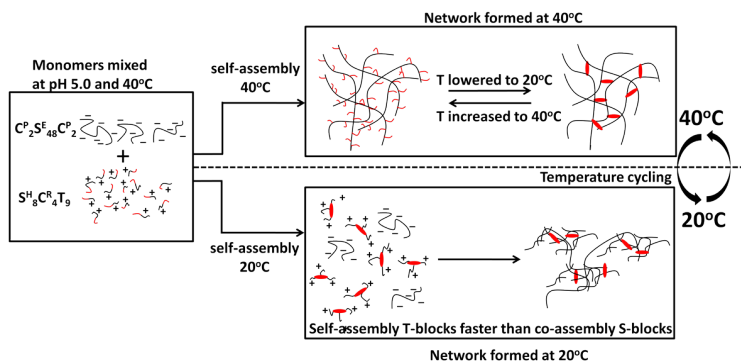
Figure 6.1: *Formation of co-assembled fibers at pH 5.0. Black lines represent compatible* **S** *blocks of* $C_2^P S_{48}^E C_2^P$ *and* $S_8^H C_4^R T_9$. *Red lines correspond to* T_9 *blocks of* $S_8^H C_4^R T_9$, *and red ellipsoids to triple helical (trimolecular) nodes formed by those* T_9 *blocks.*

6.3.1 Hydrogel formation in mixtures of $C_2^P S_{48}^E C_2^P$ and $S_8^H C_4^R T_9$

Mixed hydrogels were prepared by mixing symmetric $C_2^P S_{48}^E C_2^P$ molecules with asymmetric $S_8^H C_4^R T_9$ molecules in such a way that two positively

charged histidine residues are available per negatively charged glutamic acid residue. This charge ratio corresponds to 1.0% (w/v) of $C_2^P S_{48}^E C_2^P$ and 8.1% (w/v) of $S_8^H C_4^R T_9$. This charge ratio was chosen because at lower charge ratios the time needed to reach steady state was found to become extremely long. At a charge ratio of 1 we found that the hydrogel had not yet reached a steady state even after 170 hours. The stacking of the $S_8^H C_4^R T_9$ occurs very slowly, probably because of the high kinetic barrier of this system. First, we studied formation of hydrogels at 40°C, which is somewhat above the melting temperature of triple helices formed by the T_9 blocks present in $S_8^H C_4^R T_9$ (upper pathway in Figure 6.1). In this situation, the self-assembly of the silk blocks proceeds with very little interference of T_9 blocks. The gelation process of the $C_2^P S_{48}^E C_2^P / S_8^H C_4^R T_9$ mixture was followed by measuring the storage modulus in a rheometer. This modulus gradually increased as time proceeded and reached a plateau after approximately 40 hours (Figure 6.2A).
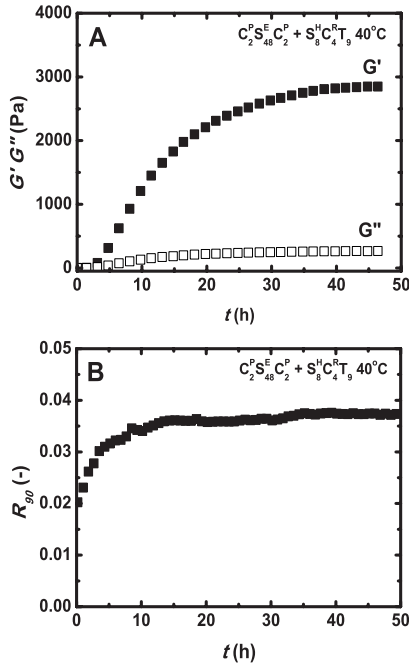

Figure 6.2: *Time-resolved gel formation at 40°C in a mixture of 1.0% (w/v) $C_2^P S_{48}^E C_2^P$ and 8.1% (w/v) $S_8^H C_4^R T_9$, as monitored by rheology and light scattering. (A) storage modulus (G′, closed squares) and loss modulus (G″, open squares). (B) Light scattering. The Rayleigh ratio was measured at 90°.*

We noted that $C_2^P S_{48}^E C_2^P$ alone also shows weak gelation at these conditions (Appendix, Figure A6.4), but this gelation happened much slower and has a final storage modulus that is at least an order of magnitude lower than observed for the mixed system. $S_8^H C_4^R T_9$ alone did not show any signs of gelation at these conditions (Appendix, Figure A6.4). As Figure 6.2B shows, gelation in the mixed system leads to increased scattering.

6.3.2   Thermo-responsive crosslinking of supramolecular $C_2^P S_{48}^E C_2^P / S_8^H C_4^R T_9$ fibers

Next, we studied further network formation resulting from thermo-responsive association of T_9 blocks. After reaching steady state, the temperature of the $C_2^P S_{48}^E C_2^P / S_8^H C_4^R T_9$ hydrogels was alternatingly set to 20 and 40 °C. After each temperature step the hydrogels were equilibrated for 15 hours during rheological experiments, and for 10 hours during light scattering experiments. The storage modulus and light scattering (measured at a q-value of 0.019 nm^{-1}) both responded in a reversible way to the changes in temperature (Figure 6.3A-B), probably as a result of the reversible formation and dissociation of triple helical crosslinks between fibers by the pendant T_9 blocks. The steady state ratio between the storage (G') and loss modulus (G''), $\frac{G'}{G''}$, was found to be 10.7 and 11.0 for 40 °C and 20 °C, respectively. Indicating that at both temperatures solid-like behavior dominates. Upon an increase of temperature, the measured Rayleigh ratio decreased as a result of triple helix dissociation. Conversely, a decrease of temperature resulted in re-association of T_9 blocks into triple helices, and a concomitant increase of the Rayleigh ratio. The dependence of the Rayleigh ratio on the wave vector q was measured at 20 and 40 °C (Figure 6.3C). At both temperatures, a q^{-1} dependence was found, indicating the presence of linear (fibrillar) objects.
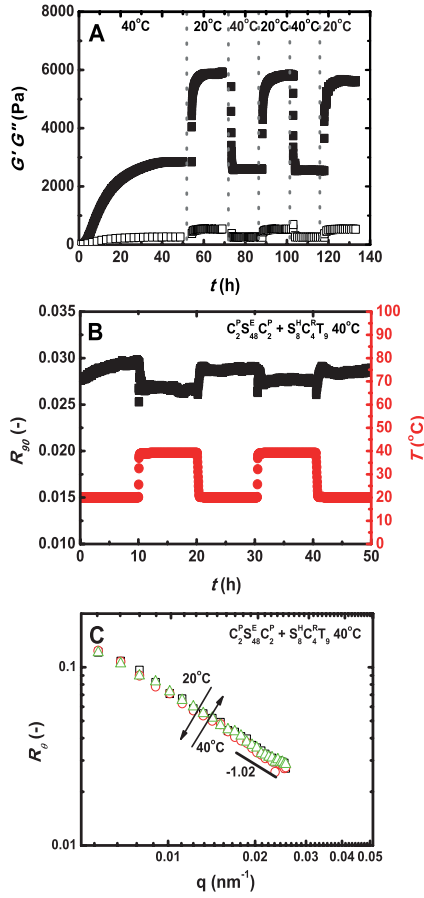
Figure 6.3: *Effect of temperature cycling on gel formation in a mixture of 1.0% (w/v)* $C_2^P S_{48}^E C_2^P$ *and 8.1% (w/v)* $S_8^H C_4^R T_9$. *(A) Storage and loss moduli (G′ closed squares and G″ open squares, respectively). (B) Rayleigh ratio from dynamic light scattering recorded at 90° (black top trace), and simultaneously recorded temperature (red bottom trace). (C) Angle-resolved Rayleigh ratio from static light scattering at different temperatures: the sample was first equilibrated to 20°C (black open squares), then at 40°C (red open circles), and subsequently again at 20°C (green open triangles). Note that the difference between the Rayleigh ratio at these two temperatures is too small to be clearly discerned in this graph.*

6.3.3 Structure of mixed $C_2^P S_{48}^E C_2^P / S_8^H C_4^R T_9$ fibers

The thermo-reversible behavior of the hydrogels observed with rheology and light scattering strongly suggests a role for the T_9 blocks as reversible cross linkers of silk-like fibers. To validate that mixed fibers are indeed co-assembled from $C_2^P S_{48}^E C_2^P$ and $S_8^H C_4^R T_9$, we labelled these two polymers with two different fluorescent dyes: Alexa Fluor 647 and 488, respectively. Figure 6.4A-C shows confocal laser scanning microscopy (CLSM) images of a mixture of labelled $C_2^P S_{48}^E C_2^P$ and $S_8^H C_4^R T_9$, two days after mixing. Both $C_2^P S_{48}^E C_2^P$ (red label) and $S_8^H C_4^R T_9$ (green label) are present in fiber bundles. This confirms that fibers are co-assembled from $C_2^P S_{48}^E C_2^P$ and $S_8^H C_4^R T_9$ at pH 5.0 and 20°C. Note the relatively high green background signal of $S_8^H C_4^R T_9$ (Figure 6.4B), which indicates the presence of a relatively high concentration of labelled $S_8^H C_4^R T_9$ monomers in the solution, probably because $S_8^H C_4^R T_9$ was present in excess. Scanning electron microscopy images of $C_2^P S_{48}^E C_2^P$, $S_8^H C_4^R T_9$, and $C_2^P S_{48}^E C_2^P / S_8^H C_4^R T_9$ hydrogels formed at different temperatures can be found in Appendix Figure A6.6.
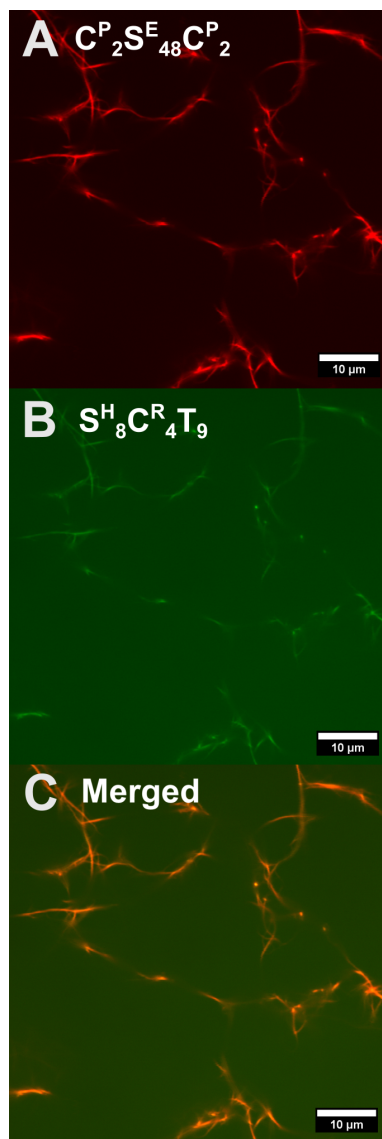
Figure 6.4: *Micrographs of mixtures of $C_2^P S_{48}^E C_2^P$ and $S_8^H C_4^R T_9$ obtained 2 days after mixing. (A) Confocal laser scanning microscopy (CLSM) showing wavelengths above 650 nm, such that the Alexa Fluor 647-labelled $C_2^P S_{48}^E C_2^P$ is visible. (B) CLSM showing wavelengths between 500 and 550 nm, and the Alexa Fluor 488-labelled $S_8^H C_4^R T_9$. The contrast and brightness of this image has been changed for viewing purposes. (C) Superposition of image A and B showing co-localization of $C_2^P S_{48}^E C_2^P$ and $S_8^H C_4^R T_9$. The $C_2^P S_{48}^E C_2^P$ and $S_8^H C_4^R T_9$ concentrations used for CSLM were 0.01 and 0.081% (w/v), respectively. All samples were prepared at $40\,^{\circ}C$.*

6.3.4 Involvement of silk-like blocks in gelation as observed by NMR spectroscopy

We used NMR spectroscopy to obtain details of the gelation process at the molecular level. ^{1}H-NMR spectra of the separate polypeptides as well as of their mixture were acquired. Immediately after mixing of $S_8^H C_4^R T_9$ and $C_2^P S_{48}^E C_2^P$, the NMR spectrum of this mixture is described by a simple sum of the spectra of $S_8^H C_4^R T_9$ and $C_2^P S_{48}^E C_2^P$ in isolation (residual intensity <1%), as would be expected (Appendix, Figure A6.7A-C). After mixing, the NMR spectrum of the mixture gradually changes as a result of co-assembly of the polymers. Figure 6.5 shows details of two spectra of the mixture that are recorded 0 and 47 hours after mixing.
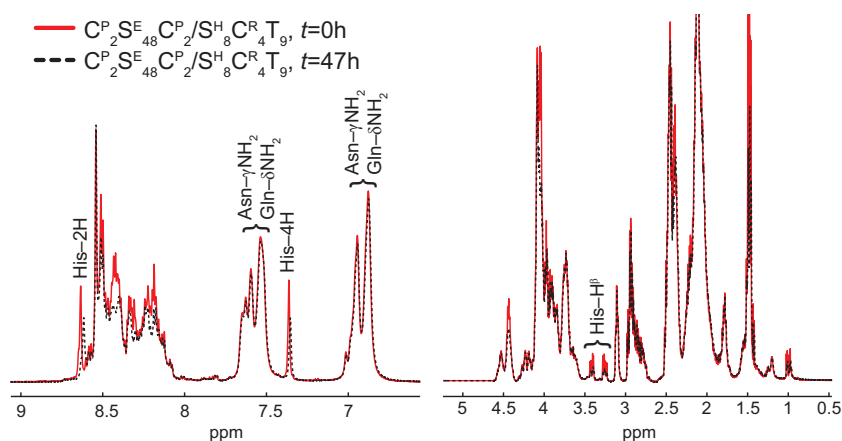
Figure 6.5: ^{1}*H-NMR spectra of mixtures of* $C_2^P S_{48}^E C_2^P$ *and* $S_8^H C_4^R T_9$ *recorded directly after mixing (red solid line), and 47 h after mixing (black dashed line). The temperature was kept at* 40 °C.

Some signals appeared to lose part of their intensity as time proceeds, whereas others did not. Upon incorporation of polypeptides into a rigid fiber network, their immobilization shortens the transverse relaxation times of constituent chemical groups, resulting in broadening of their resonances so that they can effectively disappear from the NMR spectrum. Therefore, amplitude changes are related directly to the progress of the gelation process.[28] The rate of these amplitude changes (Appendix, Figure A6.8) is comparable to the rate of increase of the storage modulus shown in Figure 6.2, confirming that these effects can be directly correlated. Besides changes in amplitude, changes of chemical shift, and thus probably

changes of molecular environment occurred in the course of gelation.

Considering the amino acid composition of $S_8^H C_4^R T_9$ (Appendix, Figure A6.3) and $C_2^P S_{48}^E C_2^P$,[19] we could assign specific resonances in the spectrum of the mixture through comparison with literature data on "random-coil" [1]H chemical shifts of amino acids.[29] Several ^{1}H resonances of histidine residues, which reside only in the S^H blocks of $S_8^H C_4^R T_9$, could be unequivocally assigned: these are the peaks of His-2H (random-coil chemical shift 8.6 ppm) and His-4H (random-coil chemical shift 7.3 ppm), and a symmetric group of signals of His-Hβ (random-coil shifts 3.3, 3.2 ppm). These signals can be observed only in the NMR spectrum of $S_8^H C_4^R T_9$, and not in that of $C_2^P S_{48}^E C_2^P$. In the spectrum of the mixture, we also observe resonances arising from asparagine (random-coil chemical shifts 7.6 and 6.9 ppm for γNH_2) and glutamine (random-coil chemical shifts 7.5 and 6.9 ppm for δNH_2) residues. Both amino acid residues are present in abundance in the random-coil blocks of both $C_2^P S_{48}^E C_2^P$ and $S_8^H C_4^R T_9$, and their resonances can also be seen in the spectra of the individual polypeptides. The aforementioned histidine resonances lose signal intensity (i.e. their peak integrals decrease) and shift. This shows that $S_8^H C_4^R T_9$ is (partly) built into the fiber network. We quantified the change in the integrals of the histidine signals (only those that do not overlap with other signals) between 0 and 48 h after mixing of the block copolymers. For His-4H, 78±3 % of the signal remains after 48 h and for His–Hβ 71±5% of the signal remains. The resonances of asparagine (γNH_2) and glutamine (δNH_2) do not show a proportional decrease in amplitude (the overall amplitude decrease is <2% in 48 h). We conclude that, upon incorporation into fibers, approximately 25% of the silk-like blocks of $S_8^H C_4^R T_9$ are immobilized, leading to the partial disappearance of the histidine signals. However, the random-coil blocks, which contain the asparagine and glutamine residues, remain flexible enough for their signal not to disappear from the NMR spectrum. The fact that the histidine residues only present in the silk-like self-assembly blocks partly disappear, while the random-coil blocks remain visible also demonstrates the incorporation of crystalline S_8^H / S_{48}^E stacks, which are specifically correlated with gel formation. Non-overlapping resonances of residues present in $C_2^P S_{48}^E C_2^P$ but not in $S_8^H C_4^R T_9$ were not found. As a result, estimation of the number of $C_2^P S_{48}^E C_2^P$ monomers that become incorporated into fibers through measurement of the amplitude decrease of such resonances is not possible. However, from confocal microscopy (Figure 6.4), we already know that both polypeptides are incorporated into fibers. Given the 12:1 molar excess of $S_8^H C_4^R T_9$ relative to $C_2^P S_{48}^E C_2^P$, and the fact that ~25% of amplitude of

histidine resonances disappear during gelation, we can conclude that the $S_8^H C_4^R T_9 / C_2^P S_{48}^E C_2^P$ ratio in the fibers is at least 3. This infers that only half of the charges present on $C_2^P S_{48}^E C_2^P$ are neutralized by $S_8^H C_4^R T_9$. By combining the results of the NMR and rheological measurements we can now estimate the fraction of T_9 blocks that is involved in a crosslink between fibers. For semi-flexible fibers a theoretical model proposed by MacKintosh and co-workers[30,31] relates the elastic shear modulus (G') to the persistence length of the fibers (l_p), the mesh size of the fiber network (ξ), and the fiber length between effective crosslinks (L_c):

$$G' \approx \frac{6 k_B T l_p^2}{L_c^3 \xi^2} \tag{6.2}$$

Here, it should be noted that the effective crosslinks can be both entanglements and triple helices that connect different fibers. We determined the persistence length of the fibers by analyzing atomic force microscopy (AFM) images with the open-source software program Easyworm.[32] A representative AFM image and details of this analysis are provided in the Appendix (Figure A6.9). The persistence length was estimated via the mean square of the end-to-end distances as $2.2 \pm 0.3 \mu m$. In previous research, the dimension of the β-roll structure along the long axis of the fiber was determined to be 0.95 nm.[33] With this, we estimate the linear density of the fibers to be 1.16×10^{-10} g.m^{-1} and the total length of fiber per unit volume, ρ_l, as 8.6×10^{-13} m.m^{-3}. We can use this to estimate the mesh size as $\xi \approx \rho_l^{-0.5} \approx 100$ nm. This is in reasonable agreement with the SEM images of the network in Appendix Figure A6.6. With equation 6.2 above and the measured moduli, we then estimate the length between effective crosslinks L_c to be 150 nm at 40°C (when there are only entanglements) and 120 nm at 20°C (when additional triple helical crosslinks are formed). We conclude that the triple helices increase the number of effective crosslinks by roughly 25 percent. Since there is approximately one T_9 block per nm along the fibers, we also conclude that the majority of triple helices does not contribute to crosslinking between fibers, but probably forms loop-like configurations, connecting three T_9 blocks on the same fiber.

6.3.5 Alternative pathways

Up to this point, we discussed formation of $C_2^P S_{48}^E C_2^P / S_8^H C_4^R T_9$ hydrogels at 40°C, when triple helix formation was kept at a low level (Figure 6.1, upper pathway). In the following, we show the formation of

$\mathbf{C_2^P S_{48}^E C_2^P} / \mathbf{S_8^H C_4^R T_9}$ hydrogels at 20 °C, where both self-assembly mechanisms are simultaneously active at a high level. The evolution of gel formation as detected by rheology is presented in Figure 6.6A. Light scattering experiments indicating hydrogel formation are presented in Figure 6.6B.
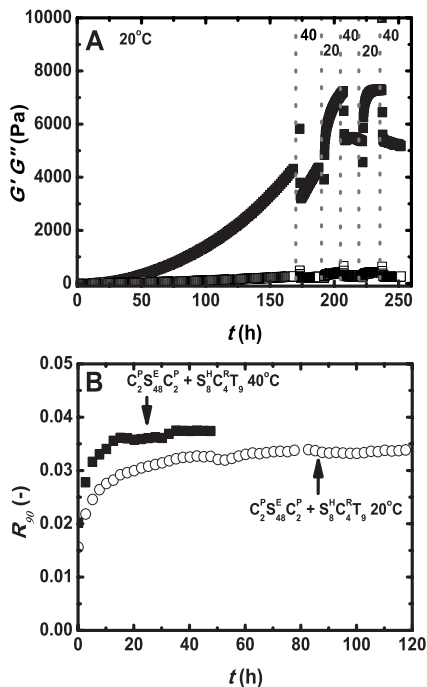
Figure 6.6: *Gel formation over time in mixtures of 1.0% (w/v)* $\mathbf{C_2^P S_{48}^E C_2^P}$ *and 8.1% (w/v)* $\mathbf{S_8^H C_4^R T_9}$*, monitored by rheology and light scattering at 20 °C. (A) Storage modulus (closed squares) and loss modulus (open squares). (B) Dynamic light scattering. The Rayleigh ratio measured at 90°. The evolution of the light scattering signal at 20 °C (lower trace, open circles) are compared to that at 40 °C (upper trace, closed black squares).*

When the hydrogel is formed at 20 °C, a steady state was still not reached after 170 hours. Slow ageing is well known in gelatin hydrogels that cannot reach equilibrium over time,[34,35] and out-of-equilibrium systems like fractal colloidal gels.[36] By contrast, hydrogels formed at 40 °C (where trimer formation by $\mathbf{T_9}$ blocks had much less influence on the assembly process) reached a steady state already after 40 hours (Figure 6.2A). A possible explanation for the differences observed at the different temperatures, is that at 20 °C, the co-assembly of fibers from the silk-like blocks in $\mathbf{C_2^P S_{48}^E C_2^P}$ and

104

$S_8^H C_4^R T_9$ competes with the crosslinking of several **S** blocks by formation of $(T_9)_3$ trimers. This competition may lead to non-equilibrium structures that relax only very slowly (Figure 6.1, lower pathway).

Interestingly, we find that temperature cycling between 20 and 40 °C significantly speeds up equilibration of hydrogels as reflected by the storage modulus (Figure 6.6A). Already after a few temperature cycles, a steady state was reached (Figure 6.6A), and towards the end of the temperature cycling experiments, reversible behavior was observed also in this hydrogel (comparable to Figure 6.3A). We hypothesize that after melting of the triple helical nodes, $(T_9)_3$, the fibers can relax faster, and thereby allow the system to reach the state of thermodynamic equilibrium faster. Temperature cycling has also been used to speed up crystal growth by promoting Ostwald ripening.[37,38]

6.4 Conclusions

We have demonstrated co-assembly of two bio-inspired protein polymers into thermo-reversibly cross-linked fiber gels. A symmetric silk-like protein polymer containing a charged silk-like assembly motif was mixed with an asymmetric silk-collagen-like protein polymer containing an oppositely charged silk-like assembly motif and a trimer-forming motif. This approach allowed us to carefully control the self-assembly, by sequential activation of both motifs. Self-assembly of silk-like motifs led to formation of long fibers. Upon cooling, these fibers were reversibly cross-linked due to triple helix formation of collagen-like motifs, leading to hydrogels with thermo-switchable stiffness. By contrast, when two self-assembly motifs were activated simultaneously, non-equilibrium structures were obtained, that could only be driven towards an equilibrium state by extensive temperature cycling. This work demonstrates how orthogonal self-assembly motifs that can be activated individually, can be used for the design of complex, hierarchically structured materials. Bio-inspired recombinant protein polymers are very suitable building blocks for achieving this, and we anticipate that our findings will inspire new designs for even more complex assemblies.

Appendix

Construction of a *P. pastoris* strain for production of $S_8^H C_4^R T_9$

The vector pMTL23-$C_4^R T_9$ was constructed analogously to the previously described pMTL23-$T_9 C_4^R T_9$,[21] and was digested with *Dra*III/*Van*91I to release the $C_4^R T_9$ insert. A double-stranded adapter with *Xho*I/*Eco*RI overhanging ends was prepared by annealing of oligonucleotides:

5′-TCGAGAAGAGAGAAGCTGAAGCTGGTCTCGGTGCTGGTGCACCCGG-TGCTGGTGCCTAAG-3′ and

5′-AATTCTTAGGCACCAGCACCGGGTGCACCAGCACCGAGACCAGCTT-CAGCTTCTCTCTTC-3′

and was ligated into *Xho*I/*Eco*RI-digested vector pMTL23ΔBsaI.[26] After linearization of the resulting vector with *Dra*III and dephosphorylation, the *Dra*III/*Van*91I-digested $C_4^R T_9$ fragment was inserted. The plasmid so obtained was linearized with *Bsa*I and dephosphorylated. The S_8^H blocks were generated as reported before for S_{24}^H,[26] and were ligated as *Bsa*I/*Ban*I-fragments into the *Bsa*I-linearized vector to obtain pMTL23-$S_8^H C_4^R T_9$. The $S_8^H C_4^R T_9$ insert was then cloned into *P. pastoris* expression vector pPIC9 via *Xho*I/*Eco*RI. The resulting vector pPIC9-$S_8^H C_4^R T_9$ was linearized with *Sal*I and used to transform *P. pastoris* GS115 by electroporation, as described previously.[13]

Purification $S_8^H C_4^R T_9$
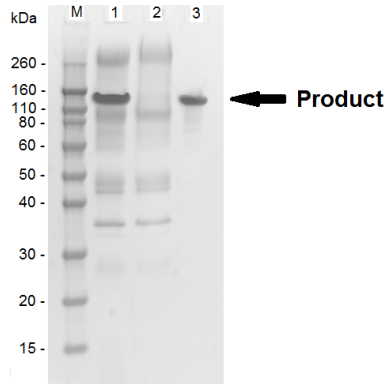
Figure A6.1: *SDS-PAGE of* $S_8^H C_4^R T_9$ *samples obtained after purification. (M) Protein marker, (1) cell-free fermentation broth, (2) Supernatant of the first 40% ammonium sulfate precipitation step, (3) Pellet after 2x 40% ammonium sulfate precipitation steps.*

Figure A6.2: *MALDI-TOF of purified* $S_8^H C_4^R T_9$*, showing molecular ions carrying single, double and higher charges.*

Figure A6.3: *Amino acid sequence of* $S_8^H C_4^R T_9$*. The* S_8^H *block is shown in red, the* C_4^R *block is shown in light blue, and the* T_9 *block is highlighted in green. Expected mass: 44,324 Da.*

Rheological controls

The gelation properties of $C_2^P S_{48}^E C_2^P$ and $S_8^H C_4^R T_9$ were studied separately at pH 5.0, which is in between the pKa-values of $C_2^P S_{48}^E C_2^P$ and $S_8^H C_4^R T_9$, 4.1 and 6.0, respectively. We find that, at pH 5.0, well above its pKa, $C_2^P S_{48}^E C_2^P$, is also able to form gels, however these hydrogels are much weaker and are formed more slowly. Possibly, at pH 5.0, a small fraction of S^E blocks is still protonated and initiates the nucleation step of $C_2^P S_{48}^E C_2^P$ self-assembly. After 48 hours, the temperature was decreased to 20 °C, which resulted in a small increase of the storage modulus. Former work done on this system at low pH showed that the storage modulus of $C_2^P S_{48}^E C_2^P$ hydrogels was independent of temperature between 20 and 30 °C, and increased with temperature above 30 °C.[19] It should be noted that the $C_2^P S_{48}^E C_2^P$ gels in both cases were formed at different pH, above and below the pKa of glutamic acid residues. This can have a considerable impact on the structure of the fiber gels, resulting in different temperature-dependent behaviour. $S_8^H C_4^R T_9$ did not form gels at pH 5.0 and 40 °C within 48 hours. As an extra control experiment, hydrogel formation of the combination of $C_2^P S_{48}^E C_2^P$ with free C_4^R polymer at pH 5.0 was studied. C_4^R is a hydrophilic random-coil that remains soluble at a wide range of temperature and pH. The same molar excess of C_4^R to $C_2^P S_{48}^E C_2^P$ (12:1) was used as in the $C_2^P S_{48}^E C_2^P / S_8^H C_4^R T_9$ mixtures. It can be observed that the addition of C_4^R resulted in a slightly increased storage modulus after 48 hours. This observation is in line with previous observations:[24] the $C_2^P S_{48}^E C_2^P$ fibers are bundled by depletion attraction resulting in higher observed moduli. This small effect cannot explain the much stronger effect in $C_2^P S_{48}^E C_2^P / S_8^H C_4^R T_9$ mixtures. It can therefore be concluded that both $C_2^P S_{48}^E C_2^P$ and $S_8^H C_4^R T_9$ are essential for the formation of strong hydrogels at pH 5.0. Finally, a mixture of $C_2^P S_{48}^E C_2^P / S_8^H C_4^R T_9$ at high ionic strength (I=600 mM) was studied. Sodium chloride was added to the mixture to reach a final salt concentration of 600 mM after the pH was adjusted to 5.0. It can be observed that after 2 days the storage modulus is significantly lower than the hydrogels at low ionic strength (I=60 mM). After the temperature was reduced, a slight increase in modulus is observed similar to the increase observed with $C_2^P S_{48}^E C_2^P$ alone. These observations indicate that electrostatic attraction contributes to the co-assembly process of the two oppositely charged protein polymers. This attraction is screened at high salt concentration.
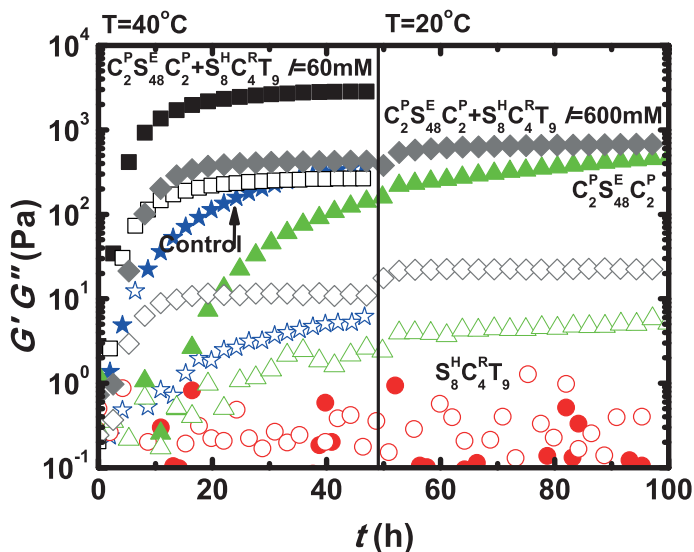
Figure A6.4: *Time-resolved progress of gel formation monitored with rheology for the control experiments at pH 5.0: $C_2^P S_{48}^E C_2^P$ alone (green triangles), $S_8^H C_4^R T_9$ alone (red circles), mixture of $C_2^P S_{48}^E C_2^P$ and C_4^R (control, blue stars), mixture $C_2^P S_{48}^E C_2^P / S_8^H C_4^R T_9$ low ionic strength (I=60 mM, black squares), mixture $C_2^P S_{48}^E C_2^P / S_8^H C_4^R T_9$ high ionic strength (I=600 mM, grey diamonds). Storage moduli (G', closed symbols) and loss moduli (G'', open symbols). Only for $C_2^P S_{48}^E C_2^P$, $S_8^H C_4^R T_9$, and the mixture $C_2^P S_{48}^E C_2^P / S_8^H C_4^R T_9$ high ionic strength (I=600 mM) the experiment was continued after 48 hours at decreased temperature. For all experiments the concentrations of $C_2^P S_{48}^E C_2^P$ and $S_8^H C_4^R T_9$ used were 1.0 and 8.1% (w/v), respectively.*

Atomic force microscopy (AFM)

Samples for AFM were prepared by mixing $C_2^P S_{48}^E C_2^P$ and $S_8^H C_4^R T_9$ at pH 5.0 and 40 °C. The concentrations were 0.01 and 0.081% (w/v), respectively. The fibers were allowed to form for 24 hours at 40 °C. Subsequently, a 5 μL aliquot of the solution was deposited on silicon wafers and equilibrated for 5 minutes. Afterward, the silicon wafers were washed with deionized water and dried under a nitrogen flow to remove nonadsorbed material. The silica wafers were glow-discharged under vacuum before being used to improve the surface hydrophilicity. Analysis was conducted with a Bruker Nanoscope V instrument in peak force tapping mode: the AFM tip is oscillated in a sinusoidal manner in the vertical direction, while the peak force is used as a feedback signal. This mode allows for direct force control and avoids damage due to lateral forces. Silicon nitride tips with a typical

radius of 2 nm (Bruker SCANASYST-AIR) were used for analysis. A corresponding height image is shown in Figure A6.5.
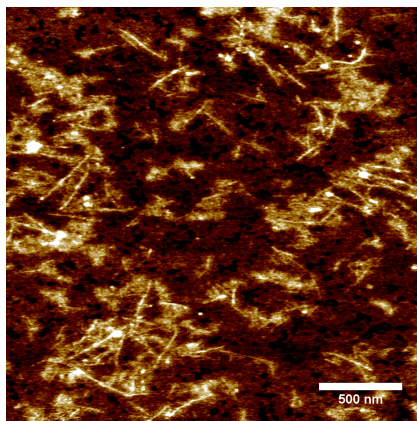

Figure A6.5: *Atomic force microscope height image of fiber formation of a $C_2^P S_{48}^E C_2^P / S_8^H C_4^R T_9$ mixture after 1 day at pH 5.0 and 40 °C. Image size is 2.5 μm x 2.5 μm, and image height is 2.0 nm. The concentrations of $C_2^P S_{48}^E C_2^P$ and $S_8^H C_4^R T_9$ were 0.01 and 0.081% (w/v), respectively. The scalebar indicates 500 nm.*

Scanning electron microscopy (SEM)

Thin slices of hydrogels were cut with a razor blade and immersed in a 5% glutaraldehyde solution for 15 minutes to fixate the hydrogels. This was done to prevent alteration of hydrogel structure due to subsequent processing steps. Water present in the hydrogels was exchanged with acetone in increasing steps of 10%. The hydrogels were equilibrated for 30 minutes at each step. After removal of water, samples were critical point dried, in which acetone was exchanged for liquid CO_2. Liquid CO_2 was subsequently removed to obtain dry samples. This preparation method avoids damage to the samples by surface tension effects. Samples were sputter-coated with a 5 nm layer of iridium to prevent charging of the sample during analysis. Analysis was performed with a FEI Magellan FESEM scanning electron microscope at a working distance of 4 mm, with SE detection at 2 kV, 6 pA. All images were recorded digitally. Figure A6.6 shows scanning electron microscope (SEM) images of $C_2^P S_{48}^E C_2^P$, $S_8^H C_4^R T_9$, and mixed $C_2^P S_{48}^E C_2^P / S_8^H C_4^R T_9$ hydrogels formed at 20 and 40 °C. For $C_2^P S_{48}^E C_2^P / S_8^H C_4^R T_9$ gels formed at 20 and 40 °C, a fibrous structure similar to the one seen for $C_2^P S_{48}^E C_2^P$ gels is observed. It should be noted that during preparation of these gels, a 5% glutaraldehyde solution was used to

fixate the hydrogels. Because glutaraldehyde can react with primary amines (lysine residues) that are present in the random-coil blocks (C_2^P and C_4^R) of $C_2^P S_{48}^E C_2^P$ and $S_8^H C_4^R T_9$, the fibers in the hydrogels are crosslinked. This might influence the morphology of the hydrogels. In addition, this preparation method might immobilize unreacted $S_8^H C_4^R T_9$ onto the fibers in the composite gel.
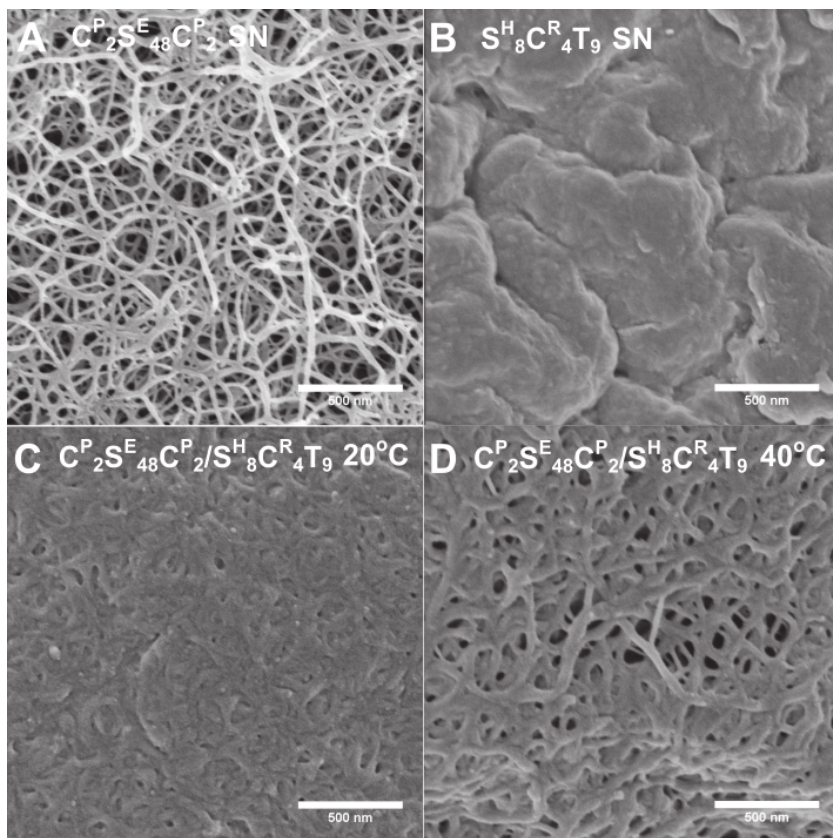
Figure A6.6: *Scanning electron micrographs (SEM) of hydrogels. (A) $C_2^P S_{48}^E C_2^P$ alone at pH 2.0 and 20°C. (B) $S_8^H C_4^R T_9$ alone at pH 10.0 and 20°C. (C) $C_2^P S_{48}^E C_2^P / S_8^H C_4^R T_9$ hydrogel formed at pH 5.0 and 20°C. (D) $C_2^P S_{48}^E C_2^P / S_8^H C_4^R T_9$ hydrogel formed at pH 5.0 and 40°C. The concentrations of $C_2^P S_{48}^E C_2^P$ and $S_8^H C_4^R T_9$ were 1.0 and 8.1% (w/v), respectively. The scalebar indicates 500 nm in all micrographs.*
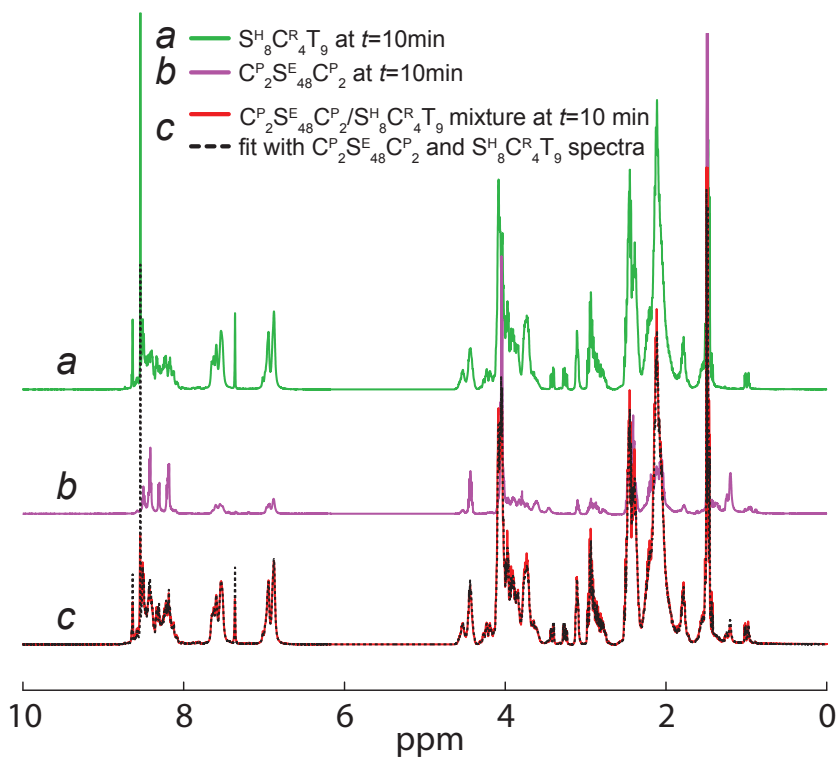
Figure A6.7: ^1H-NMR spectra. (A) $S_8^H C_4^R T_9$ (green). (B) $C_2^P S_{48}^E C_2^P$ (magenta). (C) Mixture of $C_2^P S_{48}^E C_2^P$ and $S_8^H C_4^R T_9$ immediately after mixing (red) at $40\,°C$. The spectrum of the block copolymer mixture can be described as a sum of the $S_8^H C_4^R T_9$ and $C_2^P S_{48}^E C_2^P$ spectra (dashed black line).
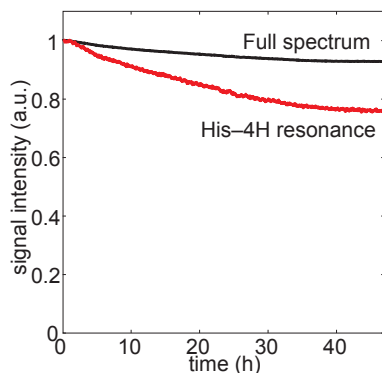
Figure A6.8: *Decrease of the normalized amplitude of the full ^{1}H-NMR spectrum and of the His-4H resonance of the $C_2^P S_{48}^E C_2^P / S_8^H C_4^R T_9$ mixture (1.0 and 8.1% (w/v)) as a function of time. The time scale of these amplitude changes corresponds to the rate increase of G′ in Figure 6.2 and A6.4. The relative decrease of amplitude of the full spectrum is less than that of the His-4H resonance, because the full spectrum also contains contributions of protons that are not immobilized, and whose resonances thus do not disappear from the NMR spectrum.*

Persistence length

To obtain the persistence length of the $C_2^P S_{48}^E C_2^P$ fibers we used the open-source software program Easyworm to analyze AFM images.[32] A representative AFM image is shown in Figure A6.9A. We measured 62 fibers with a total length of 112 μm. After all the individual fibers were selected and imported into the dataset, the dataset was fitted with the wormlike chain model via the mean square end-to-end distances (Figure A6.9B).
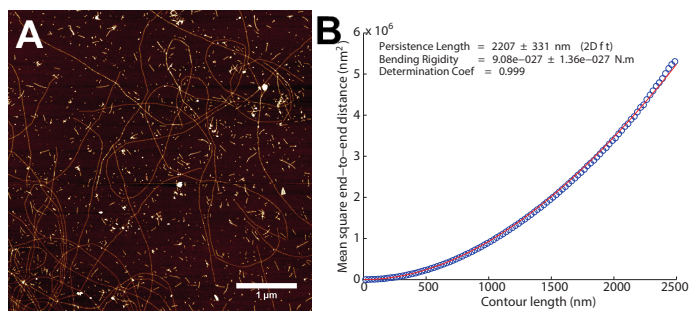
Figure A6.9: *(A) Atomic force microscope height image of $C_2^P S_{48}^E C_2^P$ fibers after 1 day at pH 2.0. Image size is 5.0μm x 5.0μm, and image height is 5.0 nm. The concentrations of $C_2^P S_{48}^E C_2^P$ was 0.005% (w/v). The scalebar indicates 1 μm. (B) Easyworm wormlike chain model fit to the dataset.*

References

(1) Whitesides, G. M.; Boncheva, M. *Proc. Natl. Aca. Sci. U.S.A.* **2002**, *99*, 4769–4774.

(2) Whitesides, G. M.; Grzybowski, B. *Science* **2002**, *295*, 2418–2421.

(3) Heeres, A.; van der Pol, C.; Stuart, M.; Friggeri, A.; Feringa, B. L.; van Esch, J. *J. Am. Chem. Soc.* **2003**, *125*, 14252–14253.

(4) Korevaar, P. A.; George, S. J.; Markvoort, A. J.; Smulders, M. M. J.; Hilbers, P. A. J.; Schenning, A. P. H. J.; De Greef, T. F. A.; Meijer, E. W. *Nature* **2012**, *481*, 492–496.

(5) Hosono, N.; Gillissen, M. A. J.; Li, Y.; Sheiko, S. S.; Palmans, A. R. A.; Meijer, E. W. *J. Am. Chem. Soc.* **2012**, *135*, 501–510.

(6) Tirrell, D. A.; Fournier, M. J.; Mason, T. L. *Curr. Opin. Struct. Biol.* **1991**, *1*, 638–641.

(7) Meyer, D. E.; Trabbic-Carlson, K.; Chilkoti, A. *Biotechnol. Prog.* **2001**, *17*, 720–728.

(8) Van Hest, J. C. M.; Tirrell, D. A. *Chem. Comm.* **2001**, *19*, 1897–1904.

(9) Haider, M.; Megeed, Z.; Ghandehari, H. *J. Controlled Release* **2004**, *95*, 1–26.

(10) Daamen, W. F.; Veerkamp, J. H.; Van Hest, J. C. M.; Van Kuppevelt, T. H. *Biomaterials* **2007**, *28*, 4378–4398.

(11) Huang, J.; Foo, C. W. P.; Kaplan, D. L. *J. Macromol. Sci.*, *Polym. Rev.* **2007**, *47*, 29–62.

(12) Nettles, D. L.; Chilkoti, A.; Setton, L. A. *Adv. Drug Delivery Rev.* **2010**, *62*, 1479–1485.

(13) Werten, M. W. T.; van den Bosch, T. J.; Wind, R. D.; Mooibroek, H.; de Wolf, F. A. *Yeast* **1999**, *15*, 1087–1096.

(14) Werten, M. W. T.; Moers, A. P. H. A.; Vong, T.; Zuilhof, H.; van Hest, J. C. M.; de Wolf, F. A. *Biomacromolecules* **2008**, *9*, 1705–1711.

(15) Pham, T. T. H.; Skrzeszewska, P. J.; Werten, M. W. T.; Rombouts, W. H.; Cohen Stuart, M. A.; de Wolf, F. A.; van der Gucht, J. *Soft Matter* **2013**, *9*, 6391–6397.

(16) Beun, L. H.; Storm, I. M.; Werten, M. W. T.; de Wolf, F. A.; Cohen Stuart, M. A.; De Vries, R. *Biomacromolecules* **2014**, *15*, 3349–3357.

114

(17) Hernandez-Garcia, A.; Kraft, D. J.; Janssen, A. F.; Bomans, P. H. H.; Sommerdijk, N. A. J. M.; Thies-Weesie, D. M. E.; Favretto, M. E.; Brock, R.; de Wolf, F. A.; Werten, M. W., et al. *Nat. Nanotechnol.* **2014**, *9*, 698–702.

(18) Włodarczyk-Biegun, M. K.; Werten, M. W. T.; de Wolf, F. A.; van den Beucken, J. J. J. P.; Leeuwenburgh, S. C. G.; Kamperman, M.; Stuart, C. M. A. *Acta biomaterialia* **2014**, *10*, 3620–3629.

(19) Martens, A. A.; Portale, G.; Werten, M. W. T.; de Vries, R. J.; Eggink, G.; Cohen Stuart, M. A.; de Wolf, F. A. *Macromolecules* **2009**, *42*, 1002–1009.

(20) Skrzeszewska, P. J.; de Wolf, F. A.; Werten, M. W. T.; Moers, A. P. H. A.; Cohen Stuart, M. A.; van der Gucht, J. *Soft Matter* **2009**, *5*, 2057–2062.

(21) Werten, M. W. T.; Teles, H.; Moers, A. P. H. A.; Wolbert, E. J. H.; Sprakel, J.; Eggink, G.; de Wolf, F. A. *Biomacromolecules* **2009**, *10*, 1106–1113.

(22) Martens, A. A.; van der Gucht, J.; Eggink, G.; de Wolf, F. A.; Cohen Stuart, M. A. *Soft Matter* **2009**, *5*, 4191–4197.

(23) Golinska, M. D.; Pham, T. T. H.; Werten, M. W. T.; de Wolf, F. A.; Cohen Stuart, M. A.; van der Gucht, J. *Biomacromolecules* **2012**, *14*, 48–55.

(24) Rombouts, W. H.; Colomb-Delsuc, M.; Werten, M. W. T.; Otto, S.; de Wolf, F. A.; van der Gucht, J. *Soft Matter* **2013**, *9*, 6936–6942.

(25) Werten, M. W. T.; Wisselink, W. H.; Jansen-van den Bosch, T. J.; de Bruin, E. C.; de Wolf, F. A. *Protein Eng.* **2001**, *14*, 447–454.

(26) Golinska, M. D.; Włodarczyk-Biegun, M. K.; Werten, M. W. T.; Cohen Stuart, M. A.; de Wolf, F. A.; de Vries, R. *Biomacromolecules* **2014**, *15*, 699–706.

(27) Wu, H. *Chem. Phys.* **2010**, *367*, 44–47.

(28) Arnaudov, L. N.; de Vries, R.; Ippel, H.; van Mierlo, C. P. M. *Biomacro-molecules* **2003**, *4*, 1614–1622.

(29) Wishart, D. S.; Bigam, C. G.; Holm, A.; Hodges, R. S.; Sykes, B. D. *J. Biomol. NMR* **1995**, *5*, 67–81.

(30) MacKintosh, F. C.; Käs, J.; Janmey, P. A. *Phys. Rev. Lett.* **1995**, *75*, 4425.

(31) Lin, Y.-C.; Yao, N. Y.; Broedersz, C. P.; Herrmann, H.; MacKintosh, F. C.; Weitz, D. A. *Phys. Rev. Lett.* **2010**, *104*, 058101.

(32) Lamour, G.; Kirkegaard, J. B.; Li, H.; Knowles, T. P. J.; Gsponer, J. *Source Code Biol. Med.* **2014**, *9*, 1–6.

(33) Schor, M.; Martens, A. A.; Cohen Stuart, M. A.; Bolhuis, P. G. *Soft Matter* **2009**, *5*, 2658–2665.

(34) Tosh, S. M.; Marangoni, A. G.; Hallett, F. R.; Britt, I. J. *Food Hydrocolloids* **2003**, *17*, 503–513.

(35) Djabourov, M. *Contemp. Phys.* **1988**, *29*, 273–297.

(36) Cipelletti, L.; Manley, S.; Ball, R. C.; Weitz, D. A. *Phys. Rev. Lett.* **2000**, *84*, 2275.

(37) Bakar, M. R. A.; Nagy, Z. K.; Rielly, C. D. *Org. Process Res. Dev.* **2009**, *13*, 1343–1356.

(38) Carless, J. E.; Foster, A. A. *J. Pharm. Pharmacol.* **1966**, *18*, 697–708.

Enhanced Stiffness of Silk-like Fibers by Loop Formation in the Corona Leads to Stronger Gels

Abstract

We study the self-assembly of protein polymers consisting of a silk-like block flanked by two hydrophilic blocks, with a cysteine residue attached to the C-terminal end. The silk blocks self-assemble to form fibers while the hydrophilic blocks form a stabilizing corona. Entanglement of the fibers leads to the formation of hydrogels. Under oxidizing conditions the cysteine residues form disulfide bridges, effectively connecting two corona chains at their ends to form a loop. We find that this leads to a significant increase in the elastic modulus of the gels. Using atomic force microscopy, we show that this stiffening is due to an increase of the persistence length of the fibers. Self-consistent-field calculations indicate a slight decrease of the lateral pressure in the corona upon loop formation. We argue that this small decrease in the repulsive interactions affects the stacking of the silk-like blocks in the core, resulting in a more rigid fiber.

7.1   Introduction

Hydrogels are of great interest for biomedical applications due to their high water content and softness which bear significant resemblance to biological tissue.[1,2] They can be prepared by crosslinking polymer chains with either permanent chemical crosslinks, or physical crosslinks that can be remodelled, or a combination of both types of crosslinks. Physical hydrogels are particularly interesting for biomedical applications, because these materials can be made stimulus-responsive, self-healing, and can be formed *in situ*.[3–5] Interesting candidates for preparing these physicals gels are bio-inspired protein polymers, which can be created by means of genetic engineering. This method allows for the design of versatile molecules with different functionalities within a single molecule. In comparison to chemical synthesis, biosynthetic production has the advantage that the product is mono-disperse, and the exact amino acid sequence can be controlled. Because self-assembly motifs, enzyme recognition sites, cellular recognition sites, and cleavage sites can be straightforwardly included into a single design, these bio-inspired protein polymers are promising materials for biomedical and tissue engineering applications.[6–12] Recently we described various designs of protein polymers based on collagen-like, silk-like, and elastin-like blocks.[13–19] Starting with the most simple design of a collagen-like hydrophilic random-coil, we gradually shifted our efforts to create more complex designs where silk-like blocks were combined with collagen-like hydrophilic random-coils. An example is the symmetric silk-like protein polymer $C_2^P S_{48}^H C_2^P$, which consists of a pH-responsive silk-like block S_{48}^H flanked by two hydrophilic random-coil blocks C_2^P. The S_{48}^H-block consists of 48 (Gly-Ala)$_3$-Gly-His repeats. As the histidine-residue in the S_{48}^H-block becomes uncharged at pH-values above 6.0, self-assembly into a semi-crystalline β-sheet-like structure occurs, ultimately resulting in long, semi-flexible fibers.[18] The folding and assembly of the silk-like blocks leading to fiber formation of $C_2^P S_{48}^H C_2^P$ is governed by hydrogen bonding and hydrophobic interactions. Circular dichroism spectroscopy experiments done to elucidate the molecular structure showed that the silk-like blocks did not contain a high fraction of β-sheets as the silk fibroin originating from *Bombyx mori* has. Instead a high turn content was found for the silk-like blocks.[14,15] With MD simulations it was predicted that a β-roll conformation of the silk-like block was the most thermodynamically stable situation for these molecules in water, because with this conformation the number of possible hydrogen bonds is increased

and the exposed surface area to water is minimized. Furthermore, as the surfaces of the β-roll structures are covered with hydrophobic alanine residues, stacking of monomers into fibers by hydrophobic interactions is promoted.[20] The $\mathbf{C}_2^{\mathbf{P}}$-block is 200 amino acids long, and assumes a random-coil conformation within a wide range of temperatures and pH, forming a hydrophilic corona around the fibers. The $\mathbf{C}_2^{\mathbf{P}}$-blocks are swollen in water and repel each other. Above the overlap concentration, the silk-like fibers entangle, leading to the formation of a physical hydrogel. A theoretical model for semiflexible fibers proposed by Mackintosh et al.[21] relates the elastic shear modulus G' of the fiber gel to the persistence length of the fibers l_p, the mesh size ξ, and the entanglement length L_e:

$$G' \approx \frac{kTl_p{}^2}{L_e{}^3\xi^2} \tag{7.1}$$

Both the entanglement length and the mesh size depend on the fiber concentration, and a concentration dependence as $G' \sim c^{2.5}$ was predicted, and found experimentally.[21] In this chapter, we investigate how a small change in the corona-forming block of the silk-like polymers modifies the self-assembly process and thereby affects the mechanical properties of the resulting hydrogels. We do this by attaching a single cysteine residue to the C-terminal $\mathbf{C}_2^{\mathbf{P}}$-block of the silk-like protein polymer, leading to the asymmetric protein polymer $\mathbf{C}_2^{\mathbf{P}}\mathbf{S}_{48}^{\mathbf{H}}\mathbf{C}_2^{\mathbf{P}}$-Cys. The cysteine residues in the protein polymers can form disulfide bridges in oxidizing conditions, effectively linking two chains in the coronae of the fibers together, to form a loop. By comparing experiments under oxidizing and reducing conditions, we investigate how loop formation of the corona chains affects the mechanical properties of the fibers. Surprisingly, we find that loop formation, which lowers the free energy of the corona chains with only a fraction of the thermal energy k_BT, leads to a significant increase of the persistence length of the fibers and thereby an enhanced shear modulus.

7.2   Experimental Section

7.2.1   Materials

Vector construction

A derivative of the previously described vector pMTL23-aII[18] was prepared via gene synthesis (Genscript, Piscataway, NJ), in which no *Ban*I and *Bsa*I sites are present except those originating from the aII adapter. The vector

pMTL23-aII-ΔBB obtained was digested with *Eco*RI/*Xho*I. An *Eco*RI/*Xho*I double-stranded DNA adapter was then prepared by annealing of the oligonucleotides:

5′-AATTCGGTCTCGGTGCTGGTGCACCCGGTGAGGGTGCCTGTTAAGC-GGCCGC-3′ and

5′-TCGAGCGGCCGCTTAACAGGCACCCTCACCGGGTGCACCAGCACCG-AGACCG-3′.

This adapter was ligated into the previously digested vector pMTL23-aII-ΔBB to obtain pMTL23-aII-ΔBB-Cys. The $\mathbf{C_2^P S_{48}^H C_2^P}$ insert[18] was digested with *Bsa*I/*Ban*I and ligated into the likewise digested and dephosphorylated vector pMTL23-aII-ΔBB-Cys. The insert was then cloned into *Pichia pastoris* expression vector pPIC9 via *Eco*RI/*Not*I. The resulting vector pPIC9-$\mathbf{C_2^P S_{48}^H C_2^P}$-Cys was linearized with *Sal*I and used to transform *P. pastoris* GS115 by electroporation, as described previously.[13]

Biosynthetic production and purification

The new protein polymer with cysteine functionality $\mathbf{C_2^P S_{48}^H C_2^P}$-Cys was produced biosynthetically in the yeast *P. pastoris*. Fed-batch fermentations were performed in 2.5 L Bioflo 3000 bioreactors (New Brunswick Scientific) according to the procedures described previously.[15,22] The secreted protein polymer was purified from the microfiltered fermentation broth by two consecutive ammoniumsulfate precipitation steps at 40% saturation, followed by desalting and lyophilisation.

Protein polymer characterization

The purification process was monitored and verified with protein electrophoresis (SDS-PAGE) using the NuPAGE Novex System (LifeTechnologies) with 10% polyacrylamide Bis-Tris gels, MES-SDS running buffer (LifeTechnologies), and a prestained protein standard (SeeBlue Plus2, LifeTechnologies). The gels were stained with Coomassie SimplyBlue SafeStain (Lifetechnologies). The molar mass of the protein polymer was verified with matrix-assisted laser desorption/ionization time-of-flight mass spectroscopy (MALDI-TOF). This was done with an ultrafleXtreme mass spectrometer (Bruker) on a 600μm AnchorChip target (Bruker) with 2,5-dihydroxyacetophenone (Sigma-Aldrich) as matrix.

7.2.2 Methods

Sample preparation

The sample preparation for all experiments was done at 20°C. A stock solution of $C_2^P S_{48}^H C_2^P$-Cys was prepared by dissolving lyophilized $C_2^P S_{48}^H C_2^P$-Cys in 10 mM HCl. To prepare the hydrogels a fixed amount of stock solution was mixed with 100 mM phosphate buffer without or with 5 mM tris(2-carboxyethyl)phosphine (TCEP, Thermo Scientific).

Rheology

Rheological measurements were performed with an Anton Paar Physica MCR 501 rheometer equipped with a Couette geometry (1 mL). With a solvent trap and direct addition of tetredecane oil on top of the samples the effects of evaporation were minimized. The temperature was controlled by a Peltier element. Samples were allowed to form a hydrogel *in situ*. *In situ* hydrogel formation was followed by measuring a time sweep (f=1 Hz, and γ=0.1%), whereby the storage (G') and loss moduli (G'') were measured. After steady state was reached, viscoelastic behavior of the steady state gel was characterized by a frequency sweep (ω=0.01-100 rad.s^{-1}, and γ=0.1%).

Atomic Force Microscopy

After 1 day of fiber growth, samples for the atomic force microscope (AFM) were prepared by depositing a 5 μL aliquot of protein solution on silica wafers, allowing the fibers to attach for 5 minutes. Afterward, the samples were washed with Milli-Q to remove all non-attached material and salts. Subsequently, the samples were dried in air. The silica wafers were glow-discharged under vacuum before use to improve surface hydrophilicity. The measurements were done with a Digital Instruments Nanoscope III in contact mode using Scanasyst. The peakforce is used as feedback mechanism. Silicon nitride tips with a typical radius of 2 nm (Bruker SCANASYST-AIR) were used.

Image analysis

To obtain the persistence length of the $C_2^P S_{48}^H C_2^P$-Cys fibers we used the open-source software program Easyworm.[23] We measured 254 fibers with a total length of 647 μm, and 243 fibers with a total length of 685 μm for the $C_2^P S_{48}^H C_2^P$-Cys fibers formed in the absence and in the presence of TCEP, respectively. After all the individual fibers were selected and imported into

the dataset, the dataset was fitted with the wormlike chain model. As we expect the persistence length l_p to be smaller than the fiber length we chose to estimate the persistence length in two ways: by determining the decay of the tangent-tangent correlations $\langle \cos \theta \rangle$, and by measuring the mean square of the end-to-end distances $\langle R^2 \rangle$.

Self consistent field calculations

To quantify the effect of connecting two polymer chains in the corona on the free energy of the assembled fibers, we use the numerical self-consistent field (SCF) approach due to Scheutjens and Fleer.[24] This method has been extensively described in the literature and therefore we only mention its key characteristics. The method uses the self-consistent field machinery which implements a mean-field approximation. Instead of particle positions, the method evaluates volume fractions. We model the self-assembled $\mathbf{C_2^P S_{48}^H C_2^P}$-Cys fiber as a cylindrical polymer brush, with a corona of $\mathbf{C_2^P}$ blocks linked to a linear core composed of the $\mathbf{S_{48}^H}$ units. In this case, the volume fraction $\varphi(\text{r})$ is a function of the radial coordinate r only. This implies an averaging of the segment concentrations in the azimuthal direction as well as along the longitudinal direction of the bottle brush. At each coordinate an incompressibility condition is applied which says that the volume fractions of solvent and polymer add up to unity. Chain conformations are evaluated on a lattice using a freely jointed chain (FJC) model. This model falls short in accounting for all excluded-volume effects; neighboring segments along the chain occupy neighboring sites on the lattice, but longer ranged correlations are ignored. A better model would be the self-avoiding chain, but such a model requires excessive computation times. The FJC model provides for an efficient method to evaluate the statistical weight of all possible conformations of the chains. In a cylindrical coordinate system we graft the brush molecules with one end to a central core. After solving the SCF equations up to 7 significant digits, we obtain an accurate free energy and lateral pressure in this cylindrical brush of linear chains. Linear chains with $N=200$ units, a bond length a of 5 nm, and a grafting density h of 1 nm were used. We compare this to a brush made of loops. These loops are composed of chains with twice the length of the linear analogue and now both the first and last segments are pinned to the core.

122

7.3 Results and Discussion

7.3.1 Biosynthetic production and characterisation

The protein polymer $\mathbf{C_2^P S_{48}^H C_2^P}$-Cys was biosynthetically produced in *P. pastoris*. The amount of dry (desalted) protein polymer obtained after purification and desalting was 3 gram per liter of cell-free broth, which is comparable to the yields observed with similar silk-like protein polymers produced before.[18] The purification of the protein polymer was in first instance checked by SDS-PAGE (Figure 7.1). In the cell-free fermentation broth, a clear product band could be distinguished. It should be noted that the migration of $\mathbf{C_2^P S_{48}^H C_2^P}$-Cys is extremely slow due to the poor SDS-binding capacity of the flanking random-coil blocks, as published before.[22] After purification, which involved two consecutive ammoniumsulfate precipitation steps, contaminating components present in the initial fermentation broth were removed (Figure 7.1, lane 2), while the main product band remained (Figure 7.1, lane 3). The molar mass of the product was verified with MALDI-TOF (Appendix, Figure A7.1), which showed a monodisperse product with a molar mass (66,275 Da) close to the theoretically predicted value (66,250 Da). The amino acid sequence of $\mathbf{C_2^P S_{48}^H C_2^P}$-Cys is presented in the Appendix (Figure A7.2).
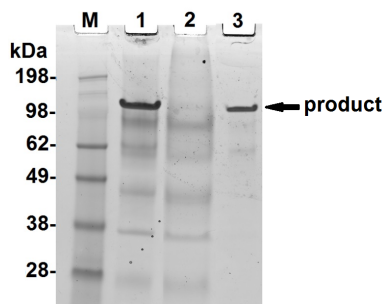
Figure 7.1: *SDS-PAGE gel of the purification process of $\mathbf{C_2^P S_{48}^H C_2^P}$ – Cys. Lane M: Marker; Lane 1: Fermentation broth; Lane 2: Supernatant after the first ammoniumsulfate precipitation at 40% saturation; Lane 3: Purified product after the second 40% ammoniumsulfate precipitation.*

7.3.2 Rheology

The effect of the new N-terminal cysteine functionality on the gelation process of $\mathbf{C_2^P S_{48}^H C_2^P}$-Cys was evaluated by comparing experiments under

reducing and oxidizing conditions (with and without 5mM TCEP) (Figure 7.2A). Under reducing conditions, the formation of disulfide bridges between cysteine residues is prevented. Therefore, this condition can be considered as the control condition, and the polymer is expected to behave similarly to the unmodified protein polymer, without cystein residue. Our results show that, under oxidizing conditions, the storage modulus of the hydrogel was about a factor of 2.5 higher than that of the hydrogel in reducing conditions, implying that disulfide bridges enhance the elasticity of the gel. The storage modulus in both conditions was independent of the shear frequency within the range evaluated (Appendix, Figure A7.3), as expected for these fibrous hydrogels.
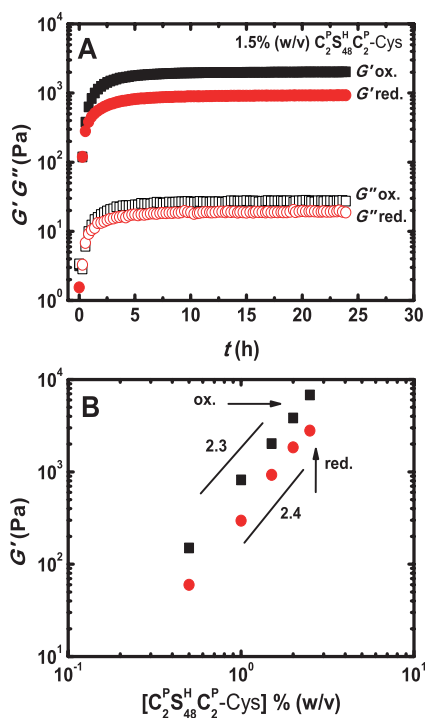
Figure 7.2: *(A) Gelation process of $C_2^P S_{48}^H C_2^P - Cys$ hydrogels in oxidizing (black squares) and reducing conditions (red circles). Storage moduli (G', closed symbols) and loss moduli (G'', open symbols). T=20°C, pH=7.0 and [$C_2^P S_{48}^H C_2^P - Cys$]=1.5% (w/v). (B) Storage moduli of $C_2^P S_{48}^H C_2^P$-Cys hydrogels in oxidizing (black squares) and reducing conditions (red circles) as a function of $C_2^P S_{48}^H C_2^P - Cys$ concentration. T=20°C and pH=7.0.*

In Figure 7.2B, the effect of the concentration of $C_2^P S_{48}^H C_2^P$-Cys on the

124

modulus is shown for both oxidizing and reducing conditions. At all concentrations, the modulus is about a factor 2.5 higher in oxidizing conditions than in reducing conditions. In both cases, the modulus increases approximately as $G' \sim c^a$, with $a \approx 2.3$, which is very close to the scaling predicted for entangled semi-flexible fibers (Equation 7.1).[21] To investigate in more detail how the gel properties depend on the number of disulfide bridges in the fibers, we mixed $C_2^P S_{48}^H C_2^P$-Cys with unmodified $C_2^P S_{48}^H C_2^P$, and measured the steady state storage modulus as a function of the mixing ratio (Figure 7.3).
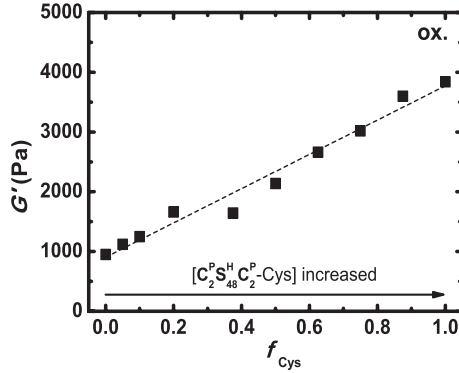
Figure 7.3: *Storage modulus as a function of fraction* $f_{Cys} = \dfrac{[C_2^P S_{48}^H C_2^P - Cys]}{[C_2^P S_{48}^H C_2^P - Cys] + [C_2^P S_{48}^H C_2^P]}$ *in a* $C_2^P S_{48}^H C_2^P - Cys / C_2^P S_{48}^H C_2^P$ *mixture in oxidizing conditions. Total protein polymer concentration = 2.0% (w/v), T=20°C and pH=7.0.*

We find that the modulus increases linearly with the fraction of cystein-modified polymer. These findings suggest that the stiffening effect of the disulfide bridges is probably not caused by inter-fiber crosslinking, as crosslinking would lead to a slightly different concentration dependence.[21] Moreover, the probability of crosslinking (rather than forming intra-fiber crosslinks) should increase strongly with increasing fiber concentration, whereas the results in Figure 7.2B and 7.3 indicate that the effect of the disulfide bridges is the same at all concentrations. Intra-fiber crosslinking may also be promoted by the pathway of self-assembly that we adopted. Under oxidizing conditions and at low pH, the $C_2^P S_{48}^H C_2^P$-Cys polymers are predominantly present as dimers, consisting of two polymers connected by a disulfide bridge. When these polymers start to self-assemble (after adding phosphate buffer), it is very likely that the two silk-like blocks in one dimer end up in the same fiber. One of the silk-like blocks in the dimer

will be stacked into a forming fiber first, which will require time for this block to adapt its conformation. This process would be counteracted if the other silk-like block present in the same dimer is built in an other nearby fiber. Hence, it is to be expected that most disulfide bridges are intra-fiber crosslinks, effectively connecting two random-coil blocks of the corona together at their ends (turning two corona chains into one polymeric loop).

7.3.3 Persistence length

If the enhanced modulus due to disulfide bridges is not caused by inter-fiber crosslinking, then what causes the increase in modulus? We hypothesize that the formation of intra-fiber disulfide bridges somehow stabilizes the fibers and thereby affects their persistence length, which should enhance the modulus according to Equation 7.1. To test this, we measured the persistence length of $C_2^P S_{48}^H C_2^P$-Cys fibers in oxidizing and reducing conditions, by analyzing AFM images of the fibers (Figure 7.4).[23] From the images, we obtain the persistence length l_p using two methods: (1) by measuring the tangent-tangent correlation function, $\langle \cos \theta \rangle = e^{-\frac{L}{l_p}}$, and (2) by measuring the mean square end-to-end distance, $\langle R^2 \rangle = 2Ll_p$, where L is the contour length.
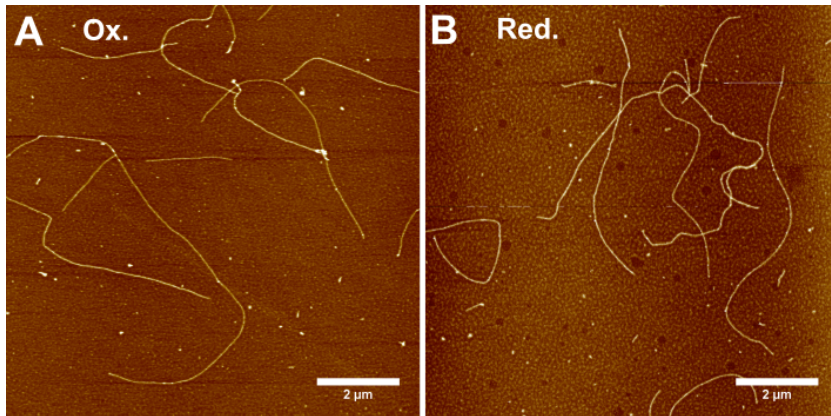
Figure 7.4: *AFM images of $C_2^P S_{48}^H C_2^P - Cys$ fibers (A) in oxidizing conditions (no TCEP), (B) in reducing conditions (5 mM TCEP). Image size is 10μm X 10μm, and image height is 5.0 nm. The fibers were formed at pH 7.0 and $[C_2^P S_{48}^H C_2^P - Cys] = 0.005\%$ (w/v).*

The estimated persistence length of $C_2^P S_{48}^H C_2^P$-Cys fibers formed in oxidizing and reducing conditions can be found in Table 7.1. The actual fits can be

found in the Appendix (Figure A7.4A-D). Clearly, the persistence length of the fibers is significantly higher in oxidizing conditions than in reducing conditions, by approximately a factor of 1.5.

Table 7.1: *Estimated persistence lengths via* $\langle \cos \theta \rangle$*, and* $\langle R^2 \rangle$ *for* $\mathbf{C_2^P S_{48}^H C_2^P} - Cys$ *fibers formed in the absence and presence of TCEP.*

Experimental condition	l_p via $\langle \cos \theta \rangle$	l_p via $\langle R^2 \rangle$
Oxidizing	$3.2 \pm 0.5 \mu m$	$3.3 \pm 0.5 \mu m$
Reducing (5mM TCEP)	$2.2 \pm 0.3 \mu m$	$2.3 \pm 0.4 \mu m$

It is this increase in persistence length, which most probably causes the increase in elastic modulus of the gels. According to the theoretical model for semiflexible fibers proposed by Mackintosh et al.,[21] (Equation 7.1), the elastic modulus increases as $G' \sim l_p^2$, when assuming that ξ and L_e are the same in oxidizing and reducing conditions. The factor of 1.5 increase in persistence length we found between oxidizing and reducing conditions would correspond to a factor $1.5^2 = 2.3$ increase in modulus, which is very close to our experimental findings (Figure 7.2B). Note that in reality the entanglement length may also depend on the persistence length,[21] which would modify the relation between G' and l_p. Nevertheless, we conclude that the increase in elasticity that we observed in oxidizing conditions can be attributed to an increased persistence length due to the formation of disulfide bridges.

7.3.4   Stiffening by loop formation

The question that remains is how the formation of intra-fiber disulfide bridges leads to an increased persistence length. Effectively, every disulfide bridge converts two coronoa chains into one polymer loop. To obtain an idea of the contribution of the corona chains to the persistence length, we pose that $\mathbf{C_2^P S_{48}^H C_2^P}$-Cys fibers can be seen as an array of $\mathbf{C_2^P}$ blocks linked to a linear core composed of compact packings of the $\mathbf{S_{48}^H}$ units. This configuration resembles a molecular bottle brush. Typically for the modelling of such structures one assumes that the backbone is a central amorphous cylindrical core onto which at regular intervals chains emanate. It should be noted, however, that the silk-like core of the fibers is a flat ribbon-like structure.[20] This means that the persistence length of the fiber is expected to be different in the length and lateral direction of the fiber. When the distance between these chains is h and the $\mathbf{C_2^P}$-block is modelled

as a string of N spherically symmetric segments with size a, we can write a Flory-like free energy per chain in a cylindrical bottlebrush:

$$\frac{F}{k_B T} \approx \frac{H^2}{Na^2} + \frac{\nu}{a^3} N\varphi \approx \frac{H^2}{Na^2} + \frac{\nu N^2}{hH^2} \tag{7.2}$$

In this equation all numerical pre-factors are ignored as these are assumed to be of order unity. The first term in Equation 7.2 is due to the entropy loss of a chain of N segments stretched to a 'height' H, which may also be identified by the cross-sectional radius of the fiber. The second term is due to the interactions inside the cylindrical brush of corona chains, wherein ν is the second virial coefficient of segment interactions. In this equation the corona is taken to have a homogeneous volume fraction, $\varphi \approx \frac{Na^3}{hH^2}$. The optimization of the free energy with respect to the height H gives $H \sim \left(\frac{\nu}{h}\right)^{\frac{1}{4}} N^{\frac{3}{4}} a^{\frac{1}{2}}$ with free energy $\frac{F}{k_B T} \approx \left(\frac{\nu N}{ha^2}\right)^{\frac{1}{2}}$. The lateral pressure $\frac{F}{ahk_B T} \approx (N\nu)^{\frac{1}{2}} h^{-\frac{3}{2}} a^{-2}$ increases with increasing chain length, improvement of the solvent quality and reducing distance between the grafts.

The side chains in a bottle brush are expected to increase the persistence length, especially when the chains are long and densely packed along the backbone. Polymer brush theory can also be used to estimate the contribution of the tethered chains to the persistence length. This induced persistence length can be shown to be proportional to the square of $\frac{N}{h}$, that is, $l_{p,induced} \sim \left(\frac{N}{h}\right)^2$.[25] This equation shows that in principle the persistence length can grow to very large values when sufficiently large chains are grafted on the backbone. However, the pre-factor for this dependence turns out to be relatively small and therefore in most practical cases the induced persistence length remains very small (of order unity). This means that in practice, the persistence length is often dominated by the stiffness of the core.

On the level of the scaling analysis of the polymer brush, a loop tethered by both ends to the core (two chains connected by a disulfide bond) is equivalent to two tethered chains with half the length of the loop. As a result, at the scaling level there is no effect of loop formation on the height of the brush, nor on the lateral pressure exerted by the brush on the core, nor on the induced persistence length. Of course, in reality there must be a (small) effect because there is an entropy loss when two free ends have to meet at a given point. This extra constraint is expected to reduce the lateral pressure in the brush.

To find a quantitative estimate of the effect of connecting in a cylindrical brush two free ends such that a loop results, we need to turn to a numerical

evaluation. We use the numerical self-consistent field approach due to Scheutjens and Fleer for this.[24] In this approach, each chain in the corona is treated as a freely-jointed chain, while interactions between chains are described within the mean-field approximation (see Methods). We calculate the free energy of corona chains in the fibers, and compare looped chains to unconnected chains. Our calculations show that loop-formation due to the cysteine residues lowers the free energy of the corona by approximately $0.1 \frac{k_B T}{a}$. This result implies that the lateral pressure in the corona is slightly decreased, which can result in a decrease in the distance between the chains h. As the induced l_p scales with the quadratic inverse of h, the l_p is slightly increased. However, it should be noted that the corona contribution is negligible compared to the intrinsic persistence length of the core of the fiber consisting of the silk-like blocks. We therefore conjecture that the observed increase in persistence length must be due to a difference in packing of the silk-like blocks in the core. This might be caused by the reduction of the lateral pressure in the coronae of the fibers due to the formation of loops. As said before, the self-assembly process is governed by a delicate balance between attraction among the silk blocks and repulsion between the corona blocks. It might well be that small changes in the corona can change the free energy landscape for self-assembly and thereby slightly modify the packing of the silk-like blocks in the core, for example by reducing the number of defects in the fibers, thereby increasing their effective stiffness. In Figure 7.5 the conjectured self-assembly and fiber reinforcement by disulfide bridges in oxidizing conditions are displayed in a schematic representation.
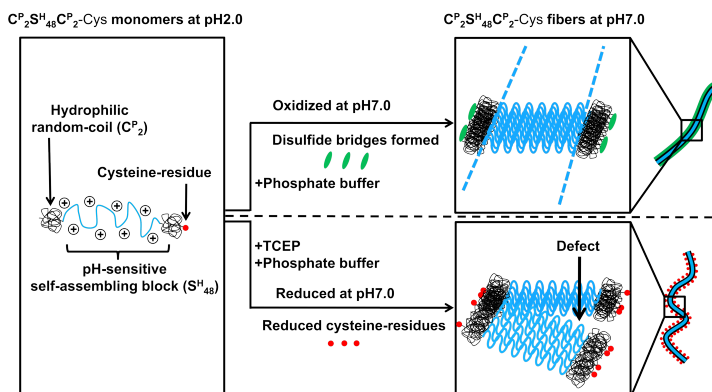

Figure 7.5: *Schematic representation of the formation of* $\mathbf{C_2^P S_{48}^H C_2^P} - Cys$ *fibers at oxidizing and reducing conditions.*

7.4 Conclusion

We have demonstrated hydrogel formation of an assymetric silk-like protein polymer with a cysteine residue attached at the end of the corona-forming block. When the hydrogel was formed in oxidizing conditions, where disulfide bridges between cysteine residues could be formed, significantly stronger hydrogels were created. This increase in mechanical strength could be directly related to a change in persistence length of the fibers. Mean field self-consistent field calculations showed that loop formation in the corona due to the disulfide bridges slightly reduces the lateral pressure in the corona. While this is in itself not enough to modify the persistence length of the fibers significantly, we conjecture that minor changes in the corona can affect the packing of the silk-like blocks. Probably the slightly lower energy barrier leads to a more crystalline structure with fewer defects and higher stiffness. This work thus shows that the self-assembly of silk-like polymers is governed by a very subtle balance between attractive and repulsive interactions, where small changes can have relatively large effects. In addition to generating an effect on fiber stiffness, the insertion of cystein residues paves the way for further functionalization of this protein polymer via chemical modification of the cysteine residue to attach fluorescent labels or reactive groups for selective covalent coupling to other blocks of interest.

Appendix
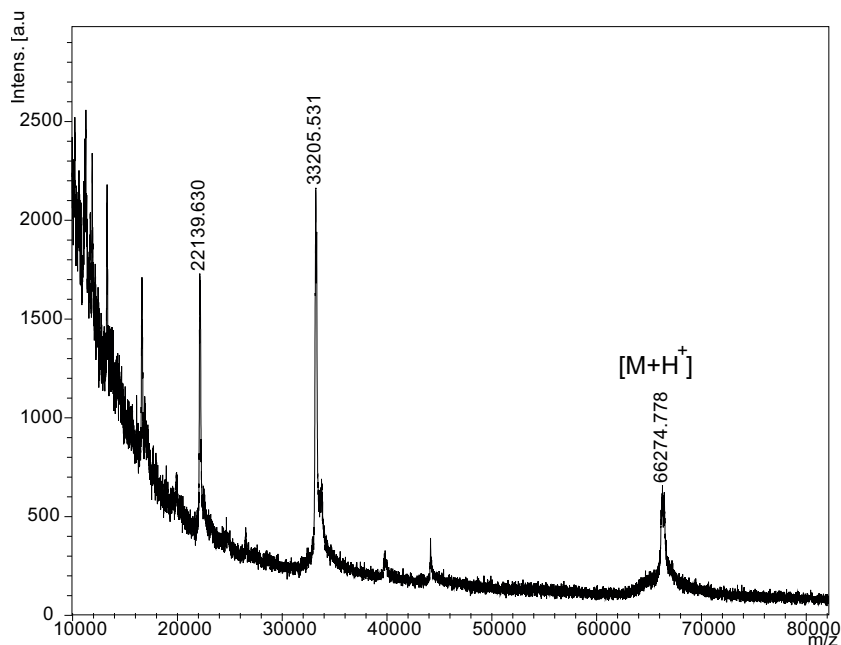
Figure A7.1: *MALDI-TOF of* $\mathbf{C_2^P S_{48}^H C_2^P}$*-Cys, showing molecular ions carying, single, double, and higher charges.*

YVEFGLGAGAPGEPGNPGSPGNQGQPGNKGSPGNPGQPGNEGQPGQPGQNGQPGEPGS
NGPQSQGNPGKNGQPGSPGSQGSPGNQGSPGQPGNPGQPGEQGKPGNQGPAGEPGNP
GSPGNQGQPGNKGSPGNPGQPGNEGQPGQPGQNGQPGEPGSNGPQGSQGNPGKNGQPG
SPGSQGSPGNQGSPGQPGNPGQPGEQGKPGNQGPAGEGAGAGAGHGAGAGAGHGAGAG
AGHGAGAGAGHGAGAGAGHGAGAGAGHGAGAGAGHGAGAGAGHGAGAGAGHGAGAGAG
HGAGAGAGHGAGAGAGHGAGAGAGHGAGAGAGHGAGAGAGHGAGAGAGHGAGAGAGHG
AGAGAGHGAGAGAGHGAGAGAGHGAGAGAGHGAGAGAGHGAGAGAGHGAGAGAGHGAG
AGAGHGAGAGAGHGAGAGAGHGAGAGAGHGAGAGAGHGAGAGAGHGAGAGAGHGAGAG
AGHGAGAGAGHGAGAGAGHGAGAGAGHGAGAGAGHGAGAGAGHGAGAGAGHGAGAGAG
HGAGAGAGHGAGAGAGHGAGAGAGHGAGAGAGHGAGAGAGHGAGAGAGHGAGAGAGHG
AGAGAGHGAGAGAGHGAGAPGEPGNPGSPGNQGQPGNKGSPGNPGQPGNEGQPGQPGQ
NGQPGEPGSNGPQGSQGNPGKNGQPGSPGSQGSPGNQGSPGQPGNPGQPGEQGKPGNQ
GPAGEPGNPGSPGNQGQPGNKGSPGNPGQPGNEGQPGQPGQNGQPGEPGSNGPQGSQG
NPGKNGQPGSPGSQGSPGNQGSPGQPGNPGQPGEQGKPGNQGPAGEGA C ←

Figure A7.2: *Amino acid sequence of* $\mathbf{C_2^P S_{48}^H C_2^P}$*-Cys (theoretical mass 66,250 Da). The cysteine residue is indicated with the arrow.*
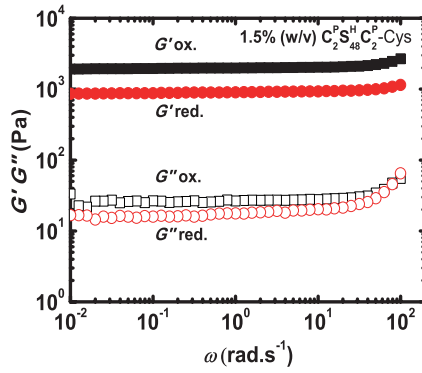
Figure A7.3: *Frequency sweep of $\mathbf{C_2^P S_{48}^H C_2^P}$-Cys hydrogels without TCEP (black squares) and with TCEP (red circles). Storage moduli (G′, closed symbols) and loss moduli (G″, open symbols). f=1 Hz, γ=0.1%, T=20°C, pH=7.0 and [$\mathbf{C_2^P S_{48}^H C_2^P}$-Cys]=1.5% (w/v).*

Figure A7.4: *Easyworm wormlike chain model fits to the datasets. (A) tangent-tangent correlations ⟨cos θ⟩ for $\mathbf{C_2^P S_{48}^H C_2^P}$-Cys fibers in oxidized conditions. (B) Me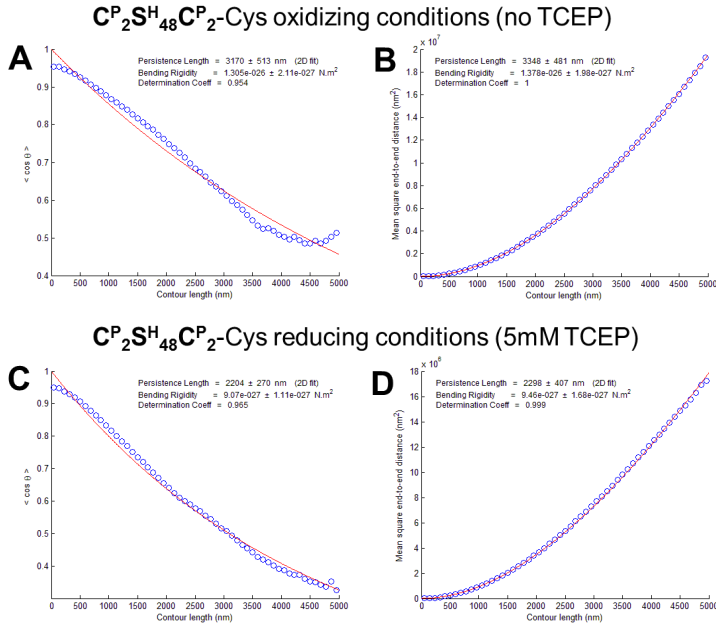an square end-to-end distance ⟨R²⟩ for $\mathbf{C_2^P S_{48}^H C_2^P}$-Cys fibers in oxidized conditions. (C) tangent-tangent correlations ⟨cos θ⟩ for $\mathbf{C_2^P S_{48}^H C_2^P}$-Cys fibers in reduced conditions. (D) Mean square end-to-end distance ⟨R²⟩ for $\mathbf{C_2^P S_{48}^H C_2^P}$-Cys fibers in reduced conditions.*

References

(1) Peppas, N. A.; Hilt, J. Z.; Khademhosseini, A.; Langer, R. *Adv. Mater.* **2006**, *18*, 1345.

(2) Geckil, H.; Xu, F.; Zhang, X.; Moon, S.; Demirci, U. *Nanomedicine* **2010**, *5*, 469–484.

(3) Imran, A. B.; Seki, T.; Takeoka, Y. *Polym. J.* **2010**, *42*, 839–851.

(4) Bawa, P.; Pillay, V.; Choonara, Y. E.; Du Toit, L. C. *Biomed. Mater.* **2009**, *4*, 022001.

(5) Vermonden, T.; Censi, R.; Hennink, W. E. *Chem. Rev.* **2012**, *112*, 2853–2888.

(6) Tirrell, D. A.; Fournier, M. J.; Mason, T. L. *Curr. Opin. Struct. Biol.* **1991**, *1*, 638–641.

(7) Meyer, D. E.; Trabbic-Carlson, K.; Chilkoti, A. *Biotechnol. Prog.* **2001**, *17*, 720–728.

(8) Haider, M.; Megeed, Z.; Ghandehari, H. *J. Controlled Release* **2004**, *95*, 1–26.

(9) Van Hest, J. C. M.; Tirrell, D. A. *Chem. Comm.* **2001**, *19*, 1897–1904.

(10) Daamen, W. F.; Veerkamp, J. H.; Van Hest, J. C. M.; Van Kuppevelt, T. H. *Biomaterials* **2007**, *28*, 4378–4398.

(11) Huang, J.; Foo, C. W. P.; Kaplan, D. L. *J. Macromol. Sci., Polym. Rev.* **2007**, *47*, 29–62.

(12) Nettles, D. L.; Chilkoti, A.; Setton, L. A. *Adv. Drug Delivery Rev.* **2010**, *62*, 1479–1485.

(13) Werten, M. W. T.; van den Bosch, T. J.; Wind, R. D.; Mooibroek, H.; de Wolf, F. A. *Yeast* **1999**, *15*, 1087–1096.

(14) Werten, M. W. T.; Moers, A. P. H. A.; Vong, T.; Zuilhof, H.; van Hest, J. C. M.; de Wolf, F. A. *Biomacromolecules* **2008**, *9*, 1705–1711.

(15) Martens, A. A.; Portale, G.; Werten, M. W. T.; de Vries, R. J.; Eggink, G.; Cohen Stuart, M. A.; de Wolf, F. A. *Macromolecules* **2009**, *42*, 1002–1009.

(16) Golinska, M. D.; Pham, T. T. H.; Werten, M. W. T.; de Wolf, F. A.; Cohen Stuart, M. A.; van der Gucht, J. *Biomacromolecules* **2012**, *14*, 48–55.

(17)   Pham, T. T. H.; Skrzeszewska, P. J.; Werten, M. W. T.; Rombouts, W. H.; Cohen Stuart, M. A.; de Wolf, F. A.; van der Gucht, J. *Soft Matter* **2013**, *9*, 6391–6397.

(18)   Golinska, M. D.; Włodarczyk-Biegun, M. K.; Werten, M. W. T.; Cohen Stuart, M. A.; de Wolf, F. A.; de Vries, R. *Biomacromolecules* **2014**, *15*, 699–706.

(19)   Hernandez-Garcia, A.; Kraft, D. J.; Janssen, A. F.; Bomans, P. H. H.; Sommerdijk, N. A. J. M.; Thies-Weesie, D. M. E.; Favretto, M. E.; Brock, R.; de Wolf, F. A.; Werten, M. W., et al. *Nat. Nanotechnol.* **2014**, *9*, 698–702.

(20)   Schor, M.; Martens, A. A.; Cohen Stuart, M. A.; Bolhuis, P. G. *Soft Matter* **2009**, *5*, 2658–2665.

(21)   MacKintosh, F. C.; Käs, J.; Janmey, P. A. *Phys. Rev. Lett.* **1995**, *75*, 4425.

(22)   Werten, M. W. T.; Wisselink, W. H.; Jansen-van den Bosch, T. J.; de Bruin, E. C.; de Wolf, F. A. *Protein Eng.* **2001**, *14*, 447–454.

(23)   Lamour, G.; Kirkegaard, J. B.; Li, H.; Knowles, T. P. J.; Gsponer, J. *Source Code Biol. Med.* **2014**, *9*, 1–6.

(24)   Fleer, G. J.; Cohen Stuart, M. A.; Scheutjens, J. M. H. M.; Cosgrove, T.; Vincent, B., *Polymers at interfaces*; Chapman & Hall: London, 1993.

(25)   Feuz, L.; Leermakers, F. A. M.; Textor, M.; Borisov, O. *Macromolecules* **2005**, *38*, 8891–8901.

General Discussion

8.1 Scientific results

As the world population is ageing rapidly, especially in the Western World, the need for donor organs to replace damaged and failing organs and tissues is increasing. However, the number of available donor organs does not match the supply, therefore alternative solutions to solve this problem are required.[1] Tissue engineering is a rapidly expanding field that thrives to meet this demand by trying to create tissues and organs through engineered combinations of cells and cell growth scaffolds.[2,3] These scaffolds act as carriers for the cells, provide structural support, and mimic the natural extracellular matrix (ECM) that embeds the cells in tissues. Therefore it is important that the structure and composition of the ECM are used as a source of inspiration for the design of scaffolds. As the ECM has many different functions (it provides structural support, is involved in cell signaling, migration, and differentiation) it has a very complex structure and composition. The components that form the ECM are excreted by cells themselves. The ECM generally consists of proteins (collagens and elastin) and polysaccharides. Depending on the tissue type, the stiffness and elasticity of the ECM can vary by several orders of magnitude, for example, between soft tissues and bone. Tissue stiffness and elasticity are determined by the amount and orientation of the fibrous proteins collagen and elastin.[4,5]

Hydrogels made from synthetic or natural polymers are interesting materials for scaffolds, because of their high water content and biocompatibility. However, most of the hydrogels have quite poor mechanical properties that limit their application as such. Recent findings in the field of hydrogels led to significant improvement of the mechanical properties. This was done by using an interpenetrating double network approach, where a stiff crosslinked network was combined with a soft loosely crosslinked network. However, in order for this method to work, at least one of the components was chemically crosslinked, requiring additional chemicals, possibly trapping toxic unreacted monomers in the hydrogel.[6] Making tough composite hydrogels from materials that are extracted from natural sources or that are biosynthetically produced is therefore particularly interesting. Nature provides a good starting point for designing these materials, because tissues can be seen as composite hydrogels. Tissues like skin and tendon can withstand large stresses and deformations before failing, due to the composite structure consisting of protein fibers embedded in a soft matrix.[7] Mimicking the composition and structure of natural tissues should ultimately lead to hydrogels that can better withstand mechanical loading. In this thesis we

136

focused on the investigation of the microscopic structure and mechanical properties of composite hydrogels made from biosynthetically produced protein polymers. This work aimed at providing a better understanding of the relation between mechanical properties and structure in complex composite hydrogel materials, and should ultimately lead to better designs of composite materials. For this research we biosynthetically produced various protein polymers that can form hydrogels based on natural collagen and silk. The protein polymers consist of combinations of different blocks, therefore both symmetric and asymmetric molecules can be made.

In the protein polymers discussed in this thesis three types of blocks were used: silk-like blocks (**S**), trimer-forming blocks (**T**) and collagen-like blocks (**C**). The **S** blocks are pH-sensitive and are able to self-assemble into semi-flexible fibers. The **T** blocks are temperature-sensitive and upon lowering the temperature, three of these **T** blocks can form triple helices similar to those formed by natural collagen. The **C** blocks ensure solubility of the protein polymers at a wide range of temperatures and pH and can act as a spacer.

8.2 Mechanical enhancement of composite hydrogels

We showed that we can create composite hydrogels with enhanced mechanical properties by using two different strategies: (1) combining a rigid silk-like fiber network with a soft elastic collagen-like network (chapter 2 and 3) and (2) combining two components that can form fibers orthogonally (chapter 4). We found that the elastic modulus, the fracture stress, and fracture strain were increased substantially by mixing fiber-forming silk-like protein polymers ($\mathbf{C_2^P S_{48}^E C_2^P}$) with collagen-like protein polymers ($\mathbf{T_9 C_4^R T_9}$) that form soft elastic networks. Up to date there are several toughening mechanisms known in literature that can result in enhanced mechanical properties. These can be split in two different categories relevant for the systems discussed here: (1) increased energy dissipation by a second network (Figure 8.1A, flexible polymer networks)[8–10] and (2) a more affine deformation of the fibers if they are embedded in a softer elastic matrix (Figure 8.1B, specific for fibers).[11–13] The first toughening mechanism uses a second, loosely crosslinked network to increase fracture resistance by delocalization of the energy at a crack site (Figure 8.1A left versus right picture). The second toughening mechanism involves the toughening of a fiber network, when it is embedded in a soft elastic matrix. The non-affine deformation modes of the fibers are

suppressed by the elastic matrix and are therefore forced to deform more affinely, resulting in a more homogeneous deformation and delocalization of the stress, leading to enhanced mechanical properties (Figure 8.1B).
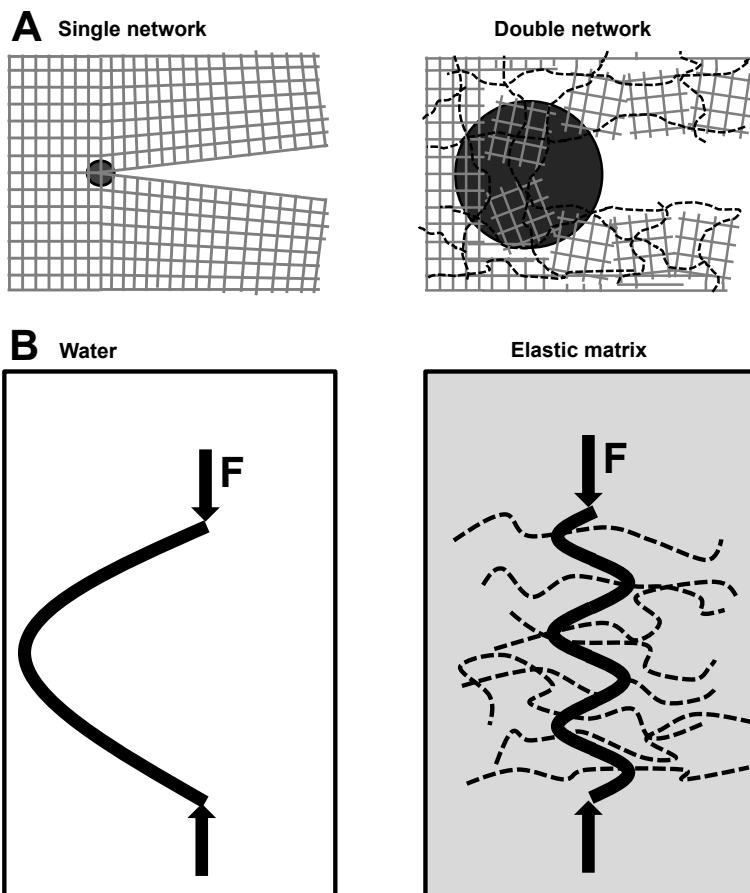
Figure 8.1: *Schematic representations of toughening mechanisms. (A) left: localization of energy in the crack tip in single networks, right: more effective distribution of energy in double networks.[8,9] (B) left: bending of fibers in water; right: buckling of fibers in an elastic matrix due to suppression of non-affine deformation modes (gelatin).[13]*

With regard to the system discussed in chapter 2 and based on the data available at that stage, we could not conclude which of these mechanisms was responsible for the toughening. Therefore, additional experiments were done in chapter 3, where the composite hydrogels were subjected to cyclic loading/unloading tests. We found that large mechanical hysteresis

occurred, which implies that energy was dissipated. This dissipated energy had two contributions: (1) a permanent part ascribed to the irreversible rupture of fibers and (2) a viscoelastic part ascribed to the disruption and reformation of the triple helical nodes. The observation that the soft elastic collagen-like network has a significant contribution to the dissipated energy supports the toughening mechanism originating from the increased energy dissipation by the presence of a second network. However, the observation that the dissipated energy related to the rupture of the fibers is also increased by an order of magnitude in the presence of an elastic matrix, supports the second toughening mechanism discussed. In addition, the observation that the strain hardening of the silk-like fibers disappears as the concentration of the collagen-like protein polymer is increased, supports the second toughening mechanism. A similar effect was observed for simulations done on a fiber network embedded in an elastic matrix.[11] It is therefore possible that the toughening we observed is caused by a combination of the two toughening mechanisms.

For the composite hydrogels we discussed in chapter 4 we combined a silk-like fiber network with a fiber network formed by a FMOC-functionalized dipeptide. With electron microscopy and atomic force microscopy we observed that both components formed different types of fibers, resulting in a composite hydrogel with enhanced mechanical properties. To investigate which toughening mechanism causes this enhancement, we subjected these composite hydrogels to cyclic loading/unloading tests as well. It should be noted that in contrast to the previously discussed composite hydrogels, these composite hydrogels already ruptured at low strains. Furthermore, the rupture strength of these composite networks was slightly increased in comparison to the single networks. We found that no significant hysteresis occurred in this system. The slight toughening observed, points at the second toughening mechanism, in which the fibers deform more affinely when they are embedded in a soft matrix, and reduces the possibility that the first toughening mechanism occurs in this system. Furthermore, we observed that the strain hardening of the dipeptide fiber network disappeared after they were embedded in the silk-like fiber network. We also observed this phenomenon in the composite hydrogel system discussed before.

The first toughening mechanism relies on the increase of the dissipative zone around the crack tip, which slows down crack propagation, and results in toughening. This effect can be more closely studied by incorporating chemo-luminescent crosslinkers in the network, that can emit light if they are broken, to see where the crosslinks are broken as the

hydrogels are deformed.[14] This would however influence the composition, structure, and rheological properties of the system. It is therefore more likely that this approach will be used in other model systems of interest. With regard to the occurrence of the second toughening mechanism, it might be worthwhile to investigate how the silk-like fibers deform if they are embedded in the collagen-like network in comparison to the fiber network alone, using a shear set-up in a confocal microscope. This can be done by using fluorescently labeled silk-like fibers. Only a small fraction of the fibers inside the fiber network should be labelled to be able to distinguish them from each other. An alternative method is to add micron-sized reflective particles to the hydrogels to study the deformation on a macroscopic scale with particle image velocimetry (PIV) measurements.

8.3 Toughening in mixed covalent/non-covalent hydrogels

In chapter 5 we combined physical crosslinks of the collagen-like network with chemical crosslinks formed between the random-coil middle blocks of these protein polymers. This procedure is abundantly used to improve mechanical properties of gelatin hydrogels and to prevent dissolution of the gelatin for biomedical and industrial applications.[15–18] At the right conditions this hydrogel should be able to recover after damage by self-healing of the triple-helical nodes, if the chemical crosslinks are not damaged in the process. In contrast to double network hydrogels, in this system both chemical and physical crosslinks are present in a single network. This approach resulted in moderately improved mechanical properties of the hydrogels, and is consistent with various studies reported in literature.[19–21] To investigate the toughening mechanism responsible for the enhanced mechanical properties, we subjected this system to cyclic loading/unloading tests. We found that no hysteresis occurred until the hydrogel was fractured. In subsequent cycles after fracture, hysteresis occurred due to the physical crosslinks present. This indicates that the chemical crosslinks were permanently fractured, and that at the point of fracture both chemical and physical crosslinks ruptured simultaneously. It is clear that the envisioned process of toughening via energy dissipation of the physical network and subsequent self-healing process is not occurring in this system. The physical crosslinks are probably too strong to function as sacrificial crosslinks in this system. In literature it was reported that in

alginate hydrogels the elastic modulus and toughness of the hydrogels could be independently controlled by varying the physical and chemical crosslink densities.[22] Therefore, tuning of the physical and chemical crosslinks in our system might lead to further toughening of these hydrogels.

8.4 Tuning the mechanics of semi-flexible fiber networks

The mechanical behavior of semi-flexible fiber networks is generally more complicated than that of flexible polymer networks, which can be described by the classical rubber theory. While the elastic modulus of flexible polymer networks depends foremost on the number of crosslinks, the elastic modulus of semi-flexible fiber networks is dependent on various factors: the persistence length, fiber length, entanglement length, and mesh size of the fiber network. The relation between these factors and the elastic modulus is described by the theoretical model proposed by MacKintosh and co-workers.[23] The persistence length, the length scale at which the fiber maintains its orientation, is a measure of the stiffness of the fiber. It is dependent on monomer composition, and can also depend on factors like temperature and ionic conditions.[24–26] Both the entanglement length and mesh size of the fiber network are influenced by concentration: they will decrease as the concentration is increased. It is clear that there are many different ways to influence the mechanical properties of fiber networks. In this paragraph we will discuss the strategies we have used to influence the mechanical properties of fiber networks in this thesis.

After studying the silk-like and collagen-like composite network (chapter 2 and 3) we were interested in the effect of an asymmetrically designed protein polymer containing a silk-like and a collagen-like block. With this design we should be able to crosslink fibers in a reversible manner with collagen-like temperature-responsive physical crosslinks. Furthermore, temperature-responsive fiber networks that are created by sequential triggering of the pH-sensitive **S** block and temperature-responsive $\mathbf{T_9}$ blocks, might result in a better control over network structure. For this purpose an asymmetric silk-like protein polymer with a trimer-forming **T** block attached to the C-terminal side $(\mathbf{C_2^P S_{48}^H C_2^P - T_9})$ of the existing silk-like protein polymer was designed with genetic engineering. Unfortunately, for unclear reasons this newly designed protein polymer was not produced by *Pichia pastoris*. However, a similar design $(\mathbf{S_8^H C_4^R T_9})$ with a short silk-block (8 instead of 48 repeats)

and a trimer-forming block separated by a hydrophilic spacer was successfully produced. In chapter 6, we demonstrated that by combining this asymmetric silk-collagen-like protein polymer with an oppositely charged symmetric silk-like protein polymer, temperature-responsive fiber hydrogels with tunable mechanical properties could be prepared. In this system, temperature was used as a switch for the assembly and disassembly of triple-helical nodes that crosslink the fibers. We demonstrated that it is indeed possible to tune the mechanical properties of the hydrogel by controlling the physical crosslinks.

In chapter 7 we altered the design of a symmetric silk-like protein polymer by adding a cysteine residue to the C-terminal side. We found that the mechanical properties of the fiber network was improved by the presence of physical crosslinks (disulfide-bridges) in the fiber coronae. This was caused by an increased persistence length due to the presence of intra-fiber crosslinks. Furthermore, the scaling between the protein polymer concentration and the elastic modulus of this system is in good agreement with the theoretical model proposed by MacKintosh and co-workers.[23]

In previous work done in our group it was shown that the mechanical properties of fiber networks can be tuned by changing the block length of silk-like protein polymers. Investigation of the self-assembly behavior of the $C_2^P S_n^H C_2^P$ series by varying the silk-block length (S_n^H, with n=8, 16, 24 and 48) showed that the protein polymers with the shortest silk-block lengths (n=8 and 16) formed spherical micelles instead of fibers.[27] However, it was found that after the flanking random-coil blocks were removed by enzymatic digestion, fibers were formed. In the absence of the random-coil blocks the fibers had the tendency to bundle. Rheological measurements comparing the hydrogels formed by the protein polymers containing 24 and 48-repeat silk-like blocks showed an order of magnitude higher storage moduli for the 48-repeat silk-block.[27] In a follow-up study the effect of the random-coil block length (C_n^P, with n=1 and 2) on hydrogel formation of di-block silk-like protein polymers ($C_n^P S_{48}^H$) was evaluated with rheology.[28] Significantly different scaling behavior of modulus versus concentration was found for $C_1^P S_{48}^H$ and $C_2^P S_{48}^H$ hydrogels, suggesting that the morphologies of the $C_1^P S_{48}^H$ and $C_2^P S_{48}^H$ fiber networks are different. With AFM it was observed that the $C_1^P S_{48}^H$ fibers had the tendency to bundle, while this effect was negligible for the $C_2^P S_{48}^H$ fibers. It was concluded that by decreasing the length of the random-coil block, the hydrophobic fiber core becomes more exposed, promoting the association of fibers, which results in additional crosslinks in the network.[28]

Fiber bundling might be an interesting way to tune mechanical

142

properties of fiber networks.[29,30] In chapter 2 we observed that the silk-like fibers were bundled in the presence of the collagen-like protein polymer. This probably occurred due to depletion attraction. This interaction is suggested to play an important role in the formation of large structures, like fibers and other assemblies in cells.[31] It was shown by Tharmann and co-workers that the mechanical and structural properties of F-actin fibers could be affected by the depletion agent polyethylene glycol (PEG): fiber bundling could be controlled by the PEG concentration.[32] Kouwer and co-workers prepared hydrogels from polyisocyanopeptides grafted with oligo(ethylene glycol) side chains.[30] By relating the bulk mechanical properties to parameters at the molecular scale they demonstrated that the polymer chains were bundled. Furthermore, it was predicted that the elastic modulus will increase with increasing bundle thickness.[30] However, there should be an optimal thickness of the fiber bundles in relation to the elastic modulus, because when the bundle thickness increases, the mesh size of the fiber network increases as well. This will ultimately result in a decrease of the elastic modulus as the bundle thickness is increased further.

8.5 Future plans and follow up research

As mentioned before, not all protein polymers that were designed could be produced with *P. pastoris*. Furthermore, preparing new protein polymer designs with genetic engineering can be a time consuming process. Therefore an alternative approach to get the desired protein polymer designs is required. Our aim is to make a toolbox of protein polymers that can be fused after production by means of incompatible domains to make various more complicated combinations possible. We were still interested to make $C_2^P S_{48}^H C_2^P - T_9$, the design we originally aimed for. To do this we adopted a two-step approach in which the **S** and **T** containing polymers were linked after production: (1) we designed and biosynthetically produced cysteine-functionalized protein polymers that can be modified via chemical means, and (2) we designed and biosynthetically produced protein polymers that contained sortaseA tags for enzymatic coupling.

8.5.1 Cysteine-functionalized protein polymers

We adapted the design of the symmetric silk-like protein polymer with genetic engineering in which a cysteine residue was added to the C-terminal side of the protein polymer ($C_2^P S_{48}^H C_2^P$-Cys). The same was done to the

design of a di-block collagen-like protein polymer ($T_9C_4^R$-Cys) consisting of a random-coil block and a trimer-forming block. Because of the rarity of cysteine residues in proteins and the unique reactivity of thiol side-chains present in cysteine residues, these residues are extensively used for chemical modifications of proteins.[33,34] We were able to produce both new protein polymers with *P. pastoris* successfully. We characterized both products with MALDI and gel electrophoresis (SDS-PAGE) (data not shown). The second step involved the selective chemical modification of the cysteine residues of both protein polymers. This step is necessary because cysteine residues in either protein polymer with cysteine residues are able to form disulfide-bridges in oxidizing conditions. Therefore, via selective reaction of the cysteine residue with a maleimide at pH 6.5, a maleimide-PEG$_4$-DBCO (Click Chemistry Tools) was coupled to the silk-like protein polymer. Similarly, we modified the di-block collagen-like protein polymer with a maleimide-PEG$_3$-azide (Click Chemistry Tools). Both chemically modified protein polymers can now be coupled covalently via a strain-promoted azide-alkyne cycloaddition (Figure 8.2), yielding a block copolymer with both a T_9 block and a S_{48}^H block.[35,36]
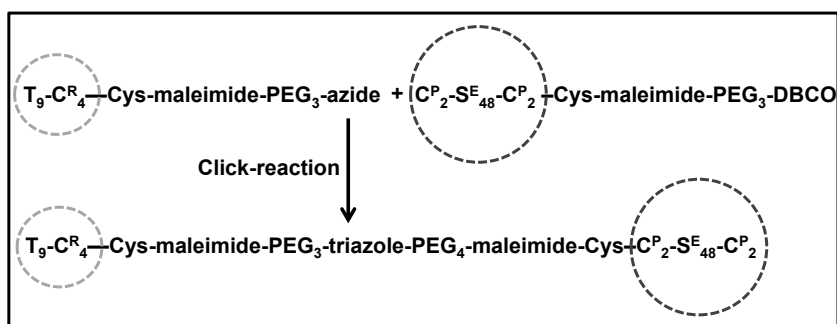
Figure 8.2: *Selective coupling of DBCO-modified $C_2^P S_{48}^H C_2^P$ – Cys and azide-modified $T_9 C_4^R$ – Cys via strain-promoted azide-alkyne cycloaddition.*

Preliminary results on the characterization of the chemically modified protein polymers indicate that the silk-like protein polymer is at least partially modified. With UV-Vis measurements a clear peak belonging to the DBCO moiety was visible, and with NMR we could clearly observe the PEG-spacer attached to the DBCO moiety (data not shown). Unfortunately, for the modified collagen-like protein polymer the characterization was more difficult: with NMR we could not distinguish the PEG-spacer, and with IR-spectroscopy we only got a weak peak which could belong to the

azide-group. Clearly, in both cases we do not know the conversion after modification. For further characterization it is worthwhile to let the DBCO-modified silk-like protein polymer react with an azide-functionalized fluorophore, and the azide-modified collagen-like protein polymer react with a DBCO-functionalized fluorophore. With fluorometry and a calibration curve we can then obtain a more quantitative idea about the conversion after the chemical modifications.

8.6 Selective enzymatic coupling with SortaseA

An alternative approach to couple protein polymers together is by using the substrate specific SortaseA enzyme. This enzyme is a bacterial transpeptidase that catalyzes the covalent coupling of a protein containing a C-terminal Leu-Pro-Xxx-Thr-Gly-Gly motif to a protein containing a N-terminal poly-glycine motif.[37–39] In recent years SortaseA has been used for many different purposes: attaching GFP to polystyrene beads,[40] immobilization of proteins to surfaces,[41] protein-protein fusion.[42] Based on the principle of sortase-coupling, new designs of protein polymers were prepared: two silk-like protein polymers with a N-terminal penta-glycine motif (Gly$_5$-$\mathbf{C}_2^{\mathbf{P}}\mathbf{S}_{48}^{\mathbf{H}}\mathbf{C}_2^{\mathbf{P}}$ and Gly$_5$-$\mathbf{C}_2^{\mathbf{P}}\mathbf{S}_{48}^{\mathbf{E}}\mathbf{C}_2^{\mathbf{P}}$), and a di-block collagen-like protein with a C-terminal Leu-Pro-Glu-Thr-Gly-Gly motif ($\mathbf{T_9}\mathbf{C}_4^{\mathbf{R}}$-Leu-Pro-Glu-Thr-Gly-Gly). The three protein polymers were successfully produced with *P. pastoris*. We characterized both products with MALDI and SDS-PAGE (data not shown). The coupling of the protein polymers with sortaseA enzyme is displayed in Figure 8.3.
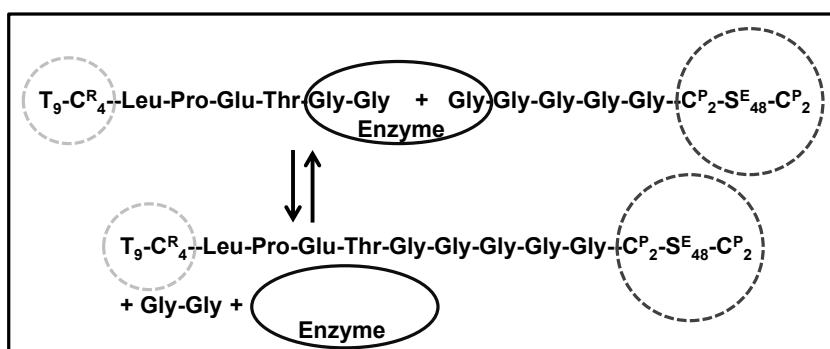

Figure 8.3: *Covalent coupling of Gly$_5$-$\mathbf{C}_2^{\mathbf{P}}\mathbf{S}_{48}^{\mathbf{H}}\mathbf{C}_2^{\mathbf{P}}$ and $\mathbf{T_9}\mathbf{C}_4^{\mathbf{R}}$-Leu-Pro-Glu-Thr-Gly-Gly with sortaseA enzyme.*

Preliminary experiments coupling the protein polymers together with SortaseA enzyme, monitored with SDS-PAGE, were not succesfull. Clear bands of the SortaseA enzyme and both protein polymers were distinguished with SDS-PAGE (data not shown). A fourth band belonging to the fused protein polymer was not observed. However, it should be noted that the protein polymers poorly bind to SDS (especially the collagen-like protein polymers), and therefore migrate slower than expected based on the molar mass of the protein polymers. It is therefore possible that there was considerable overlap between the fused protein polymers and the non-fused protein polymers. The coupling of protein polymers should be checked with size exclusion chromatography (SEC) to get a definite answer on the success of coupling. Furthermore, optimization of various reaction conditions is necessary: reactant concentrations, enzyme concentration, temperature, and reaction time.

8.7 Toward application

Although the aim of this thesis was not focused on application, the materials that were discussed can have many potential applications (Figure 8.4). Genetic engineering, the tool that is used to generate the production host for the recombinant protein polymers, provides control over the amino acid sequence, mono-disperse products, and a stable system for fast and reproducible polymer (re)production. Furthermore, protein polymers are promising candidates for biomedical applications, because they consist only of natural building blocks.
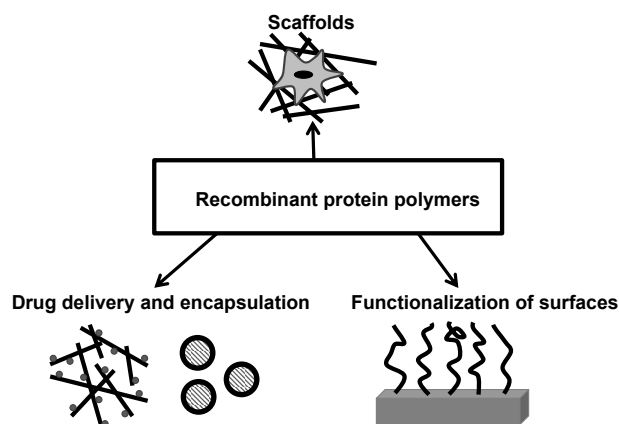
Figure 8.4: *Various possible applications of recombinant protein polymers.*

146

8.7.1 Scaffolds

There are five important factors when determining if a biomaterial is suitable to use as a scaffold for tissue engineering: biocompatibility, biodegradability, mechanical properties, architecture, and processability.[43] In short, biocompatibility infers that the scaffold should not adversely affect cell adhesion, proliferation, and functioning. The scaffold should be biodegradable to allow cells to form their own ECM and eventually replace the scaffold gradually over time. With regard to the first two criteria, the recombinant protein polymers consist of natural building blocks (amino acids) and are therefore considered biocompatible in comparison to synthetic materials, and can possibly be degraded via enzymatic degradation and hydrolysis. The mechanical properties of the scaffold should match those of the target tissue and should allow material handling during implantation procedures. It was demonstrated that the mechanical properties of the composite hydrogel were significantly improved in comparison to the single networks: this effect was observed in mixtures of soft and stiff components (chapter 2), as well as two fiber-forming components (chapter 4). Also, introduction of chemical crosslinks to physical hydrogels (chapter 5) and introduction of cysteine residues in comparison to the single components (chapter 7) significantly improved the mechanical properties.

Depending on the intended scaffold application, the mechanical strength of composite hydrogels can be tuned by varying the amounts of the protein polymers. The mechanical strength of the ECM, a biological composite, is mainly determined by the amount and ordering of the collagen fibers.[4,5] The composite fiber-containing hydrogels discussed here, partially mimic the ECM, and therefore they can be considered as scaffold materials. The architecture of a scaffold involves the porosity, pore size, and cell-binding ligands. The porosity and pore size are crucial for diffusion of nutrients into the scaffold and metabolites out of the scaffold. The presence of cell-binding ligands such as RGD-sequences can promote cell attachment.[44] These RGD-sequences can be incorporated into the designs of the protein polymers with genetic engineering. In addition, BMP-2 or other growth factors of interest can be incorporated in the scaffold, that can direct cell differentiation, via chemical modification of cysteine residues or sortaseA-coupling.[45,46] With regard to the porosity and pore size of silk-like protein polymer hydrogels, analysis with scanning electron microscopy (SEM) demonstrated pore sizes in the range 50-150 nm (chapter 6), which is roughly an order of magnitude lower than the size of cells. It might be possible for the cells to remodel the fiber matrix in

such a way that they can migrate within the scaffold. Probably, the diffusion of nutrients to the cells and metabolites from the cells will be the limiting factor for using these scaffolds for 3D tissue culture. With regard to the processability of the material, proteins in general cannot withstand heat treatment and treatment with aggressive chemicals, however they can be filter sterilized. Recently, 2D cell culture studies performed on silk-like protein polymer hydrogels proved that rat bone mesenchymal stem cells were able to proliferate and mineralize *in vitro*.[47]

8.7.2   Drug delivery and encapsulation

Hydrogels are interesting candidates for drug delivery applications, because of their high water content, porosity, and biocompatibility.[48] However, this high water content is also a point of concern: drugs can be released too rapidly, which can be potentially harmful to the patient. Therefore, an important requirement is that release of drugs from the hydrogel can be controlled. The drug release is a very complex process that is dependent on many factors such as: geometry of drug carrier, swelling of the polymer in the drug carrier, interaction between the drug and hydrogel, and the location of drug delivery.[48–50] Drug release can be controlled by designing a drug carrier that can interact with the drug. There are several strategies that use this principle: covalent bonding of the drug to the drug carrier,[51] electrostatic physical interactions,[52] controlled surface diffusion by a reduced-permeability film at the surface.[53] When hydrogels are formed, and mixed with the drug outside of the body, problems can arise due to the viscosity of the gelling solution. Therefore a better control over the gelation time of the hydrogel, or preparing hydrogel microspheres that are loaded with the drug and are injectable, might be alternative solutions. Some of the protein polymers can be considered for drug delivery applications. The collagen-like polymers ($T_9C_4^RT_9$) can form gels at physiological pH. The collagen-like network has a small mesh size and thus porosity, which might have a favorable drug release profile. However, the melting temperatures of the T_9 gels at the concentrations used in this thesis are close to body temperature. This probably results in weak gels that are unsuitable for drug delivery purposes. Furthermore, erosion of polymers from the gel surface will occur already far below the melting temperature of the gel. This problem can be solved by increasing the length of the T block. Collagen-like triblock copolymers with T_6, T_{12} and T_{16} blocks at the ends were designed and investigated in previous work. It was shown that the melting temperature of the triple helices could be increased

to 60 °C by increasing the **T** block length.[54] The silk-like protein polymer functionalized with the cysteine residue ($C_2^P S_{48}^H C_2^P$-Cys), and the silk-like protein polymer with the sortaseA tag (Gly$_5$-$C_2^P S_{48}^H C_2^P$), both can form rigid hydrogels at physiological pH and temperature. Here, the mesh size of the fiber network is bigger than that of the gelatin-like networks. For $C_2^P S_{48}^H C_2^P$-Cys, drugs can be covalently coupled to the silk-fibers via chemical modification of the cysteine residue. For Gly$_5$-$C_2^P S_{48}^H C_2^P$, the conjugate sortaseA tag is coupled to the drug and via enzymatic coupling with sortaseA the drug can be coupled to the silk fibers.

8.7.3 Surface modification

Implants used in the medical industry often contain materials that are alien to the human body, and can therefore invoke adverse reactions such as inflammation and infection. To prevent these adverse reactions from happening, the surface of the implant needs to be screened from the surrounding environment. This can be done by modifying the surface of the implants in various ways: chemical grafting, self-assembled monolayers, and plasma medication.[55] As we are discussing the possible application of protein polymers, the focus will be on the chemical grafting method only. This method is used to immobilize proteins or polymers on surfaces to introduce desired functional groups or bioactive groups on the surface, and to minimize contact of the alien material with the surrounding environment. This method generally involves covalent coupling of the protein or polymer to the surface of interest. The silk-like protein polymers discussed in this thesis can be of potential interest for this purpose. Adaptions to the protein polymer design can be easily made with genetic engineering to introduce sortaseA tags, cysteine residues, and bio-active RGD sequences. Via selective coupling with the sortaseA enzyme,[41] or via chemical modification of cysteine residues,[33,34] these protein polymers can be coupled to surfaces. In case of the silk-like proteins, this procedure can be done after the fibers are formed to get a fiber-coating on an implant. As fibers are present in abundance in the ECM, introducing these silk-like fibers on the surface of an implant might improve cell attachment. The random-coil middle block C_4^R might be used to make implant surfaces more biocompatible, because the amino acid composition of this block is similar to that of natural collagen.

8.8 Concluding remarks

With regard to the engineering of hydrogels for tissue engineering purposes, we have shown that there are various strategies to improve the mechanical properties of fiber networks: by embedding the fibers in a soft elastic matrix (chapter 2 and 3), by adding a second fiber network (chapter 4), by crosslinking the fibers with physical interactions (chapter 6), and by intra-fiber crosslinking via cysteine residues (chapter 7). At this stage, combining two different networks is the most promising method to prepare stronger hydrogels, because the improvement of the mechanical properties observed was the largest in these composite networks. The synergy of two different components leads to improved mechanical properties. This is probably also the reason that composite materials are present in abundance in nature.

In terms of the mechanical properties of the hydrogels discussed, there is still a long way to go when they are compared to the moduli of tissues (~MPa). Considering the fact that the hydrogels presented in this thesis contain more than 90% (w/v) water, it is possible to improve the mechanical properties by increasing the concentration of the protein polymers. It should be noted however that the biosynthetic production of genetically engineered protein polymers is relatively expensive (~1,000 € per gram). By mixing silk-like protein polymers with FMOC-dipeptides as is shown in chapter 4, the cost of these hydrogels can be reduced, because the amount of silk-like protein polymers in the composite can be reduced, to obtain similar mechanical properties as the silk-like hydrogels would have.

References

(1) Smith, C. M.; Beasley, G. C.; Cheng, Y.; Ormond, D. B.; Spain, P. *US Department of Health and Human Services*, *Health Resources and Services Administration*, *United Network for Organ Sharing*, *Richmond*, *Va* **2000**, *2000*, 351–410.

(2) Langer, R.; Vacanti, J. P. *Science* **1993**, *260*, 920–926.

(3) Fisher, M. B.; Mauck, R. L. *Tissue Eng. Part B* **2013**, *19*, 1–13.

(4) Alberts, B.; Bray, D.; Hopkin, K.; Johnson, A.; Lewis, J.; Raff, M.; Roberts, K.; Walter, P., *Essential cell biology*; Garland Science: 1998.

(5) Holzapfel, G., *Biomechanics of soft tissue. In: The handbook of Materials Behavior, Nonlinear Models and Properties*; Academic New York: 2000.

(6) Hennink, W. E.; van Nostrum, C. F. *Adv. Drug Deliv. Rev.* **2002**, *54*, 13–36.

(7) Hiltner, A.; Cassidy, J. J.; Baer, E. *Ann. Rev. Mater. Sci.* **1985**, *15*, 455–482.

(8) Gong, J. P.; Katsuyama, Y.; Kurokawa, T.; Osada, Y. *Adv. Mater.* **2003**, *15*, 1155–1158.

(9) Webber, R. E.; Creton, C.; Brown, H. R.; Gong, J. P. *Macromolecules* **2007**, *40*, 2919–2927.

(10) Gong, J. P. *Soft Matter* **2010**, *6*, 2583–2590.

(11) Zhang, L.; Lake, S. P.; Barocas, V. H.; Shephard, M. S.; Picu, R. C. *Soft matter* **2013**, *9*, 6398–6405.

(12) Onck, P.; Koeman, T.; Van Dillen, T.; Van der Giessen, E. *Phys. Rev. Lett.* **2005**, *95*, 178102.

(13) Brangwynne, C. P.; MacKintosh, F. C.; Kumar, S.; Geisse, N. A.; Talbot, J.; Mahadevan, L.; Parker, K. K.; Ingber, D. E.; Weitz, D. A. *J. Cell Biol.* **2006**, *173*, 733–741.

(14) Ducrot, E.; Chen, Y.; Bulters, M.; Sijbesma, R. P.; Creton, C. *Science* **2014**, *344*, 186–189.

(15) Zhang, X.; Do, M. D.; Casey, P.; Sulistio, A.; Qiao, G. G.; Lundin, L.; Lillford, P.; Kosaraju, S. *Biomacromolecules* **2010**, *11*, 1125–1132.

(16) Gerrard, J. A.; Brown, P. K.; Fayle, S. E. *Food Chem.* **2002**, *79*, 343–349.

(17) Gerrard, J. A.; Brown, P. K.; Fayle, S. E. *Food Chem.* **2003**, *80*, 35–43.

(18)   Olde Damink, L. H. H.; Dijkstra, P. J.; Van Luyn, M. J. A.; Van Wachem, P. B.; Nieuwenhuis, P.; Feijen, J. *J. Mater. Sci.:Mater. Med.* **1995**, *6*, 460–472.

(19)   Hellio, D.; Djabourov, M. In *Macromol. Symp.* 2006; Vol. 241, pp 23–27.

(20)   Xing, Q.; Yates, K.; Vogt, C.; Qian, Z.; Frost, M. C.; Zhao, F. *Sci. Rep.* **2014**, *4*.

(21)   Bigi, A.; Bracci, B.; Cojazzi, G.; Panzavolta, S.; Roveri, N. *Biomaterials* **1998**, *19*, 2335–2340.

(22)   Kong, H. J.; Wong, E.; Mooney, D. J. *Macromolecules* **2003**, *36*, 4582–4588.

(23)   MacKintosh, F. C.; Käs, J.; Janmey, P. A. *Phys. Rev. Lett.* **1995**, *75*, 4425.

(24)   Hagerman, P. J. *Annu. Rev. Biophys. Biophys. Chem.* **1988**, *17*, 265–286.

(25)   Geggier, S.; Vologodskii, A. *Proc. Natl. Acad. Sci.* **2010**, *107*, 15421–15426.

(26)   Geggier, S.; Kotlyar, A.; Vologodskii, A. *Nucleic acids research* **2010**, *39*, 1419–1426.

(27)   Beun, L. H.; Storm, I. M.; Werten, M. W. T.; de Wolf, F. A.; Cohen Stuart, M. A.; De Vries, R. *Biomacromolecules* **2014**, *15*, 3349–3357.

(28)   Beun, L. H. Molecular design, self-assembly, and material properties of silk-like protein polymers., Ph.D. Thesis, 2015.

(29)   Gardel, M. L.; Shin, J. H.; MacKintosh, F. C.; Mahadevan, L.; Matsudaira, P.; Weitz, D. A. *Science* **2004**, *304*, 1301–1305.

(30)   Kouwer, P. H. J.; Koepf, M.; Le Sage, V. A. A.; Jaspers, M.; van Buul, A. M.; Eksteen-Akeroyd, Z. H.; Woltinge, T.; Schwartz, E.; Kitto, H. J.; Hoogenboom, R., et al. *Nature* **2013**, *493*, 651–655.

(31)   Marenduzzo, D.; Finan, K.; Cook, P. R. *J. Cell Biol.* **2006**, *175*, 681–686.

(32)   Tharmann, R.; Claessens, M. M. A. E.; Bausch, A. R. *Biophys. J.* **2006**, *90*, 2622–2627.

(33)   Chalker, J. M.; Bernardes, G. J. L.; Lin, Y. A.; Davis, B. G. *Chem. Asian J.* **2009**, *4*, 630–640.

(34)   Baslé, E.; Joubert, N.; Pucheault, M. *Chem. Biol.* **2010**, *17*, 213–227.

(35)   Agard, N. J.; Prescher, J. A.; Bertozzi, C. R. *J. Am. Chem. Soc.* **2004**, *126*, 15046–15047.

(36) Van Berkel, S. S.; Floris, P. J. T.; van Hest, J. C. M.; van Delft, F. L., et al. *Chem. Commun.* **2010**, *46*, 97–99.

(37) Mazmanian, S. K.; Liu, G.; Ton-That, H.; Schneewind, O. *Science* **1999**, *285*, 760–763.

(38) Marraffini, L. A.; DeDent, A. C.; Schneewind, O. *Microbiol. Mol. Biol. Rev.* **2006**, *70*, 192–221.

(39) Bentley, M. L.; Lamb, E. C.; McCafferty, D. G. *J. Biol. Chem.* **2008**, *283*, 14762–14771.

(40) Parthasarathy, R.; Subramanian, S.; Boder, E. T. *Bioconjugate Chem.* **2007**, *18*, 469–476.

(41) Sijbrandij, T.; Cukkemane, N.; Nazmi, K.; Veerman, E. C. I.; Bikker, F. J. *Bioconjugate Chem.* **2013**, *24*, 828–831.

(42) Levary, D. A.; Parthasarathy, R.; Boder, E. T.; Ackerman, M. E. *PLoS One* **2011**, *6*, e18342.

(43) O'Brien, F. J. *Mater. Today* **2011**, *14*, 88–95.

(44) Bellis, S. L. *Biomaterials* **2011**, *32*, 4205–4210.

(45) Poldervaart, M. T.; Wang, H.; van der Stok, J.; Weinans, H.; Leeuwenburgh, S. C.; Oner, F. C.; Dhert, W. J.; Alblas, J. *PloS one* **2013**, *8*, e72610.

(46) Lee, K.; Silva, E. A.; Mooney, D. J. *J. R. Soc., Interface* **2011**, *8*, 153–170.

(47) Włodarczyk-Biegun, M. K.; Werten, M. W. T.; de Wolf, F. A.; van den Beucken, J. J. J. P.; Leeuwenburgh, S. C. G.; Kamperman, M.; Stuart, C. M. A. *Acta biomaterialia* **2014**, *10*, 3620–3629.

(48) Hoare, T. R.; Kohane, D. S. *Polymer* **2008**, *49*, 1993–2007.

(49) Siepmann, J.; Göpferich, A. *Adv. Drug Deliv. Rev.* **2001**, *48*, 229–247.

(50) Brandl, F.; Kastner, F.; Gschwind, R. M.; Blunk, T.; Teßmar, J.; Göpferich, A. *J. Controlled Release* **2010**, *142*, 221–228.

(51) Schoenmakers, R. G.; van de Wetering, P.; Elbert, D. L.; Hubbell, J. A. *J. Controlled Release* **2004**, *95*, 291–300.

(52) Rodríguez, R.; Alvarez-Lorenzo, C.; Concheiro, A. *Eur. J. Pharm. Sci.* **2003**, *20*, 429–438.

(53) Matsusaki, M.; Sakaguchi, H.; Serizawa, T.; Akashi, M. *J. Biomater. Sci., Polym. Ed.* **2007**, *18*, 775–783.

(54) Silva, C. I. F.; Skrzeszewska, P. J.; Golinska, M. D.; Werten, M. W. T.; Eggink, G.; de Wolf, F. A. *Biomacromolecules* **2012**, *13*, 1250–1258.

(55)   Thevenot, P.; Hu, W.; Tang, L. *Curr. Top. Med. Chem.* **2008**, *8*, 270–280.

9 Summary

In this thesis we presented various combinations of custom-designed protein polymers that formed composite hydrogels. In **chapter 2**, composite hydrogels were prepared by mixing fiber-forming silk-like block copolymers ($C_2^P S_{48}^E C_2^P$) with collagen-like block copolymers ($T_9 C_4^R T_9$). We found that by adding the collagen-like protein polymer the storage modulus, the critical stress, and critical strain values of the composite hydrogels were significantly improved in comparison to the single networks. With cryo-transmission electron microscopy (cryo-TEM) we observed that the silk-like fibers were bundled in the presence of the collagen-like protein polymer, probably due to depletion attraction interactions. In follow-up research on these composite hydrogels in **chapter 3**, we tried to get more insight into the exact toughening mechanism and self-healing capabilities of the composite network by performing cyclic loading/unloading tests. We found that mechanical hysteresis occurred in these composite hydrogels. The energy that was dissipated could be split into two contributions: a permanent part belonging to the irreversible rupture of silk-like fibers, and a viscoelastic part belong to the disassembly and assembly of collagen-like triple helices. Both these contributions increased as the concentration of the collagen-like protein polymer in the composite network was increased, resulting in toughening of the composite network. Furthermore, it was observed that the silk-like fiber network was not able to recover, while the composites could recover up to 70% of the original storage modulus after failure. In **chapter 4** we studied composite networks of silk-like block copolymers ($C_2^P S_{48}^E C_2^P$) and a FMOC-functionalized dipeptide (FMOC-LG) which could both form fibers. With cryo-TEM and atomic force microscopy (AFM) we found that two different types of fibers were formed, indicating that orthogonal self-assembly occurred in this system. We found with rheology that the storage moduli of the composite fiber networks were significantly higher (75 kPa vs 400 kPa) than that of the single networks. Strain hardening present in the FMOC-LG fiber network disappeared when the silk-like protein polymer was present. In **chapter 5** hydrogels with both physical and chemical crosslinks were prepared from collagen-like protein polymers ($T_9 C_4^R T_9$). The chemical crosslinks were introduced by crosslinking lysine residues present in the random-coil middle blocks with glutaraldehyde. We found with rheology that the order in which the physical and chemical networks were formed did not influence the final storage modulus of the hydrogel. Depending on the amount of glutaraldehyde added, we found an increase of up to an order of magnitude in the storage modulus for the collagen-like hydrogels. To investigate

effects on the nonlinear rheological properties, cyclic loading/unloading tests were performed. It was observed that before hydrogel failure occurred, no hysteresis was observed between consecutive cycles. Both physical and chemical crosslinks ruptured when the hydrogel was fractured. In **chapter 6** we studied hydrogels formed by the co-assembly of an asymmetric silk-collagen-like protein polymer ($S_8^H C_4^R T_9$) with a symmetric oppositely charged silk-like protein polymer ($C_2^P S_{48}^E C_2^P$). This was done in a step-wise approach: (1) the **S** blocks were co-assembled into silk-like fibers. (2) the **T** blocks were assembled into triple helical nodes by reducing the temperature. We confirmed with confocal laser scanning microscopy (CLSM) and NMR that both monomers were present in the same fibers. With rheology we found that these composite hydrogels did respond in a reversible manner to temperature changes, with which the mechanical strength of the hydrogel can be tuned. In **chapter 7** hydrogel formation of a modified silk-like protein polymer with a cysteine residue attached to the C-terminal side ($C_2^P S_{48}^H C_2^P$-Cys) was studied. With rheology we showed that hydrogels that were formed in oxidizing conditions, where disulfide-bridges could form, were much stronger than those formed in reducing conditions. Both hydrogels formed in oxidizing and reducing conditions showed a scaling of modulus versus concentration consistent with entangled semi-flexible networks. This result implies that the disulfide-bridges formed between cysteine residues formed loops in the coronae of the fibers. The increase in mechanical strength of the fibers was related to the increase in persistence length of the fibers in oxidizing conditions observed with AFM. With self-consistent field theory-simulations it was shown that the formation of loops in the corona resulted in a slight reduction of the lateral pressure in the corona of the fibers. However, this effect is by itself not sufficient to cause a significant change in persistence length. Due to the reduction in lateral pressure, the stacking of monomers into fibers is probably influenced: fibers with a more crystalline structure and with less detects are formed, resulting in improved mechanical properties of the hydrogels. In the general discussion in **chapter 8**, we reflect on our work, discuss about future directions of research, and possible applications of protein polymers.

Samenvatting

In dit proefschrift beschrijven we de mechanische eigenschappen en structuur van composiete hydrogelen gemaakt van verschillende combinaties van bio-geïnspireerde eiwitpolymeren. In **hoofdstuk 2** bestuderen we een hydrogel die gemaakt is uit een combinatie van zijde-achtige ($C_2^P S_{48}^E C_2^P$) en collageen-achtige eiwitpolymeren ($T_9 C_4^R T_9$). We hebben aangetoond dat na toevoeging van de collageen-achtige eiwitpolymeren de elastische modulus, de kritische schuifspanning en de kritische deformatie van de composiete hydrogelen significant verbeterd zijn in vergelijking met de hydrogelen gemaakt van de losse componenten. Met cryo-transmissie elektronen microscopie (cryo-TEM) hebben we gezien dat de zijde-achtige fibers in aanwezigheid van het collageen-achtige eiwitpolymer gebundeld zijn. Dit wordt vermoedelijk veroorzaakt door depletie interacties. In vervolg-onderzoek naar dit systeem (**hoofdstuk 3**) hebben we ons gericht op het verkrijgen van meer inzicht in het exacte versterkingsmechanisme en de zelf-helende eigenschappen van dit composiete netwerk. Dit is gedaan door herhaalde belasting/ontlasting experimenten uit te voeren. We hebben gezien dat er hysterese optreedt in de composiete hydrogelen. De gedissipeerde energie kan in twee catagorieën worden onderverdeeld: permanente beschadiging door het onomkeerbaar breken van de zijde-achtige fibers, en een viscoelastische bijdrage die afkomstig is van het ontvouwen en vouwen van de collageen-achtige drievoudige helices. Zowel de permanente en viscoelastische bijdrages aan de gedissipeerde energie nemen toe als de concentratie van het collageen-achtige eiwitpolymer in het composiete netwerk toeneemt, wat in een versterking van het composiete netwerk resulteert. Hydrogelen die alleen bestaan uit de zijde-achtige eiwitpolymeren zijn niet in staat om zich te herstellen na breuk, dit in tegenstelling tot de composiete hydrogelen die zich tot 70% van de originele elastische modulus kunnen herstellen. In **hoofdstuk 4** hebben we composiete hydrogelen gemaakt van een zijde-achtige eiwitpolymeer ($C_2^P S_{48}^E C_2^P$) en een FMOC-gefunctionaliseerde dipeptide (FMOC-LG). Beide

componenten kunnen fibers vormen. Met cryo-transmissie elektronen microscopie en atoomkrachtmicroscopie (AFM) laten we zien dat er twee verschillende typen vezels aanwezig zijn, wat betekent dat er orthogonale zelf-assemblage heeft plaats gevonden in dit systeem. Met reologie tonen we aan dat de elastische modulus van het composiete netwerk significant hoger (75 kPa versus 400 kPa) is dan die van de enkele netwerken. Niet-lineair gedrag (strain hardening) dat aanwezig is in het FMOC-LG netwerk, verdwijnt als het zijde-achtige eiwitpolymeer wordt toegevoegd. In **hoofdstuk 5** bestuderen we hydrogelen gemaakt van collageen-achtige eiwitpolymeren ($T_9C_4^RT_9$), waarin zowel fysische als chemische crosslinks aanwezig zijn. De chemische crosslinks worden gevormd door lysine residuen, die aanwezig zijn in het oplosbare middenblok, met behulp van glutaraldehyde met elkaar te verbinden. Met reologie laten we zien dat de volgorde van het vormen van de fysische en chemische crosslinks geen effect heeft op de uiteindelijke elastische modulus. Afhankelijk van de hoeveelheid glutaraldehyde hebben we een orde van grootte verschil geobserveerd in de elastische moduli van de collageen-achtige hydrogelen. We hebben de niet-lineaire eigenschappen van de hydrogelen bestudeerd door herhaalde belasting/ontlasting experimenten uit te voeren. Er treedt geen hysterese op in deze hydrogelen voordat breuk optreedt. Zowel de fysische als chemische crosslinks breken op het moment dat er breuk in de hydrogel optreedt. In **hoofdstuk 6** hebben we hydrogelen gevormd door middel van co-assemblage van een asymmetrisch zijde-collageen-achtig eiwitpolymeer ($S_8^HC_4^RT_9$) met een tegengesteld geladen symmetrische zijde-achtig eiwitpolymeer ($C_2^PS_{48}^EC_2^P$). Dit is in twee stappen gedaan: (1) de co-assemblage van de **S**-blokken die aanwezig zijn in beide polymeren, (2) Het vormen van drievoudige helices door zelf-assemblage van de **T**-blokken als de temperatuur verlaagd wordt. Met confocale laserfluorescentiemicroscopie (CLSM) en kernspinresonantie (NMR) laten we zien dat beide polymeren aanwezig zijn in de fibers. Met reologie tonen we aan dat de elastische modulus van deze hydrogelen reversibel reageert op verandering van de temperatuur. Door het veranderen van de temperatuur kan de mechanische sterkte van deze hydrogelen gecontroleerd worden. In **hoofdstuk 7** hebben we hydrogel formatie bestudeerd van een gemodificeerd zijde-achtig eiwitpolymeer ($C_2^PS_{48}^HC_2^P$-Cys), waarbij aan de C-terminale zijde een cysteine residu aanwezig is. Met reologie laten we zien dat wanneer de hydrogelen in geoxideerde omstandigheden gevormd worden, de hydrogelen significant sterker zijn dan gelen die in gereduceerde omstandigheden zijn gevormd. Beide typen hydrogelen hebben een

schaling tussen de elastische modulus versus concentratie die consistent is met die van verstrikte semi-flexibele netwerken. Dit resultaat impliceert dat de cysteine residuen disulfide-bruggen vormt in de coronae van de fibers. Met atoomkrachtmicroscopie hebben we laten zien dat het verschil in mechanische sterkte tussen de hydrogelen gevormd in oxiderende en reducerende omstandigheden kan worden verklaard door een toename van de persistentielengte van de fibers. Met zelf-consistente-veld theorie simulaties hebben we aangetoond dat het vormen van lussen in de coronae van de fibers leidt tot een kleine afname van de laterale druk in de corona van de fibers. Dit effect is echter niet genoeg om tot een significante toename van de persistentie lengte te leiden. Vermoedelijk is door het verlagen van de laterale druk in de corona het assembleren van de monomeren in de fibers beïnvloed: meer kristallijne fibers worden gevormd, waarin minder defecten aanwezig zijn, wat resulteert in betere mechanische eigenschappen van de hydrogelen. In de algemene discussie (**hoofdstuk 8**), reflecteren we op ons werk, bediscussiëren we toekomstige onderzoeksplannen en mogelijke toepassingen van de eiwitpolymeren.

List of publications

This thesis:

Chapter 2: Rombouts, W. H.; Colomb-Delsuc, M.; Werten, M. W. T.; Otto, S.; de Wolf, F. A.; van der Gucht, J. Enhanced rigidity and rupture strength of composite hydrogel networks of bio-inspired block copolymers. *Soft Matter* **2013**, *9*, 6936–6942.

Chapter 3: Rombouts, W. H.; van der Gucht, J. Breaking and Self-Healing of Composite Hydrogels Formed by Silk-like and Collagen-like Block Copolymers. *Submitted*

Chapter 4: Rombouts, W. H.; Giesbers, M.; van Lent, J., de Wolf, F. A.; van der Gucht, J. Synergistic Stiffening in Double-Fiber Networks. *Biomacromolecules* **2014**, *15*, 1233-1239.

Chapter 5: Rombouts, W. H.; Galerne, M.; van der Gucht, J. Linear and nonlinear properties of collagen-inspired hydrogels with both physical and chemical crosslinks. *In preparation*

Chapter 6: Rombouts, W. H.; de Kort, D. W.; Pham, T. T. H.; van Mierlo, C. P. M.; Werten, M. W. T.; de Wolf, F. A.; van der Gucht, J. Reversible temperature-switching of hydrogel stiffness of co-assembled, silk-collagen-like hydrogels. *Biomacromolecules* **2015**, *16*, 2506–2513.

Chapter 7: Rombouts, W. H.; Domeradzka, N. E.; Werten, M. W. T.; Leermakers, F. A. M.; de Vries, R.; de Wolf, F. A.; van der Gucht, J. Enhanced stiffness of silk-like fibers by loop formation in the corona leads to stronger gels. *Submitted*

Other work:

Cingil, H. E.; Rombouts, W. H.; van der Gucht, J.; Cohen Stuart, M. A.; Sprakel, J. Equivalent pathways in melting and gelation of well-defined biopolymer networks. *Biomacromolecules* **2014**, *16*, 304-310.

de Kort, D. W.; Rombouts, W. H.; Hoeben, F. J. M.; Janssen, H.; van As, H.; van Duynhoven, J. Scaling Behavior of Dendritic Nanoparticle Mobility in Semidilute Polymer Solutions. *Macromolecules* **2015**, DOI: 10.1021/acs.macromol.5b01530

Pham, T. T. H.; Skrzeszewska, P. J.; Werten, M. W. T.; Rombouts, W. H.; Cohen Stuart, M. A.; de Wolf, F. A.; van der Gucht, J. Disulfide bond-stabilized physical gels of an asymmetric collagen-inspired telechelic protein polymer. *Soft Matter* **2013**, *9*, 6391-6397.

Pham, T. T. H.; Kleijn, J. M.; Rombouts, W. H.; Fokkink, R. G.; Stuart, M. C. A.; Cohen Stuart, M. A. Templated silk-like fibril growth on pluronic nanospheres: curved and circular fibrils. *Submitted*

164

Dankwoord

Dit hoofdstuk is voor iedereen die voor mij een belangrijke rol gespeeld heeft om tot deze mijlpaal te komen. Ondanks dat het afleveren van een proefschrift een test van individuele academische bekwaamheid is, had ik dit zonder jullie goede adviezen, hulp en steun niet gered.

Allereerst wil ik Jasper en Martien bedanken om mij de kans te geven om me te bewijzen als onderzoeker bij de vakgroep fysische chemie. Dit was voor mij na drie jaar vertoeven als docent in het middelbaar onderwijs een flinke uitdaging! Jasper, ik wil je ontzettend bedanken voor de leuke discussies tijdens onze bijeenkomsten, je adviezen en hulp bij het naar het hoger plan trekken van mijn onderzoek. Ik vond het erg fijn dat ik veel ruimte van jou kreeg om mijn eigen draai aan het onderzoek te geven, en ik denk dat er veel goede ideeën uit zijn voort gekomen ook voor toekomstig onderzoek. Ondanks dat ik soms wat pessimistisch en veeleisend was over bepaalde zaken, hebben we door jouw positieve kijk en pragmatische aanpak een goed resultaat kunnen neerzetten.

Graag wil ik de Nederlandse Organisatie voor Wetenschappelijk Onderzoek (NWO) bedanken voor de financiering van dit project.

Ik wil Renko, Joshua, Mieke, Joris, Marleen, Martien en Frans bedanken voor de leuke discussies en adviezen voor mijn onderzoek. Hannie, Diane, Remco, Anton en Ronald heel erg bedankt voor jullie hulp bij het opzetten van mijn experimenten en bij het leren werken met de apparatuur. Zonder jullie zou het een stuk minder soepel gelopen hebben!

Lieve Anita, Josie en Mara ik wil jullie bedanken voor het regelen van de financiën, de bestellingen en de reizen tijdens mijn project, maar vooral voor de steun en dat ik mijn verhaal bij jullie kwijt kon als ik ergens mee zat. Mara, voor mij was kletsen met jou aan de koffietafel een heerlijk begin van de dag. Bedankt voor het inschrijven voor de spinningritten in de laatste jaren. Je zorgde er steeds voor dat we op onze 'eigen' fiets konden zitten vooraan. Verder was het geweldig om samen 'foute' nummers te bedenken en op te sturen voor tijdens de spinningritten. Bert, bedankt voor de hulp met het binden van de proefschriften en de goed gevulde snoepbak op jouw

kantoor.

Thao, thank you for all your help and assistance during the first months of my PhD. I learned a lot from you. Later on, we started collaborating on various projects, which resulted in several publications. I enjoyed working together with you and I think you are a great scientist, and I hope that you will find a nice job in the near future!

Natalia, thank you for your help with the fun part of my PhD; designing the new protein polymers. In the end I did not have much time left to properly characterize them all, there is only one chapter in this thesis on them. Fortunately, this work will be continued in a postdoc.

Melodie, bedankt voor jouw bijdrage aan mijn proefschrift. Ik vond het leuk om jou bij je bacheloropdracht te mogen begeleiden en ik hoop dat je er veel van geleerd hebt. Daarnaast hoop ik dat je plan om in Frankrijk je Master voort te zetten geslaagd is.

Mijn kantoor heb ik de laatste vier jaar gedeeld met Katarzyna, Kamuran, Inge en Marcel. Bedankt voor de goede (werk)sfeer in het kantoor! Inge, ik heb genoten van onze hikes op Hawaï na afloop van de PhD-trip en onze gedurfde hike in Israël, waarbij ik nog bijna het ravijn in donderde. Marcel ik vond het leuk om met jou samen een aantal dingen te ontwerpen in SolidWorks. Ondanks dat 3D-printen weinig directe toepassing had in mijn onderzoek, had ik er veel plezier in.

Ik wil Inge, Marcel, Hélène, Maarten en mijn broer(tje) Jaldert bedanken voor hun hulp bij het leren van LateX. Heeft heeft wat moeite gekost, maar uiteindelijk ziet het boekje er met jullie hulp gelikt uit!

Verder wil ik mijn andere collega's: Hans, Jacob, Jeroen, Jan-Bart, Jan Maarten, Joanne, Gosia (G'), Gosia (G"), Hande, Yuan, Ties, Ruben, Lione, Hanne, Ilse, Lennart, Maarten, Stan, Hélène, Duc, Nadia, Rui, Merve, Maria, Christian, Peter, Rene, Dirk, Jan, Aldrik, Aljosha, HuanHuan, TingTing, Dmitry, Evan, Marc, Sabine, Gerben, Frank, Stan, Celine, Johan, Vittorio en Anton bij Fysko bedanken voor de gezelligheid tijdens de pauzes en lunches. Met in het bijzonder Jeroen en Jan-Bart voor het halen van de kroketten en kibbeling.

Mijn onderzoek is onder andere tot stand gekomen door samen te werken met veel mensen buiten de vakgroep. Graag wil ik Mathieu Colomb-Delsuc, Sybren Otto, Jan van Lent, Marcel Giesbers, Daan de Kort, Carlo van Mierlo, Jan van Hest en Lise Schoonen bedanken voor hun bijdrage aan mijn onderzoek.

Bij FBR wil ik Frits en Marc bedanken voor hun hulp. Marc, ik heb er van genoten om met jou op het lab van FBR samen te werken aan de fermentaties en het maken van nieuwe eiwitpolymeren. Je bleef altijd geduldig en nam

About the author

Wolf Rombouts was born on the 17th of May 1982 in Groningen, The Netherlands. In 2001 he graduated from the Maartenscollege in Haren. He obtained both his Bachelor and Master degree in Biomedical Engineering at Twente University, with a specialization in Cellular, Molecular and Tissue Engineering. During his Master he did his internship at the Helmholtz-Zentrum Geesthacht near Berlin on chemical modification and cytotoxity tests on polyetherimide membranes. After finishing his Master, he started another Master to obtain his degree in teaching. In September 2009 he started teaching Chemistry and Design & Research (O & O) at C.S.G. Reggesteyn in Nijverdal.

In September 2011 he started as a PhD-candidate at the department of Physical Chemistry and Soft Matter at Wageningen University. He worked on the project 'Tough and Smart' on designing hybrid polymer networks and was supervised by Prof. Dr Jasper van der Gucht, and was financed by Netherlands Organisation for Scientific Research (NWO). The results of this research are presented in this thesis. After finishing the project in September 2015 he started a postdoc within the Foundation for Fundamental Research on Matter (FOM), where he will be working on the functionalization of polymer particles with proteins.

Overview of completed training activities

Displine specific

Winterschool	Han-Sur-Lesse, Belgium	2012
Small Angle Scattering School	Delft	2012
Dutch Polymer Days*	Lunteren	2013
Physics@FOM	Veldhoven	2013
'Chemistry in Relation to Physics and Material Sciences'[†]	Veldhoven	2013
European School of Rheology	Leuven, Belgium	2013
Polyelectrolytes conference*	Ein Gedi, Israel	2014
Gordon Research Conference 'Bio-inspired Materials'*	Maine, USA	2014
Scattering Summer School [†]	Bombannes, France	2014
Dutch Polymer Days	Lunteren	2014
Solid Works Software Training	Wageningen	2014
Chains: Chemistry Matters for the Future[†]	Veldhoven	2015

General

Techniques for Writing and Presenting a Scientific Paper (WGS)	Wageningen	2013
Competence Assessment (WGS)	Wageningen	2013
Career Perspectives (WGS)	Wageningen	2014
Effective behavior in professional surroundings (WGS)	Wageningen	2014

Entrepeneurship in and outside Science (StartLife)	Wageningen	2014
Data Management (WGS)	Wageningen	2014
Journal Club (PCC)	Wageningen	2014–2015

Optionals

Writing research proposal	Wageningen	2011
Advanced Soft Matter	Wageningen	2013
PhD-trip California[†]	USA	2013
Organisation committee PhD-trip UK	Wageningen	2014–2015
PhD-trip UK[† † ★]	UK	2015
Group meetings and colloquia	Wageningen	2011–2015

Notes: [†]oral presentation, [★]poster presentation